# PERFORMANCE ENHANCEMENT OF GRID CONNECTED SOLAR PV SYSTEM

A Thesis Submitted in Partial Fulfillment of the Requirements for the Degree of

## **DOCTOR OF PHILOSOPHY**

in

**Electrical Engineering** 

by

**SUKHBIR** 

(2k19/PHDEE/10)

Under the Supervision of

Prof. J N RAI
Department of Electrical Engineering
Delhi Technological University, Delhi



#### DEPARTMENT OF ELECTRICAL ENGINEERING

#### DELHI TECHNOLOGICAL UNIVERSITY

(Formerly Delhi College of Engineering) Shahbad Daulatpur, Main Bawana Road, Delhi-110042, India

August, 2025



#### **DELHI TECHNOLOGICAL UNIVERSITY**

(Formerly Delhi College of Engineering) Shahbad Daulatpur, Main Bawana Road, Delhi-110042

#### **CANDIDATE'S DECLARATION**

I **Sukhbir** hereby certify that the work which is being presented in the thesis entitled "**Performance Enhancement of Grid Connected Solar PV System**" in partial fulfillment of the requirements for the award of the degree of Doctor of Philosophy, submitted in the Department of Electrical Engineering, Delhi Technological University is an authentic record of my own work carried out during the period from August 2019 to May 2025 under the supervision of Prof. J N Rai.

The matter presented in the thesis has not been submitted by me for the award of any other degree of this or any other institute.

Sukhbir (2k19/PHDEE/10)

This is to certify that the student has incorporated all the corrections suggested by the examiners in the thesis and the statement made by the candidate is correct to the best of our knowledge.

**Signature of Supervisor** 

**Signature of External Examiner** 

ii



#### **DELHI TECHNOLOGICAL UNIVERSITY**

(Formerly Delhi College of Engineering) Shahbad Daulatpur, Main Bawana Road, Delhi-110042

#### **CERTIFICATE BY THE SUPERVISOR**

Certify that Sukhbir(2K19/PHDEE/10) has carried out the research work presented in this thesis entitled "Performance Enhancement of Grid Connected Solar PV System" for the award of Doctor of Philosophy from Department of Electrical Engineering, Delhi Technological University, Delhi under my supervision. The thesis embodies result of original work, and studies are carried out by the student himself and the contents of the thesis do not from the basis for the award of any other degree to the candidate or to anybody else from this or any other University/Institute.

Prof. J N Rai
Professor
Department of Electrical Engineering
Delhi Technological University, Delhi

Date:

#### **ACKNOWLEDGEMENTS**

I want to express my deep and sincere gratitude to my supervisor, **Prof. J N Rai**, for his valuable guidance and continuous monitoring of my research work. It was a great honor to pursue my research work under his supervision. **Prof. J N Rai** has been the motivating and inspiring factor behind my research work. His vigor and hunger to perform in an adverse situation have inspired me to strive for excellence. It is a lifetime experience to work under my supervisor and humbly acknowledge lifetime gratitude to him.

I would like to express my thanks to Prof. Rachana Garg, HOD (EE), for her kind support.

I want to thank the SRC members **Prof. Vijender Kumar**, **NSUT**, **Delhi** who has given me valuable advice to improve the quality of my research work. I am extremely grateful to the other member of SRC, **Prof. Uma Nangia**, **Prof. Narendra Kumar II and Prof. A K Sahoo** for their valuable advice. I want to thank other office staff, central library and computer centre staff members for their valuable cooperation and support. I would like my sincere thanks to

I am incredibly grateful to my research group and friends Dr. Sombir Kundu, Dr. Hemant Saxena, Dr. Rajesh Kumar, Dr. Hitanshu Saluja, Pardeep Parashar, Anuj Sinha, Pardeep Sharma, Yogendra Rathi and Rohit Gupta for their valuable assistance, cooperation, and an excellent source of learning.

**Dr. Ajendra Singh** who guided me at an initial level of my research work.

If I get any success today for my research work, the entire credit should go to my father, Late Sh. Bhim Singh, mother Smt. Krishna Devi, and my younger brother Somit Sheokand. I sincerely convey my gratitude to my wife Ms. Jyoti, daughter Priyanshi Sheokand, and son Shiven Sheokand who has encouraged me to carry out my research work. I want to thank other family members who directly or indirectly support my research work.

Lastly, I thank Mother Nature and Almighty God for allowing me to pursue doctoral studies		
Place: Delhi		
Date:		
Sukhbir (2k19/PHDEE/10)		

#### **ABSTRACT**

Solar photovoltaic (PV) based electricity generating system is becoming increasingly popular for managing energy consumption of remote and isolated communities. Solar energy source is the most promising renewable energy source (RES) due to its clean and unbounded supply, low maintenance requirements, lesser mechanical components, no green house gas emission, and ability to be put in remote regions for power generation.

The design, control, and analysis of a grid-connected photovoltaic system have been given in this thesis work. It makes three-phase load balancing, active and reactive distribution adjustment, and power quality enhancement. The proposed system is implemented in both the single-phase and three-phase distribution networks. Maximum Power Point Tracking (MPPT) technique has been implemented to extract maximum power from the PV. A voltage source converter (VSC) in the system provides power compensation (active and reactive), harmonics elimination, load leveling, and enhancement in the overall power quality of the system.

An appropriate control algorithm is needed for the proper operation of power electronic converters in a grid connected solar PV system. The control techniques ensure synchronization of different voltages, estimate fundamental components of voltages and currents and regulation of DC-link voltage of converters. Different conventional approaches for estimating synchronizing signals have been described, and novel advanced techniques for the systems have been proposed.

Frequency Locked Loops (FLLs) and Phase Locked Loops (PLLs) are being extensively employed to estimate synchronization signals and can compute the phase, amplitude, and frequency of the load current. These approaches have been implemented under a variety of operating situations, including fluctuations in solar intensity and harmonics in the loads for the grid connected solar PV system.

Conventional algorithms such as fourth ordered generalized integrator (FOGI), and Reduced-Order Generalized Integrator (ROGI) based FLL have been used for the proposed system. Furthermore, a novel technique using All-Pass Filter-PLL based control techniques

have been presented, which are adaptive and provide fast dynamic response without compromising steady-state performance.

Further advanced techniques like Coati Optimization Algorithm tuned Fuzzified-Phase Locked Loop (COA Fuzzified-PLL) and single-phase complex band-pass filter-based frequency locked loop (1φ-CBF-FLL) has been developed, rejecting the DC-offset and have faster dynamic response for the system. A Complex-Coefficient Reduced-Order Generalised Integrator-based Frequency-Locked Loop (CC-ROGI-FLL) control technique used for harmonic reduction.

A novel ensembled Deep Reinforcement Learning (EDRL) MPPT controller has been developed. The ensembled DRL MPPT controller leverages the power of deep learning and reinforcement learning techniques to optimize the MPPT process, enabling the mitigation of inter-harmonics and efficient power extraction with a constant reference DC voltage at the DC link.

In the present work, three primary components of the power circuit of the system are the grid, loads at common point of interfacing (CPI), and solar energy conversion system (SECS). A boost converter, VSC, an interacting inductor, and a ripple filter make up the power circuit of SECS. A boost converter is the first stage and a VSC is the second. The PV array is linked to the input of the boost converter. MPPT is served by the first stage of the boost converter. The output of the boost converter is linked to the DC link of VSC. The second stage of VSC adds PV power to the grid and aids in improving the PQ of the distribution network. The proposed system and algorithms have been simulated and examined in the MATLAB/Simulink environment. The experimental results validate the effectiveness of the proposed control schemes in a standalone system.

## **TABLE OF CONTENTS**

Candidate's De	claration	ii
Certificate by t	he Supervisor	iii
Acknowledgme	nts	iv
Abstract		vi
Table of Conte	nts	viii
List of Tables		xiii
List of Figures.		xiv
List of Symbols	S	xvii
List of Abbrevi	ations	xix
1. Introduc	etion	1-9
1.1 Gene	eral	1
1.2 Rene	ewable Energy based Sources	4
1.2.1	Solar	4
1.2.2	Wind	4
1.2.3	Hydro	5
1.2.4	Biomass	5
1.2.5	Geothermal	5
1.3 State	of Art	5
1.4 Scop	e of the Present Work	6
1.4.1	Design of Grid Connected Solar PV System	7
1.4.2	Development of Control, Synchronization and MPPT	7
	Techniques	
1.4.3	Application of Control Techniques	8
1.5 Thes	is Organisation	8

2.	Literatur	re Survey	10-29
	2.1 Gene	ral	10
	2.2 Litera	ature Survey on PV System Modeling and MPPT Control	10
	Algor	ithms	
	2.3 Litera	ature Survey on PQ Problems and their Solution	12
	2.4 Litera	ature Survey on Grid-Connected PV System	14
	2.5 Litera	ature Survey on Synchronization and Control Algorithm	15
	2.6 Litera	ature Survey on Analysis of Interharmonic Component	26
	2.7 Identi	ified Research Gap	27
	2.8 Autho	ors Contribution in the Proposed Work	28
	2.9 Object	ctives of the proposed Research Work	29
	2.10 Su	nmary	29
3.	Design a	nd Development of Single & Three-Phase Grid-Connected	30-44
	Solar PV	System	
	3.1 Gener	al	30
	3.2 Design	n and Development of Single-Phase Grid-Connected Solar PV	30
	System		
	3.2.1	Design of PV System	32
	3.2	2.1.1 Design of PV Module	32
	3.2	2.1.2 Design of PV Array	35
	3.2.2	Calculation of DC-Link Reference Voltage	37
	3.2.3	Design of DC-Link Capacitor	37
	3.2.4	Design of Interfacing Inductor	38
	3.2.5	Design of DC-DC Boost Converter	38
	3.3 Design	n and Development of Three-Phase Grid-Connected Solar PV	40
	System		
	3.3.1	Calculation of DC-Link Reference Voltage	42
	3.3.2	Design of DC-Link Capacitor	43
	3.3.3	Design of Interfacing Inductor	43
	3.3.4	Design of PV Array	44
	3.4 Summ	nary	44

4.	Implementation of Advance Control Algorithms for Single-Phase	45-75
	Grid-Connected Solar PV System	
	4.1 General	45
	4.2 1φ-CBF-FLL Control Approach	45
	4.2.1 Evaluation of 1φ-CBF-FLL	46
	4.2.2 Examining 1φ-CBF-FLL	46
	4.2.3 Modeling	47
	4.2.4 Calculation of Fundamental Load Current Component	50
	4.2.5 Estimation of Reference Currents	51
	4.2.6 Simulation Results	51
	4.2.6.1 Dynamic Behaviour of System in Case of Variation in	51
	Solar irradiance	
	4.2.6.2 Dynamic Behaviour of System in Case of Load	53
	Removal/Insertion	
	4.2.6.3 Dynamic Behaviour of System in Case of Load Variation	54
	4.2.6.4 Performance of the System in Case of DC-Offset	55
	Condition	
	4.2.6.5 Harmonics Analysis	56
	4.2.6.6 Performance Comparison	57
	4.2.7 Test Results	58
	4.2.7.1 Dynamic Behaviour of System in Case of Load Variation	59
	4.2.7.2 Harmonics Analysis	60
	4.3 APF-PLL Control Approach	61
	4.3.1 Modeling	61
	4.3.2 Phase Estimation Dynamics	61
	4.3.3 Amplitude Estimation Dynamics	63
	4.3.4 Simulation Results	64
	4.3.4.1 Steady State Output of Proposed System in Case of	64
	Constant Solar Irradiance	
	4.3.4.2 Dynamic Output of Proposed System in Case of Variation	65
	in Solar Irradiance	

	4.3	3.4.3 Dynamic Output of Proposed System in Case of Load	66
		Variation	
	4.3	3.4.4 Power Curve Under Different Loading Conditions	66
	4.3	3.4.5 Harmonic Analysis	67
	4.3	3.4.6 Comparative Performance	68
	4.4 FOGI-	-FLL Control Approach	69
	4.4.1	MPPT Control	69
	4.4.2	Calculation of Maximum Value of Fundamental Load Current	70
		Component	
	4.4.3	Simulation Results	70
	4.4	4.3.1 Static Response of the Suggested System Under Fixed	71
		Solar Irradiance and Load	
	4.4	4.3.2 Effective Response of the Suggested System Under	72
		Change in Solar Irradiance	
	4.4	4.3.3 Effective Response of the Suggested System Under Fixed	74
		Solar Irradiance Feeding Unbalanced Load	
	4.4	4.3.4 Harmonic Analysis of the System	74
	4.5 Summ	nary	75
5.	Control	Techniques for Three-Phase Grid-Connected Solar PV	76-107
	System		
	5.1 Gener	al	76
	5.2 CC-R	OGI-FLL control approach	78
	5.2.1	P&O-based MPPT Control	78
	5.2.2	CC-ROGI-FLL control approach for VSC	79
	5.2.3	Simulation Results	80
	5.2	2.3.1 Response in case of Steady State Condition	80
	5.2	2.3.2 Response in case of Varying Solar Insolation	81
	5.2	2.3.3 Response in case of Unbalanced Load	83
	5.2	2.3.4 Harmonic Analysis	83
	5.3 Interh	armonic Mitigation via DRL-MPPT	85

	5.3.2	Action Space	86
	5.3.3	Reward	87
	5.3.4	DQN (Discrete)	91
	5.3.5	DDPG (Continuous)	92
	5.3.6	PPO (Discrete)	93
	5.3.7	rlTD3 twin-delayed deep deterministic policy gradient	94
		(Continuous)	
	5.4 DC of	fset Mitigation Using Improved PLL	95
	5.5 Simula	ation Results	100
	5.6 State-o	of-Art Comparison	106
	5.7 Summ	nary	107
6.	Conclusio	ons, Future Scope and Social Impact	108-110
	6.1 Concl	usions	108
	6.2 Future	e Scope and Social Impact	110
	6.3 Social	Impact	110
	Reference	es	111-134
	Appendix		135
	List of Pu	blications	136
	Bio Data		137

## LIST OF TABLES

S.No.	Title	Page No.
3.1	Ideality factor	33
3.2	PV string parameters at STC for single-stage grid-connected PV	36
	system	
3.3	PV string parameters at STC for double-stage grid-connected PV	37
	system	
3.4	The parameter setting of PV	42
3.5	The parameter setting of PV	44
4.1	Performance overview of various controllers	58
4.2	Comparative performance of proposed APF-PLL with conventional	68
	control algorithms	
5.1	The range values for the input/output of fuzzy controller	98
5.2	Constraints for Fuzzy Controller	98
5.3	Fuzzy rule for output variable $\Delta\theta$	99
5.5	The summary of performance of Different controller	107

## LIST OF FIGURES

S.No.	Title	Page No
3.1	System configuration of single-phase grid-connected solar PV system	31
3.2	Practical single diode model of PV cell	32
3.3	(a) P-V and I-V curve at different temperatures and fixed solar	34
	insolation	
	(b) P-V and I-V curve at different solar insolation and fixed temperature	35
3.4	System configuration of three-phase grid-connected solar PV system	40
3.5	Topology of three-phase grid-connected solar PV system	41
4.1	(a) 1φ -CBF-FLL configuration	47
	(b) Second order CBF in the continuous time domain	47
4.2	(a) Model of 1φ-CBF-FLL	50
	(b) Its alternate	50
4.3	Digital model of 1φ-CBF-FLL	50
4.4	(a) & (b) Dynamic response of GTSPV in case of change in solar	52
	irradiance	
4.5	(a) & (b) Dynamic response of GTSPV in case of load	53-54
	removal/insertion	
4.6	Dynamic response of GTSPV system in case of change in load	55
4.7	(a) & (b) Performance of GTSPV system in case of DC-offset condition	55-56
4.8	(a)-(c) Harmonics analysis of 1-φ GTSPV system	57
4.9	Comparative performance of proposed 1¢-CBF-FLL with LKF-FLL and	58
	SOGI-FLL	
4.10	(a)-(d) Dynamic response of the proposed system in case of change in	59-60
	load	
4.11	(a) & (b) Harmonic spectra of the proposed system	60
4.12	APF-PLL control algorithm	63
4.13	Steady state output of proposed system in case of constant solar	64
	irradiance given to a balanced load	
4.14	(a) & (b) Dynamic output of proposed system in case of variation in	65

	solar irradiance	
4.15	Dynamic output of single phase grid interfaced solar-PV system in case	66
	of constant solar irradiance	
4.16	Power curve under different loading conditions	67
4.17	(a)-(c) Harmonic analysis of (a) source voltage (b) source current, and	67-68
	(c) load current	
4.18	FOGI-FLL control algorithm	69
4.19	(a) & (b) Static response of the suggested system under fixed solar	71-72
	irradiance feeding balanced nonlinear load	
4.20	(a) & (b) Effective performance of GCSPV system under change in	73
	solar insolation	
4.21	Effective response of the system under fixed solar irradiance level	74
	feeding unbalanced nonlinear load	
4.22	THD of GCSPV system under nonlinear load condition	75
5.1	CC-ROGI-FLL control algorithm	78
5.2	Response at steady state condition	81
5.3	(a) and (b) Response in case of varying insolation	82
5.4	Response in case of unbalanced load	83
5.5	(a)-(c) Examination of harmonic	84
5.6	Three-phase grid-connected photovoltaic system using ensembled DRL	87
	for MPPT control	
5.7	The average reward per episode during training of EDRL	91
5.8	COA Fuzzified-PLL based Controller	97
5.9	(a) Coati optimised membership function for input E	99
	(b) Coati optimised membership function for input $\Delta E$	99
	(c) Coati optimised membership function for output $\Delta\theta$	100
5.10	The output of DC coupling voltage of (P&O) and EDRL	102
5.11	The output of grid current during (P&O) and EDRL MPPT Technique	102
5.12	The magnitude of fundamental frequency component during (P&O) and	103
	EDRL MPPT Technique	
5.13	The frequency variation during (P&O) and EDRL MPPT Technique	103

	with conventional PLL	
5.14	The Phase angle error during (P&O) and EDRL MPPT Technique with	104
	conventional PLL	
5.15	The output of grid current during EDRL-COA Fuzzified PLL	105
	synchronization technique	
5.16	The frequency variation during EDRL MPPT with COA-Fuzzified PLL	105
	Technique	
5.17	The Phase angle error during EDRL MPPT Technique with COA-	106
	Fuzzified PLL	

#### LIST OF SYMBOLS

PQ Power Quality

SPVS Solar Photovoltaic System

VSC Voltage Source Converters

PLL Phase Locked Loop

DSTATCOMs Distribution Static Compensators

RESs Renewable Energy Sources

MPPT Maximum Power Point Tracking

EDRL Ensembled Deep Reinforcement Learning

COA Coati Optimization Algorithm

CBF-FLL Complex Band-Pass Filter Based Frequency Locked Loop

FOGI-FLL Four Ordered Generalized Integrator Frequency Locked Loop

APF-PLL All-Pass Filter-Based Phase Locked Loop

SOGI Second Order Generalized Integrator

CC-ROGI-FLL Complex-Coefficient Reduced-Order Generalised Integrator-based

Frequency-Locked Loop

PCC Point of Common Coupling

CSI Current Source Inverter

BES Battery Energy Storage

PWM Pulse Width Modulated

ANN Artificial Neural Networks

DTOGI Dual Third Order Generalized Integrator

THD Total Harmonic Distortion

LMS Least Mean Sqaure

MLMS Modified Least Mean Square

SRFT Synchronous Reference Frame Theory

VGC Variable Gain Controller

ROGI Reduced-Order Generalized Integrator

SECS Solar Energy Conversion System

DGS Distributed Generation System

#### LIST OF ABBREVIATIONS

PV Voltage  $\mathbf{v}_{pv}$ **PV** Current **PV** Power  $p_{pv}$ Minimum DC-link voltage  $V_{dcm}$ Maximum Power  $P_{mp}$  $V_{mp}$ Voltage at maximum power point Current at maximum power point  $I_{mp}$  $V_{dc}$ DC link voltage DC-link Capacitor  $c_{dc}$ Grid Voltage  $v_g$ Reference DC-link voltage  $V_{dcref}$ **Switching Frequency**  $f_{S}$ Compensator Current  $i_c$  $I_f$ Interfacing Inductor Fundamental Load Current Component  $I_{fL}$  $i_g^*$ Reference Current Net Current  $I_{net}$  $D_c$ Duty Cycle State Space X

**Reward Function** 

r

U Action Space

 $\pi$  Policy

 $J_{\pi}$  Cumulative Expected Reward

 $I_{rms}$  RMS value of the individual harmonic current components

 $Tp_b$  Weighted average of the duty cycle obtained from individual DRLs

## **CHAPTER 1**

#### INTRODUCTION

#### 1.1 General

In the absence of electricity, modern existence would be nearly unfeasible, rendering it one of the most significant contributions of science to humanity. As a clean and efficient energy source, it plays a crucial role in daily activities and industrial development. However, a substantial portion of the global population still lacks access to stable and high-quality power. While many remote and isolated areas are officially classified as electrified, they often receive electricity only for a few hours due to planned and unplanned outages. Planned outages are imposed by distribution companies for commercial reasons, whereas unplanned outages result from environmental and human-related factors such as overloads, conductor snapping, and short circuits. Even when electricity is available, issues like low supply voltage and phase imbalances frequently arise due to uneven load distribution across three phases. Bulk of electricity is generated in thermal power plants using fossil fuels and transmitted through transmission network to load centres. The energy consumption is continuously increasing globally and due to increased generation the huge amount of carbon emission is produced and resulting disastrous greenhouse effect. Further, fossil fuels are continuously depleting and their increasing prices are imposing several challenges to power producers. Distributed generation (DG) employing locally accessible renewable energy sources (RESs) has garnered significant interest from scientists and researchers for power generation that is cost-free and abundantly available. Principal sources of renewable electricity include solar, wind, hydroelectric, and tidal energy. Wind and solar energies are two fast growing RES now a day. Solar energy via solar PV systems has gained popularity for applications like grid connection.

Solar PV, or PV, arrays are essential solutions to environmental deterioration and the exhaustion of fossil fuel resources, driven by the increasing global need for clean, sustainable energy. Growing popularity of solar PV systems is anticipated as costs come down and

technology improves, helping to create a more sustainable energy environment. Grid-connected solar PV systems are highly efficient at harnessing solar energy and integrating it into the electrical grid, leading to their growing popularity. Grid-connected solar PV networks, capable of generating energy without carbon emissions, are a promising unconventional energy source that will significantly enhance environmental conditions. Nonetheless, direct integration with the utility grid poses challenges due to the sporadic characteristics of solar PV systems. As the weather and time of day affect the energy output variations, asynchronous coupling becomes a necessity.

It is common practice to use an advanced control method in conjunction with an AC/DC converter to securely and efficiently connect PV systems to the power grid, which allows them to satisfy energy demands while keeping the grid stable. These requirements include grid harmonization, improved quality of electricity, stability, harmonic reduction, and electrical power flow control [1]. The inclusion of solar panels is presently regarded as the gold standard for grid construction. Maximum Power Point Tracking (MPPT) is a technique that enhances energy transfer efficiency by continually assessing and adjusting the power output to the load in response to variations in the load and external conditions. Its primary objective is to effectively manage output voltage fluctuations caused by changes in PV power. Additionally, the non-linear relationship between output current and voltage in solar systems poses a significant challenge, as it can substantially impact efficiency [2].

The grid interface circuit primarily performs three key functions: filtering, voltage sensing, and conversion from analog to digital. A likely explanation for the detected offset of DC in the captured voltage of the grid could be attributed to the nonlinear behaviour of voltage sensors, along with thermal drift in analogue components and the conversion process from analogue to digital. Employing a well-engineered grid interface circuit may not avert this situation. [3]. The addressed DC offset is the undesired component of the input sine signal on the PLL structure's output waveform. One of the common applications sine signal is as a reference signal in the production of reference currents for PV converters. Numerous recognized standards, such as IEC 61727, EN61000-3-2, and IEEE 1547-200, delineate the allowable thresholds for direct current (DC) infusion into the grid through the connected solar energy converters. Diverse methodologies might be utilized to eradicate the offset of DC

detected in the voltage of the grid. Having interharmonics, on the other hand, can make the power system work less well. There are several problems that can happen when a lot of nonlinear loads are linked to the power system. These include low power factor, high heat production from transformers and power lines, protection device failure, higher transmission losses, and bad voltage regulation [4]. Energy loss from interharmonic components is substantial. Variable frequency drives, converters, and inverters are examples of non-linear power electronic loads that are strongly linked to the power system's increasing interharmonics. Environmental factors that might impact PV module and inverter performance include temperature changes and variations in solar radiation. Inter-harmonic oscillations as well as output power and current harmonic oscillations may result from these changes.

Grid-connected PV systems dominate the major section of the market (99%) of the total PV installed, compared to stand-alone systems that rely on batteries. Grid-connected systems does not require batteries since the PV plant sends power directly to the grid, where it is transferred, distributed, and consumed. This reduces the demand for other energy sources, such as hydropower or fossil fuels, effectively offsetting their use. These savings serve as virtual energy storage, fulfilling the same roles of power regulation and backup typically provided by batteries in islanded systems. Isolated systems are less expensive and necessitate more maintenance and reinvestment compared to the systems which are connected to grid due to their non requirement connected batteries. This approach, in addition to technological advancement, environmental consciousness, economic efficiency, and appropriate subsidies and regulations, has harnessed solar energy's potential. Again, in a standard PV system, solar irradiation, temperature, and terminal voltage affect DC power production. PV inverters convert DC electricity into grid power. For better performance and flexibility, an intermediate DC-DC converter can be added across the grid-tied inverter and PV modules. This supplementary stage clearly differentiates the operational point of the PV system from the grid management of the PV inverter. Furthermore, it may augment the DC output voltage of the PV system as required, ensure galvanic isolation, and enable MPPT management. The PV power conversion stage has been continuously evolving as a result of the rise in installed PV capacity. Over time, contemporary power converters for PV has evolved as dependable, compact, and highly efficient, facilitating optimal power extraction from solar radiation in homes, businesses, and factories. During the past two decades, the PV converter industry has matured significantly, emerging as a distinct category within power conversion technology. This rapid development has been driven by stringent market demands for advanced specifications, including high efficiency, extended warranty periods, superior power quality (PQ), transformer less operation, and specialized control features like MPPT.

The system overall reliability is enhanced by integrating PV systems with the grid. Inverters are responsible for this integration. If the PV system cannot be linked to the grid using appropriate synchronization mechanisms, it will add to the existing number of PQ issues in the grid. Therefore, we need to learn about PQ difficulties, their causes, and how to fix them.

#### 1.2 Renewable Energy Based Sources

Government support, improving economic conditions and significant advancements in renewable energy technologies are major factors to shift towards usages of renewable energy. The following are few common sources of renewable energy systems.

- **1.2.1 Solar:** The solar PV effect established the basis for solar energy in 1839. Solar has developed into one of the RESs with the fastest rate of growth over the last two decades. Solar technology is classified into two types:
  - Solar thermal
  - Solar PV array

Solar thermal systems focus sun energy and convert it to heat using a network of reflecting collectors. Solar PV systems use a panel of connected solar cells to directly convert sunlight into electrical power.

1.2.2 Wind: As we move toward a low-carbon energy future, wind power will play an important role as a renewable resource. Ongoing technical advancements and encouraging policies are further enhancing the efficiency, reliability, and cost-effectiveness of wind turbines, making them an increasingly vital component of the global energy mix. Offshore and onshore wind energy technologies have advanced significantly in recent years, focusing on increasing electricity generation through the

use of larger turbines.

- **1.2.3 Hydro:** The force or energy of moving water generates hydropower. Small power plants rely on naturally flowing water sources, whereas larger hydro plants require dams to hold the required water head to produce hydropower for running hydro turbines attached to generator shafts. Hydro power relies on rain fall pattern and can be impacted by climate change which causes less rain.
- **1.2.4 Biomass:** Biomass fuel is made from organic materials including, manure, forest trash, crops, and sugar cane residue. Biomass energy may be transformed into electricity. The process of extracting energy from biomass varies based on the substance used. Most biomass is used in rural areas for cooking, lighting and heating in developing countries.
- 1.2.5 Geothermal: One nonconventional energy source is geothermal heat and power, which draws on the Earth's inherent thermal energy to power various heating and cooling systems. It takes advantage of the natural heat reservoirs found underground, which are a result of geological processes and the planet's residual heat from its formation. The oil and gas sector typically uses techniques like digging wells below the earth's surface and moving water through them to extract energy from hot rocks. The water is then heated and pushed to the surface, where it powers a turbine and generator to generate electricity. The process is then repeated with recycled water[5],[6].

#### 1.3 State of Art

The enhancement of PQ amidst intermittent conditions and the provision of unbalanced linear or non-linear needs have been the subject of much research on the management and coordination of grid-connected solar systems. Owing to the intrinsic non-linear characteristics of PV systems, the implementation of MPPT approaches is imperative.

Solar PV system efficiency in grid-connected setups can be affected by fluctuations in solar irradiation, changing climatic conditions, and grid voltage distortions caused by nonlinear loads and conversion processes. DC-offset and interharmonics are two examples of

these aberrations. Several factors contribute to the presence of unwanted direct current components in the recorded system output currents. Imprecision and errors in PWM signals may result from various factors, including the non-linear characteristics of switching devices, minor inaccuracies, and compensate shifts in the current and voltage the reading instruments utilized for control system feedback [7].

Interharmonics in the context of PV inverters could be related to the MPPT control mechanism. The fluctuations in irradiance caused by partial shedding may influence the efficiency of inverters and PV modules. These variations can lead to inter-harmonic oscillations, changes in output power, and variations in current harmonics. The traditional methods used to achieve grid synchronisation and MPPT are limited by interharmonics problems. In addition, common synchronization techniques like Phase Locked Loop (PLL) may have trouble keeping in sync with the grid when there are voltage distortions or changes in frequency, which might lead to DC-offset issues.

This study offers a novel MPPT controller based on Ensembled Deep Reinforcement Learning (EDRL), accompanied with an improved PLL tuned to COA in an attempt to address these challenges. Additionally, a band-pass filter called 1φ-CBF-FLL (single-phase) has been presented. This thesis further proposes a synchronizing system based on APF-PLL and a FOGI-FLL utilizing four ordered generalized integrators. A CC-ROGI-FLL control technique used for harmonic reduction.

By optimizing the MPPT process and employing reinforcement and deep learning techniques, the integrated DRL MPPT controller can effectively minimize interharmonics and maintain power retrieval, and provide a reference voltage with stability to the DC link.

To attain a dependable integration with the electrical grid, under the distorted voltage and fluctuating frequency, the synchronizing systems that rely on COA Fuzzified-PLL, CC-ROGI-FLL, 1φ-CBF-FLL, FOGI-FLL, and APF-PLL strive to reject DC-offset. These control algorithms have made good improvements in the mitigation of PQ problems.

## 1.4 Scope of the Thesis

Through the comprehensive literature surveyon the performance enhancement of gridconnected solar PV systems, numerous significant gaps have been observed. There is a need for advanced control techniques to improve PQ in grid-connected PV systems. Modification in some advanced techniques which I have been studied for shunt compensators are required thorough studies and investigation. A number of PLL based circuits are available in literature. Additional PLLs for the management of grid-connected PV systems, utilized for synchronization, are required to be efficient and rapid. Fast and effective synchronization approaches utilizing various types of adaptive filters are essential for grid-connected PV systems. Advanced control techniques for different loading conditions are required and a comparison of these is also required based on simulation studies.

The primary objectives of the thesiscan be summarized as

- To design, model, and create a solar PV system that is connected to the grid.
- To develop and evaluate novel techniques of grid-connected PV system synchronization under DC-offset situations.
- To analyze the interharmonic component and find ways to reduce it; to create new
  methods for dealing with partial shade and changing irradiance; and to conduct
  mathematical stability tests to ensure that the synchronization approach can operate
  reliably under different grid voltage situations.

A brief description of some of the related work on grid-connected solar PV systems is given below:

#### 1.4.1 Design of Grid-Connected Solar PV System

The grid-connected PV system was created and simulated using MATLAB. It is suitable for both single-phase and three-phase systems. To ensure the simulation models were accurate, an experimental prototype was built and tested under a controlled laboratory environment.

#### 1.4.2 Developments of Control, Synchronization and MPPT Techniques

This work describes both old and modern methods of synchronization. We have tried these synchronization approaches under various operational situations. In an attempt tocoordinate a grid-connected solar PV system, systems like: COA Fuzzified-PLL, CC-ROGI-FLL, 1\phi-CBF-FLL, FOGI-FLL, and APF-PLL have been employed and evaluated. To minimize interharmonics and optimise power extraction from solar PV in dynamic

environments, many MPPT methods have been developed and put into use, including EDRL and P&O.

#### 1.4.3 Application of Control Techniques

The primaryelement of distorted load current may be attained by applying certain single-phase and three-phase control methods. The control and synchronization of the grid-connected solar PV systems have been handled using the COA Fuzzified-PLL, CC-ROGI-FLL, 1φ-CBF-FLL, FOGI-FLL, and APF-PLL control algorithms. The developed techniques have been employed for reactive power compensation, DC-offset rejection, load leveling, harmonics abatement, and reducing PQ problems. The EDRL based MPPT technique have been used to mitigate the interharmonics.

#### 1.5 Thesis Organisation

Entire thesis is organized in six chapters describing the proposed work in a comprehensive way as follows

**Chapter-1:** This chapter provides an overview and background on grid-connected solar PV systems, highlighting PQ challenges, their underlying causes, associated issues, and potential solutions.

**Chapter-2:** This chapter incorporates an extensive literature survey on control and system description for grid-connected solar PV systems, fundamental component estimation techniques, MPPT and techniques for synchronization, and methods for interharmonics analysis.

**Chapter 3**: The modeling of PV systems and the design of PV arrays for integration with the grid have been discussed in this chapter. This chapter also discusses the design of power components and equipment for single-phase and three-phase systems.

Chapter-4: The control methods employed in a single-phase solar PV grid system operating under the irregular conditions of solar energy supply to an unbalanced load have been explored. The 1φ-CBF-FLL, FOGI-FLL, and APF-PLL control algorithms are developed to enhance the system power quality.

Chapter-5: A grid-connected solar PV system based on three-phase is discussed in this chapter, which aids in the construction of control algorithms. An innovative COA-fuzzified

PLL is proposed to eliminate DC-offset, a CC-ROGI-FLL control technique used for harmonic reduction and it leads to the removal of interharmonics via an EDRL-based MPPT approach.

**Chapter-6:** This chapter summarizes the primary benefits of several grid synchronization techniques, control algorithms, and PV grid integration for single-phase and three-phase systems under the primary contribution of the thesis. This chapter also presents the proposed future work in this domain.

## **CHAPTER 2**

#### LITERATURE SURVEY

#### 2.1 General

The previous chapter provided an overview of the requirements for solar PV systems, power quality issues, their implications, and potential solutions in grid-connected PV systems. The thesis's present condition, scope, and organization were also addressed. Precise modeling is crucial to align with actual PV behaviour, facilitated by the PV systems integration into the grid, which permits active power injection and enables comprehensive investigation of PV characteristics and power extraction. The impact on power quality of the present distribution system, associated with various types of loads, has been analyzed. The chapter provides an extensive literature review of synchronization and control algorithms to guarantee the reliable operation of grid-connected solar PV systems under fluctuating grid voltage and load variation conditions. Moreover, many designs for the transmission of excess power to the grid have been meticulously examined.

## 2.2 Literature Survey on PV Modeling and MPPT Techniques

Power semiconductor technology has gained superiority during the last few decades. The cost of PV cells has also decreased extensively, hence, solar energy has emerged as one of the most promising forms of energy production and distribution solutions. Furthermore, using direct sunlight is inexpensive and has no impact on the environment[8]. As of December 2013, India's total solar energy installed capacity was 2180MW, with the potential to contribute a solar installed capacity of 63.303 GWAC by December 31, 2022. However, due to significant advancements in solar technology over the years to improve efficiency and reduce costs are reported. Innovation and advancement efforts are focused on enhancing the response of solar cells and modules, increasing their efficiency, and making them more affordable[9]. The choice between series/shunt connections of solar PV cells depends on the specific needs of the system and the load being served. For medium power demands, a series connection can provide a higher output voltage, but the current will be limited to that of each

module. If higher power demands are expected, a combination of series and shunt connections, such as using multiple series-connected strings in parallel used to generate the desired amount of power [10].

The system voltage in a shunt configuration is equivalent to the voltage of a single module, however, the current is a combination of the currents delivered by all the modules. As a result, for solar PV modules, a range of inter-connection patterns such as series-parallel (combination of series & shunt connection scheme), Total Cross Tied, Bridge linked, and Honey Comb are offered[11]. The most common topologies are series-parallel connections, which are commonly used to meet load power requirements. However, the output power may be drastically decreased if any of the PV system are shaded. Partial shadowing can be caused by large trees, hoardings, poles, and towers, among other things[12]. As a result, partial shadowing distributes the shadow over the solar PV array unevenly. Partial shadowing is a critical consideration in PV system design and installation, and addressing its effects is essential for maximizing power generation and ensuring the long-term reliability of the system.

The perturbing effects of partial shade are numerous peaks in the PV characteristics and steps in the characteristics[13], [14]. Multiple MPPT control approaches have been investigated in the literature[15]. As classical MPPT methods, P&O[16], hill climbing (HC)[17], and IC [18] are discussed. Despite being easier to implement in hardware, the HC and P&O approaches exhibit considerable oscillations that are closer to the MPP, which causes power losses. An IC approach is accurate and adaptable in changing atmospheric conditions[19]. P&O & IC are conventional algorithms that are easy to implement, less complex and works effectively under varying solar insolation and temperature condition[20].

The efficiency of solar cells varies from 6% for amorphous silicon-based solar cells to 44% for multi-junction production cells, and is achieved in laboratories [21], [22], [23]. In practical solar cells, the efficiency of solar cells varies from 15% to 22% [24], [25]. Solar irradiance, temperature, dust, and other airborne particulates are environmental elements that substantially affect the solar cells' performance efficiency. Usually, a solar cell is designed in the form of a single-diode model or a diode model [26], [27], [28]. A single-diode model with

series & shunt resistance considered identical with the practical solar cell with less complexity. Solar cell is the current source type, and its characteristics are non-linear. A single cell cannot produce enough energy to be used for power applications. A solar PV module has many cells interconnected in series, and one may connect numerous modules in either series or parallel configurations to produce substantial power. One of the key instruments of optimizing the performance of a PV module or array is the MPPT technique. The MPPT methodology has been addressed in several published studies [29], [30], [31], [32]. Two of the conventional algorithms, which are easy to implement, are P&O and INC, which are less complex and work well under varying irradiance and temperature conditions[33], [34], [35], [36].

## 2.3 Literature Survey on PQ Problems and Their Solutions

Modern distribution networks are quite complicated and are linked to several sorts of loads. Different PQ difficulties can emerge owing to varying loading situations and natural disturbances. Voltage flicker, Transients, short and long-duration voltage transients, voltage imbalance, and waveform distortion are the most common PQ concerns. Lightning strikes, capacitor switching, single line to ground faults, switching on/off loads, single-phase loads connected to three-phase supply, adjustable speed drives, power electronic converters, halfwave rectification, arc furnaces, and other non-linear loads are the primary causes of poor PQ [37], [38]. These PQ difficulties induce failure, improper operation of electrical equipment, and energy loss, all of which result in direct or indirect economic loss [39]. Power experts are deeply concerned about the introduction of harmonics at the CPI in current distribution systems. Contemporary power electronics integrated into the distribution system significantly contribute to system harmonics [40]. A distribution system composite of large-scale PV and fast-charging EV batteries may assert a negative influence, particularly on voltage magnitude and harmonics [41]. These harmonic currents cause higher losses and heating in a variety of electromagnetic equipment. Again, the introduction of reactive power compensating capacitors to electrical systems in an attempt to power factor may lead to the risk of resonant conditions occurring. Resonance can happen when the capacitance of the power factor correction capacitors matches the inductance of the system or specific components within it, such as transformers or cables. PQ standards have been proposed by the IEEE and the

International Electrochemical Commission (IEC) [42]. IEEE 1159:2019 (revision of IEEE Std 1159-2019) [43] the prescribed standards are focused on the characterization, measurement, quantification, and interpretation of electromagnetic disturbances in power systems. Its purpose is to provide guidelines for understanding and addressing variations that may arise from internal factors within the power supply or load machinery[44].

IEEE 519:1992 [45], explores the IEEE guidelines and standards for mitigating harmonics in electrical systems. Specifically, an updated version of IEEE 1547-2003, the IEEE 1547-2018 standard specifies the necessary steps for combining electric power networks with distributed energy resources. Each DER shall meet at PCC[46]. It is essential to come up with global standards and guidelines in order to establish a reliable, operationally efficient, and safe wind and solar energy-based Electric Power Systems (EPSs). These criteria and standards address various aspects of DER integration, including technical requirements, communication protocols, operational procedures, and safety guidelines [47]. To address the PQ difficulties, various strategies have been employed. One of the stages is the Active power filters (APFs), which are found to be one of the most employed filters under this context. These active filters can be broadly classified into three categories such as: shunt active filters, series active filters, and hybrid active filters [48]. A series active compensator is linked in series at the load end and is employed to alleviate voltage-based PQ issues like voltage sag/swell, flickers, voltage perturbations, voltage imbalance, and harmonics. Solid State Static Series Compensators (SSSCs) [49], [50] and DVRs are examples of series APFs[51]. DSTATCOM is a term used to describe shunt APFs used in distribution systems. The Current Source Inverter (CSI) and VSC act as a Control Power Inverter (CPI) as it is coupled in shunt configuration, offering several possible applications. DSTATCOM has tackled current power quality concerns, including harmonic reduction, reactive power support, load balancing, and voltage management[52]. Because of advancements in switching devices, DSTATCOM is currently rather common for mitigating PQ difficulties [53]. Previously, MOSFET and GTO were used as switching devices, but now they employ IGBT for easy operation and improved performance [54]. The hybrid APF configuration offers a more comprehensive solution for PQ problems by combining the advantages of both series & shunt APFs[56]. Nevertheless, there are available solutions that can improve voltage and current-related PQ problems.

However, this technology has some drawbacks, including complex control, requiring more switches, and therefore being more expensive [57].

## 2.4 Related Work on Grid-Connected PV System

In[58], the author describes a grid-tied solar PV system characterized by three phases and two stages. Boost converters are usually employed in the first phase to attain a MPPT by transferring solar energy to the PV inverter. In the second phase, the energy from the boost converter is applied to the grid with the help of a two-level voltage source converter, which additionally operates as a PV inverter. The proposed system features an adjustable reference DC link voltage that may be altered based on the PCC value. The main objective of the introduction of this adaptive DC link regulation of voltage is to minimize switching power losses. In[59] a three-phase PV generating system that is grid-supportive is discussed. Grid support refers to the fact that the proposed technology helps enhance PQ at the distribution system's front end in addition to feeding energy produced by solar PV systems into the grid. The suggested two-stage architecture consists of a grid-interfaced VSC in the second stage and a boost converter in the first, which harvests energy from the PV array. A refined step adaptive neuron-based control method has been created to ascertain the overall power-consuming element of the load current.

In[60], through the utilization of a digital multistage interpolation (DMSI)-based approach, the researchers shed light on a multi-objective solar PV system that is incorporated into a three-phase and four-wire (3P4W) distribution network. In order to achieve power conditioning and transmission from solar systems to the 3P4W grid, a VSC with four legs is utilized. When it comes to power tracking MPPT, the utilization of the P&O technique is applied. In addition, a control mechanism that is based on DMSI is offered in order to effectively manage the operation of the grid-connected VSC. The control of a hybrid system that is based on single-phase PV battery energy storage (BES) is described by the author in [61]. This system includes characteristics that improve power quality and smooth transmission. A single-phase system that is based on PV-BES technology provides uninterrupted power to the nonlinear loads that have been selected, even when the grid is down. This is accomplished by a seamless changeover to islanding. The suggested

synchronized system can be controlled in grid-integrated mode thanks to the current regulation, which is based on learning quantization (LQ) and a PV feed-forward (PVFF) loop.

single-phase & three-phase distribution system have been existed and different type of loads have been connected as per user need [62], [63]. Incorporation of PV to the distribution grid is possible in both the case with the help of single-phase H-bridge VSC and three-phase VSC [64], [65]. Researchers have proposed a novel PWM control technique for PV systems with grid connectivity through a single-phase and a multilevel approach in PV inverter[66], [67]. In literature, we may observe the PV systems being integrated to distribution grid in single-stage [68], [69], [70], [71], [72] and double-stage configuration for PQ improvement along with the capability of active power injection[73]. Design of PV array is most important thing for the solar PV integration for effective power injection [74], [75]. Battery storage system has also been deployed for reducing the intermittency effect of solar PV and power backup under power failure [76], [77]. In [78], the authors conduct an investigation on the power loss that occurs in grid-connected solar systems that are configured with either a single stage or a dual stage. The loss study reveals that the overall power loss is equivalent to that of a two-stage system, despite the fact that a boost converter stage is not required in a singlestage solar system that is linked to the grid. When the amount of power produced exceeds the requirements of the load, the installation of solar systems makes it easier to inject active electricity into the grid. A direct current to direct current converter is utilized in the two-stage system, although it is not present in the single-stage configuration. According to the findings of the research, MPPT strategies are utilized in both of the above instances. Literature suggests the use of both single-stage topologies [79], [80] and two-stage topologies to be employed to create the operating cycle of the DC-DC converter [81], [82]. The technique based on power tracking MPPT is employed for regulating the DC-link voltage at its apex in both of these setups.

## 2.5 Literature Survey on Synchronization and Control Algorithm

The calculation of synchronizing signals and the extraction of essential components from the distorted load current are both required by control algorithms. The unit template technique is the simplest way for producing the synchronizing signal; nevertheless, it is only effective in

the ideal condition of a system that is isolated from other systems[83], [84]. However, if the isolated system has multiple PQ difficulties, such as noise and DC-offset, it is essential to have novel and enhanced techniques for estimating synchronizing signals. Furthermore, researchers have developed many PLL approaches, some of which do not perform well under non-ideal or intermittent situations. Researchers in an attempt to produce a synchronizing signal have been found to employ the SRF-PLL as a typical PLL for frequency and phase computation[85]. Similarly, it is observed that the EPLL is capable of reducing dualfrequency oscillations and mitigating harmonics [86]. The ROGI-PLL technique is frequently employed in standalone systems for synchronization because of its simplicity and efficacy [87]. The ROGI-PLL's performance is shown to be unsatisfactory under unbalanced load and DC-offset conditions. ROGI-FLL has been employed for effective ROGI operation under variable frequency conditions [88]. Whereas the FLL block is utilized to assess the frequency of the input signal. Regrettably, ROGI-FLL's inadequate filtering capacity renders it insufficient when the grid voltage exhibits a DC-offset. An approach known as CC-ROGI-FLL has been proposed to reduce the DC-offset in grid voltage[89]. Under situations of steady-state on a grid that has been extensively distorted, the frequency that is detected by the FLL displays variable degrees of oscillation depending on the situation. In a three-phase system, a PLL based on the CDSC has been examined. This necessitates the use of transform equations as well as an extra Proportional Integral (PI) controller [90]. Under intermittent RESs and distorted load current, a robust frequency estimate technique has been presented[91]. Furthermore, an Affine Projection Like (APL) approach for estimating synchronizing signals in isolated microgrid has been proposed [92]. These techniques were used under variations in frequency and distorted conditions, but the DC-offset condition was not covered. Except under DC-offset conditions, these algorithms produce the minimum steady-state error in the computation of frequency. In recent years, the use of Artificial Neural Networks (ANN) for predicting power system characteristics has acquired significant popularity and has been utilized in several applications, including phase detection, symmetric component analysis, and harmonic identification[93], [94]. Particle Swarm Optimization [95] and recurrent training of neurons for proper weight estimation[96] were two of the earliest ANN approaches. Furthermore, if real-time implementation algorithms based on ANN methodologies are to replace conventional PLLs, they must be quick, precise, and converge

within a few cycles. By using the per-phase model and the multi-loop control system, the four-leg converter can effectively handle unbalanced load conditions and provide better orthogonal signals. This improves the converter's performance, enhances the quality of the output power, and ensures reliable operation in practical applications. By removing the requirement to deal with symmetrical components, the suggested control technique can deliver balanced output voltages under varying load demands[97].

The PQ enhancement technique necessitates the use of proper control algorithms. In the literature a wide range of control algorithms, such as IRPT [98]-[100], SRFT [101], [102], LMS [103], TOGI [104] and MLMS [105], [106] have been used for the grid-connected PV architecture. The control approach is designed in a specific manner to estimate the basic component. The unpredictable and non-linear nature of load current, however, necessitates that the developed algorithms produce accurate and timely results under all circumstances. Although several methods have been developed for shunt compensation, it is still required to carefully examine changes in convergence time, mathematical level of complexity, quick dynamic response with fewer oscillations, and steady-state response. The most efficient method to develop a control algorithm for improving PQ in grid-connected PV system, according to recent literature on FLL-based control techniques, is to use a filter that is both effective and efficient[107], [108]. Various PLL variants have been reported in the literature [109]-[111] as well as recent advances in the study of PLLs [112]. ROGIs were developed[113] and are thought to be less difficult than SOGIs, however, they require a fundamental component from the load current. The authors in [114] has successfully showcased that with the help of a spline-based controller as a phase-locked loop the power quality of the three-phase and three-wire power distribution can be improved. The evaluation and mitigation of harmonics in an autonomous system are achieved by control strategies based on FLL in the scholarly articles. EPLL-based algorithms have also been described in the literature for various applications [115], and they can also be employed as SAPF control algorithms.

Much research and development in recent years has concentrated on improving the gridconnected solar scheme's PQ with relation to harmonics and DC-offset. Numerous investigations into the origins and effects of interharmonics have highlighted the need for effective reduction techniques. Furthermore, transformer saturation and increased losses are caused by direct current offset in solar systems. The academic community has expressed interest in determining and getting rid of DC-offset. Various methodologies have been explored and executed to address DC-offset and harmonics, including phase-locked loop (PLL) [3], grid synchronization, variable gain controller enhanced PLL (VGC-IPLL) [117], all-pass filter with PLL [118], synchronous reference frame PLL (SRF-PLL) [116], second-order generalized integrator (SOGI) [119]. The SRF-PLL can effectively provide an accurate estimate and eliminate the undesirable periodic ripple even in the presence of an input signal contaminated with a DC-offset. The study in [116] proposed a novel PLL that employed Extended SOGI.

A novel type of PLL is introduced in [116], utilizing the Extended SOGI, which is guided by an APF. Furthermore, research reveals that ESOGI-PLL can operate successfully even when there are substantial DC-offset values and enhanced low-order harmonic frequencies present. Furthermore, because of its straightforward architecture, the ESOGI-PLL that was presented in this research might be simply implemented on a microcontroller that is not exceptionally expensive.

The research work in [120] specifies that the SOGI-PLL possesses a significant capability for disturbance rejection and demonstrates robust performance. Furthermore, it has a rather rapid transient reaction. A type of filter with comb-like structure that employs an improved PLL based on sliding Goertzel discrete Fourier transform (SGDFT) is presented in [1]. In order to reduce the influence of components of non-fractional frequency, it incorporates the three degrees of freedom that are associated with second-order fractional delay functions. Synchronization is improved by the SGDFT-based PLL, which does this by finding the amplitude, phase angle, and fundamental frequency while maintaining a constant sampling frequency.

A solar system featuring a two-stage and three-phase design, integrated with an Advanced Third Order Generalised Integrator(ATOGI) is proposed in [121], which covers the management of the PQ. The extraction of relevant components is made easier by the application of the ATOGI to distorted grid voltages and non-linear load currents. Traditional SOGI systems have been hampered by factors such as integrator delay and interharmonics, but the solution that has been offered is able to effectively overcome these concerns. The DC-

Offset Estimator component has an exceptional performance in terms of DC-offset rejection characteristics. The study's findings indicate that the control strategy utilising globally linear reduced complexity (WL-RC-QLMS) could enhance the performance of the system with integrated system with three-Phase [122]. This methodology attempts to eliminate the unbalanced load currents resulting from various order harmonic components. The Luenberger observer is generally employed for the stable regulation of voltage at the DC-link, and the overall harmonic distortion quantifies the irregularities in the grid current, assessed by following the IEEE 519 standard against diverse operating conditions. These findings illustrate the effectiveness of the implemented controls.

The paper [123] demonstrates an exemplary implementation of two generalized integrators inside a cascade setup: the SOGI generalized integrator and the ROGI controller. The SOGI-ROGI exhibits several advantageous traits, such as excellent filtering capability, tolerance against phase shift, excellent dynamic response, and limited harmonic distortion. Initiatives to alleviate these problems have concentrated on filtering methodologies, including active power filters and passive filters. Challenges endure despite advancements; for instance, the demand for enhanced detection techniques requires the use of novel technology. The SOGI and ROGI controllers may initiate a cascade connection. These controllers, being applied to remove the distortions in the grid voltage, facilitate the provision of a synchronization signal. Consequently, the study in [124] does an extensive analysis of the impact of employing cascaded generalized integrator (GI) blocks in a single-phase distribution system to enhance power quality. This research focuses on employing several cascaded SOGI blocks to mitigate PQ issues. The study investigates various SOGI blocks up to the tenth order to ascertain the best quantity of cascaded GI blocks. concentrates on a specific phase of grid-interfaced solar PV systems [125]. The suggested multifunctional system additionally enhances power quality in a single-phase system. The submitted work involves a two-step approach. The initial stage of MPPT is accomplished using the boost converter. Step two entails a VSC, which integrates solar energy into the grid while eliminating harmonics and reactive power. A SOGI-FLL based control strategy was presented to regulate VSC.

The study in [126] explored the single-phase SECS in the context of grid grid-connected PV system. The multifunctional SECS proposed in this study enhance common

coupling power quality. Furthermore, Luenberger observer-based control technique has been presented for the regulation of VSC. The Luenberger observer functions as a basic extractor to get the average power component used by the load current. The authors in [127]proposed a technique to adjust the load for a single-phase, two-stage solar PV system linked to the grid. The technique achieves two objectives concurrently: first, it improves the output power of the PV unit, and second, it reduces the power quality concerns, leading to a correction of power factor and harmonic reduction. The objective of creating a straightforward notch filtering control method is to enable the elimination of the PLL's functions from the load current extraction procedure. Again, the authors in [128] introduce a control system based on PEF for an energy conversion system that runs on a single phase. The system regulates reactive power, reduces harmonics, and reinstates a unity total power factor while also providing electricity to the grid. We employ an adjustable DC link voltage scheme to further reduce switching losses. The work focuses on an integrated, three-phase, multi-functional SECS [129]. This study employs a two-stage power circuit layout. The MPPT process begins with the utilization of a boost converter in the early operation phase. In the second stage, a variable speed controller (VSC) with four legs is utilized in order to inject the energy that has been extracted into the distribution system and to enhance the PQ. A four-leg VSC can be regulated using the SOGI-Quadrature approach, which is the way that has been recommended.

Again in [130], a multifunctional device with an architecture of two stages and a three-phase system has been proposed. To manage multifunctional VSCs, which are responsible for supplying active electricity into the grid from solar systems and also function as APFs, an adaptive noise reduction approach is utilized. Similarly, the work in [131] demonstrates the application of an Adaptive Notch Filter (ANF) algorithm in the two-stage PV system. The suggested PV system not only converts direct current from solar PV sources to alternating current for mains use but also mitigates harmonic currents and regulates reactive power. It is grid-connected and possesses other additional beneficial features. The study demonstrates the implementation of an hybrid autonomous diesel and solar PV system utilizing a control mechanism in [132]. The suggested technique not only improves power quality but also considers the PV array's erratic energy generation. A MPPT method is employed in this study to control and optimize the PV array under varying operating circumstances. A control methodology for an S-DSTATCOM (Solar-Distribution Static Compensator) utilizing an

offset reduction SOGI is elucidated in [133]. The suggested approach improves power quality while converting solar PV array electricity to single-phase distribution. The proposed solar PV system employs a singular VSC to perform many functions, including harmonic reduction and MPPT, while consistently maintaining a uniform power factor for grid current.

The work in [134] presents a dual-stage grid-connected 3P4W PV system with a crosscorrelation control approach. This provides electricity to the grid as well as regulates power factor and reduces harmonics. Again, the work in [135] describes a direct current link voltage that is adaptive to the voltage fluctuations in the point of common coupling (PCC) of the gridsupported solar energy conversion system. The study proposes a two-stage system, of which the initial stage consists of a boost converter, whilst the subsequent phase entails a gridconnected VSC. The VSC regulates transfers energy from solar PV panels to the three-phase distribution system, and mitigates reactive power and harmonics. A dual-frequency control approach utilizing SOGI is presented for this multifunctional VSC. Despite abrupt fluctuations in load at the PCC, this VSC exhibits robust steady-state performance and a rapid dynamic response. In [136], the authors introduce an enhanced PLL control methodology for two-stage PV system capable of power generation in grids. It also reduces PQ issues in a 3P4W distribution system when solar intensity fluctuates. The suggested enhanced EPLLbased synchronization system is applied to fulfil grid needs, including power quality enhancement, distortion-free signals under fluctuating solar intensity, and load balancing. Again in [137], the work presents a lattice wave digital filter (LWDF) regulated PV system. This multifunctional PV system can rectify nonlinear loads at the common coupling point, utilizing variable PV insolation. The grid-tied VSC can be regulated by an LWDF-based approach. This approach is capable of evaluating the reference current of the grid by identifying the basic components of a sinusoidal. Furthermore, a two-stage solar PV system based on SOGI algorithm has been proposed in [138]. The suggested architecture encompasses power factor correction, harmonic reduction, load balancing, and grid integration of PV energy. A bifurcated methodology is suggested to resolve this problem. A DC-DC boost converter is applied at the first stage. This stage tracks the maximum power point by adjusting the duty ratio. SOGI regulates the VSC and estimates the significant active components of the load currents along.

A PV battery energy storage for a microgrid, which is grid-synchronized for household application, is proposed by the authors in [139]. The primary aim of the proposed microgrid is to provide a completely autonomous power management system. The SNE algorithm is augmented with a PV feed-forward component to improve the dynamic performance of the PV-BES-based microgrid. The study in [140] looks at how to handle a single-stage as well as the 3P3W solar-grid interfaced system using a dual DSOGI-PLL when there is irregular grid voltage. The methodology also takes care of the imbalanced load and the variation of solar insolation. The system is controlled by a dual DSOGI-PLL with an inloop filter-based control technique being utilized. For the purpose of estimating sequence components, lowering DC-offset, and lowering harmonics for both voltage and current, the DSOGI with in-loop filter technique is utilized. The filtering capabilities of this algorithm are significantly improved. Using a technique that is based on incremental conductance, the DC link voltage is kept at the Maximum Power Point throughout the process. The work that is presented in [141] is a method to control a DG system that makes use of RES. This technique makes use of proportional resonant (PR) control and Improved Affine Projection Versoria, and it is distinguished by its speed and robustness. Two different modes of operation are available for the system: grid-connected and islanded. In order to improve synchronization performance and provide smooth mode transitions between the island and the grid connection, a modified second-order sequence FLL is implemented. This allows for the estimation of frequency and phase angle to be performed in a quick and accurate manner, even when the grid voltages are distorted and imbalanced. This work details the planning and modeling of a microgrid that employs a PV-hydro system regulated by batteries using a bidirectional converter [142]. The suggested independent microgrid system is economical and dependable, attributed to a 50% decrease in battery capacity. This isolated microgrid derives its power from hydroelectric dams. The suggested system may control electricity generation from renewable resources, including solar panels and hydropower. Nonetheless, the battery storage system controls the load, and the INC-based control mechanism optimizes of power output from the SPV array.

The work [143] provides a description of a microgrid system that utilizes solar PVs and battery energy storage technology. The utilization of a bidirectional DC-DC converter (BDDC) is employed by the PV array in order to maximize its performance. The converter is

responsible for regulating the DC link voltage to the maximum power point (MPP) value. In the event that the solar array stops producing electricity, the BDDC will automatically adjust its settings in order to keep the DC connection at a constant voltage. A RL1-LMSF and an enhanced multi-variable filter-based frequency-locked loop (IMVF-FLL) are the two algorithms that are evaluated in the study that can be found in [144]. The purpose of this study is to demonstrate the effectiveness of these two algorithms by conducting a performance analysis of a three-phase solar-grid interfaced system that makes use of a double-stage topology. The asymmetrical DC-offset, voltage sag/swell, imbalanced loads, imbalanced grid voltages, and fluctuations in solar irradiation are some of the elements that are taken into consideration when determining the efficiency of the system. The solar array is kept at the maximum power point by the utilization of a boost converter in conjunction with an incremental conductance-based approach at all times. The approach under investigation in research [145] is termed the Reweighted Zero Attracting Maximum Correntropy Criterion (RZAMCC). The method is designed to connect with a solar panel system using a three-phase procedure and single-stage architecture. The control approach facilitates the generation of reference grid currents by isolating essential components from distorted load currents. This approach functions exceptionally well in both steady-state and dynamic environments. A solar PV array produces maximum power with the Incremental Conductance method. Again in [146], a control approach to smooth transition between island and grid-connected modes for a distributed PV system is proposed. The suggested Distributed Generation System (DGS) comprises a VSC along with a PV array and a DC-DC boost converter. Moreover, local nonlinear loads and an array of PV cells are also attached to the system. The control strategy utilizes a normalized advanced robust shrinkage technique to reduce the load reactive power harmonics with a unity power factor. A Fast Fourier transform phase-locked loop and a synchronization control (SYC) algorithm are employed for resynchronization and synchronization of the grid. Similarly, the study in [147] proposed a multifunctional VSC for a microgrid architecture that runs on a PV system and a standalone battery management system. The configuration not only optimizes the power output of a solar array but also concurrently minimizes reactive power, which assists a smooth transition between standalone and grid-connected mode. Hence remains immune to grid failure by autonomously transitioning to isolated mode, conforming an uninterrupted supply to the load. The work

in[148] devised, implemented, and verified a unique adaptive algorithm using hardware to improve the practical dependability and functionality of distributed generating systems. The suggested AMLMS management algorithm for off-grid VSC systems effectively alleviates power disturbances while preserving power quality. To enhance the simplicity of the LMS, the VSC control methodology modifies the circuitry's coefficients and incorporates multipliers into the finite impulse response (FIR) filter.

A robust conceptual foundation for the development of a grid-connected system has been proposed in [149]. The study outlines contemporary synchronization techniques for both single and three-phase systems. One of the conventional methods of grid synchronisation is the PLL, which must withstand oscillations in the power supply since its vulnerability affects the generated reference signal. The review study compares several PLL algorithms based on their advantages and disadvantages and focuses on the design of PV supplied grid synchronization's power stages. Researchers working in the field of PV-fed grids will find this publication to be their one-stop resource. This paper[150] demonstrates how, because of their sluggish dynamic performance, DC-offset rejection techniques based on in-loop filtering have gotten less attention in the literature. Thus, as an alternative to DC-Offset rejection, this research suggests in-loop PLL filtering. Results from simulations and experiments verify the usefulness of the suggested PLL. In[151], a single-phase PLL is presented to reduce the impact of certain non-idealities. This PLL is built around the widely used structure of the SOGI. The impacts of input DC-offsets are removed by modifying the SOGI structure. Highpass filtering is a feature of the final SOGI structure. The high-pass generalized integratorbased PLL (HGI-PLL) is the name given to this PLL as a result of the SOGI-based PLLs with DC-cancelling capabilities, it is demonstrated that the HGI-PLL has the lowest resource utilization. Through the use of systematic design techniques, a design that, for given non-ideal input circumstances (frequency deviation and harmonic distortion), keeps the unit vector THD within 1% has been created. The proposed controller in [152] is a cascade of a second-order integrator-based frequency-locked loop and a pre-filter called CESOGI-FLL-WPF. The proposed approach utilizes the existing solar PV power to meet the power requirement of local loads. The excess electricity from the solar PV is then returned to the grid after fulfilling the requirements of the local load. In certain instances, the CESOGI-FLL-WPF controller may segregate important components from nonlinear load currents, enhancing harmonic

compensation and the overall dynamic response time and stability of the system. To regulate a unified PQ conditioner (UPQC) system that integrates solar PV arrays, the researchers in the study [153] devised a modified generalized integrator UPQC-solar PV system capable of eliminating DC-offsets. To create reference currents for the shunt active filter of the UPQC-solar PV system, this approach initially separates the essential component of the load current. This control algorithm enhances PQ by mitigating voltage swell and sag in the grid, balancing grid currents, eliminating harmonics, and compensating reactive power.

The estimation of grid voltage synchronizing signals and the estimation of the load component from the load current are prerequisites for control algorithms that are used in shunt compensation. The unit template approach is the most straightforward for producing the synchronizing signal, but it is only effective under optimal grid voltage scenarios[115]. However, the advanced techniques are needed to estimate synchronization signals under the grid voltage with DC-offset and distortion. Additionally, researchers have put forth a variety of PLL approaches, some of which perform poorly in non-ideal grid scenarios. In order to generate synchronizing signals, researchers have utilized SRF-PLL, a standard PLL, for phase and frequency estimation[154], [155], [156]. Double-frequency oscillations can be eliminated with EPLL[157], [158], [159]. Because of its ease of use and efficiency in grid synchronisation, the SOGI-PLL algorithm is frequently utilized [160]. When there are significant grid distortions and DC-offset situations, the SOGI-PLL performance is shown to be inadequate. The successful operation of SOGI in the event of variable frequency conditions has been proposed by SOGI-FLL[161], [162]. To determine the input signal frequency, the FLL block is implemented. However, the filtering performance of SOGI-FLL is limited and fails to yield satisfactory results when the voltage of the grid undergoes a DC-offset. Consequently, the studies in [163], [164] proposed an advanced SOGI-FLL method to deal with such offsets in grid voltage. Additionally, it is noted that, in a severely distorted grid, the frequency calculated by the FLL exhibits oscillations to variable degrees in a steady-state scenario. Again, in studies [165], [166] three-phase system using a PLL called CDSC(Cascaded Delayed Signal Cancellation Operator) has been proposed. This method was not designed to estimate synchronizing signals, and to tackle this issue, the authors in [167] developed a robust frequency estimation approach. Moreover, they proposed a three-phase grid synchronizing signal estimation approach, which is primarily guided by the Three Consecutive Sampling (3CS) system. These methods have been primarily designed to operate under the distorted and frequency-changing environments, which shall yield no steady state error for frequency estimation, with the exception of DC-offset scenarios.

The application of ANN in the estimation of power system parameters, such as the detection of phase and symmetrical components, harmonics, etc can also be observed[168]. Some of the earliest ANN techniques employed back-propagation techniques and repeated training of neurons for correct weight estimation [169]. Offline training techniques have found better alternatives in the form of online and supervised training algorithms. Moreover, real-time implementation algorithms designed based on ANN techniques should be fast, accurate, and converge approximately within a few cycles if it has to replace the conventional PLL. Within the scope of the research presented in [170], an expanded Adaline technique is investigated in terms of its creation, modelling, simulation, and implementation. This approach was initially applied for grid synchronization and was then extended for load adjustment. Adaline is made up of a single neuron that is designed to accept stimulation from different input nodes, train according to appropriate weights, and generate a single output node. Due to the simple architecture of Adaline-based PLL, it can be employed in the identification of instantaneous changes in frequency, voltage, and phase values.

# 2.6 Literature Survey on Analysis of Interharmonic Component

Power oscillations are caused by voltage disturbances in solar arrays, as was covered in the introductory section. This is especially true when partial shedding is implemented. There are interharmonics in these power fluctuations. Over the years, methods for controlling MPPT have been proposed to maximise output and improve PQ. Several methods for MPPT in PV power systems have been put forth in the literature[171], [172], [173]. The study in [171] proposes a hybrid MPPT control strategy, the technique utilizes an improved perturb along particle swarm optimizer and an observation algorithm. Again, the work in [172], a modified fuzzy logic MPPT control algorithm is presented and tested over simulation and a hardware environment.

The extensive use of heuristics can also be observed in the literature, such as the MPPT method discussed in [7] which is built on an application-adaptable ANN model immune to system parameter variance. Most of these methods are model-dependent and

intended to control different PV systems; nevertheless, they are unable to forecast the interharmonics properties. These harmonic issues with PV panels in different configurations may be resolved by obtaining an accurate model for PV systems and the characteristics that go along with it. It forces the author to look for an approach that is not dependent on any one paradigm.

The article [174] outlines the qualities of a suitable technique for analyzing and estimating interharmonics in PV systems and makes a connection between these qualities and the elements of the techniques that have been studied. Thus, the peculiarities of interharmonic emissions associated with PV systems are given. The different approaches are categorized, condensed, and a checklist is created to highlight the points that need to be considered when choosing an appropriate approach for the analysis of a PV system with inner harmonics. In[175], the author looks into the process underlying inter-harmonic emission by testing an industrial PV inverter. Several factors may influence the interharmonics in the grid current, including perturbations to the MPPT algorithm. These sources are most evident while running at low power. This leads to the discussion of three mitigation strategies to deal with the problem; the efficacy of the strategies is confirmed through simulations. In [176], the author examines the characteristics and mechanisms that result in interharmonics in PV systems. According to the findings of the investigation, the disruption that is caused by the MPPT algorithm is one of the factors that contribute to a grid current of PV system with inner harmonics. As a result, the inter-harmonic features are affected by the parameters of the MPPT controller, which include the sampling rate and the perturbation step size. Hence, the study proposed a model that is capable of predicting interharmonics by applying the frequencies and amplitudes of the controller parameters that have been selected. In [177], the author suggests a unique way to reduce interharmonics in PV systems using the P&O MPPT algorithm. This is accomplished by using a fuzzy-based controller to manage the MPPT parameters while taking the real-time irradiance value and the frequency components in the PV output into consideration.

## 2.7 Identified Research Gap

1) To have an enhanced power quality in grid-connected PV systems, it is necessary to have an advanced control technique. Modifications to several sophisticated approaches

- I have explored for shunt compensators necessitate comprehensive analysis and inquiry.
- 2) A variety of PLL-based circuits are documented in the literature. Additional PLLs for the management of grid-connected PV systems, utilized for synchronization, are required to be efficient and rapid.
- 3) For grid-connected PV systems, rapid and effective synchronization approaches utilizing various types of adaptive filters are essential.
- 4) Advanced control techniques for different loading conditions are required, and a comparison of these is also required based on simulation studies.

### 2.8 Authors Contribution in the Proposed Work

The primary contributions in the thesis can be summarized as:

- The design of single-phase and three-phase grid-based Solar-PV systems has been done in this study. Moreover, the study provides an extensive analysis of the designed systems.
- 2) The study implements a diverse range of algorithms for the synchronization of the proposed system under different operating conditions, like fluctuating solar intensity, while accommodating the dynamics of coupled unbalanced non-linear loads.
- 3) Development and implementation of methods for MPPT such as EDRL and P&O to optimize power extraction from solar PV systems under dynamic situations and to reduce interharmonics.
- 4) The developed control algorithms enhance system stability, reduce the steady-state error, and provide a faster dynamic response during the extraction of the fundamental load current component.
- 5) Additionally, the algorithms utilizing VSC to regulate all parameters of the proposed system facilitate the harmonics mitigation, elimination of DC-offset, load leveling, power compensation, and improve the quality of the proposed system.
- 6) A State-of-the-art analysis of the methodologies has been done under different operating circumstances has been taken into consideration. The work regards the IEEE-519 standard norms of harmonics level and keeps the THD level below 5% under nonlinear load.

### 2.9 Objectives of the Proposed Research Work

The proposed research work shall mainly focus on the following aspects of the gridconnected PV system.

- 1. Designing and performance evaluation of grid-connected PV system.
- Developing novel synchronization methods for a grid-connected PV system under DC-offset situations and analyzing their performance.
- 3. New techniques for varying irradiance and partial shading conditions, and mathematical stability analysis for stable operation of the synchronization technique under various grid voltage conditions.
- 4. Analysis of interharmonic component and its mitigation.

# 2.10 Summary

This chapter presents a comprehensive literature review of PV modelling, MPPT approaches, synchronization methods, control algorithms, interharmonic reduction, and power management for single as well as three-phase grid-connected PV systems. Through the literature evaluation and the rationale for the use of PV technology, research gaps and objectives have been delineated.

# **CHAPTER 3**

# DESIGN AND DEVELOPMENT OF SINGLE AND THREE-PHASE GRID-CONNECTED SOLAR PV SYSTEM

### 3.1 General

This chapter addresses the development and design of single-phase and three-phase solar PV system. Comprehensive mathematical computations of the design parameters for diverse system components have been executed for simulation objectives. It encompasses the design and modeling of the PV, together with the design proposed system. The design of the system's components for the simulation research is offered in compliance with the requisite requirements.

# 3.2 Design and Development of Single-Phase Grid-Connected Solar PV System

Figure 3.1 illustrates the proposed grid-connected solar PV system operating on a single phase. The system's power circuit has three main components: the SECS, the loads at the PCC, and the single-phase grid. The SECS power circuit comprises a boost converter, a ripple filter, an interacting inductor, and a single-phase VSC. The boost converter serves as the primary stage, whilst the variable speed controller functions as the secondary stage. Linking the PV array to the input of the boost converter enables the MPPT implementation. The output of the boost converter is then connected to the DC input of the VSC. The PV electricity is integrated into the grid, enhancing the power quality of the 1-φ distribution network at the second step of the voltage source converter. A single-phase bridge voltage source converter is utilized in the proposed project. The VSC comprises two legs of Insulated Gate Bipolar Transistor (IGBT) circuits, amounting to four IGBTs in total. A single-phase grid is linked to

the voltage source converter via an interacting inductor. A ripple filter is installed at CPI to further decrease voltage switching waves. The controller that regulates the SECS consists of a signal conditioning unit and sensors. Interpreting and processing the available instantaneous signals in a certain manner generates switching pulses for the VSC.

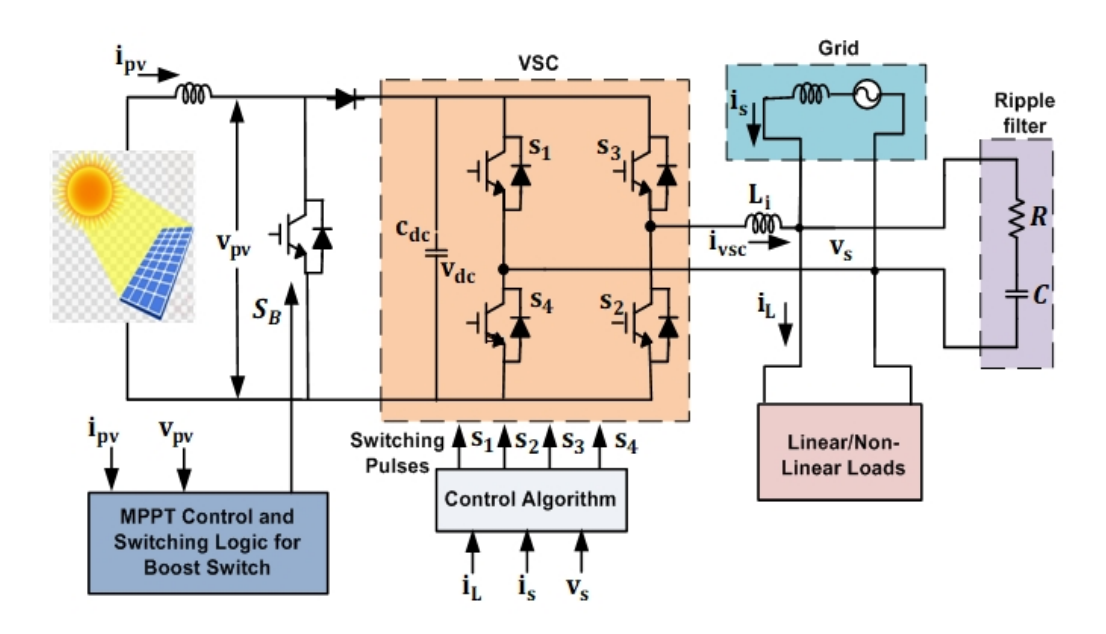


Fig. 3.1 Configuration of a single-phase solar PV system linked to the grid

The subsequent discussion pertains to the design of all components of a single-phase grid, both with and without PV systems. Design of the following quantities is considered:

- 1. Design of PV system
- 2. DC-link reference voltage
- 3. DC-link capacitance
- 4. Interfacing inductor
- 5. DC-DC boost converter

### 3.2.1 Design of PV System

### 3.2.1.1 PV Module Design

Various parameters can be considered while modeling a solar cell. According to [178], a more realistic and manageable model would be a single-diode circuit with series and parallel resistance. Figure 3.2 shows a one-diode model with series and shunt resistance that is suitable for practical applications.

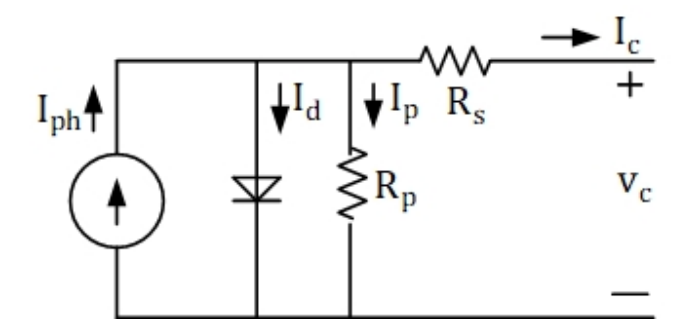


Fig.3.2 Practical PV cell model based on a single diode[179]

With the help of Kirchhoff's current law, the output current (I<sub>c</sub>) of the PV cell is estimated as

$$I_{c} = I_{ph} - I_{d} - I_{p} \tag{3.1}$$

$$I_{c} = I_{ph} - I_{o} \left[ exp \left( \frac{V_{c} + I_{Ra}}{\alpha} \right) - 1 \right] - \frac{V_{c} + IR_{s}}{R_{p}}$$
(3.2)

Where,  $(I_{ph})$ ,  $(I_{d})$ ,  $(I_{p})$  and  $(\alpha)$  is the diode current, photon current, leakage current and modified ideality factor in the parallel resistor [180]. Equation for  $\alpha$  is given as

$$\alpha = \frac{N_s AkT_c}{a} \tag{3.3}$$

Where, k = Boltzmann's constant  $(1.381 \times 10^{-23} \, \text{m}^2 \text{kg} - \text{s}^{-2} \text{k}^{-1})$ ,  $N_s = \text{number of series}$  cells in PV panel, A is the ideality factor, and  $q = \text{electron charge} \ (1.6 \times 10^{-19} \, \text{coulombs})$ . The ideality factor of different PV technologies has different values, and is shown in Table 3.1. Here, the value of the ideality factor (IF) is 1.3 as the considered module is silicon polycrystalline.

The photo current  $(I_{ph})$  is affected by the two variables, solar insolation and temperature  $(T_c)$ , as shown in the equation below.

Table 3.1: Ideality factor (A)

Technology	Si-Mono	Si-ploy	a-Si-H	a-si-H triple	CdTe	AsGa	a-Si-H tandem
IF	1.2	1.3	1.8	1.5	1.5	1.3	3.3

$$I_{ph} = \frac{G}{G_{ref}} (I_{phref} + \mu_{sc} \Delta T)$$
 (3.4)

Ideally,  $I_{phref} \approx I_{scref}$  and  $\Delta T = T_c - T_{cref}$ . Here,  $T_{cref}$  is the PV cell temperature at 298K,  $G_{ref}$  denotes the solar insolation at standard test conditions (STC=1000 $\omega/m^2$ ). The short-circuit current temperature is denoted as  $\mu_{sc}$  and is given by the manufacturer. The short-circuit current and photon current at STC are denoted as  $I_{scref}$  and  $I_{phref}$  respectively, whereas the diode current ( $I_d$ ) of the PV can be defined as

$$I_{d} = I_{o} \left[ exp \left( \frac{V_{c} + IR_{s}}{\alpha} \right) - 1 \right]$$
 (3.5)

Again, the reverse saturation current of a diode is defined as

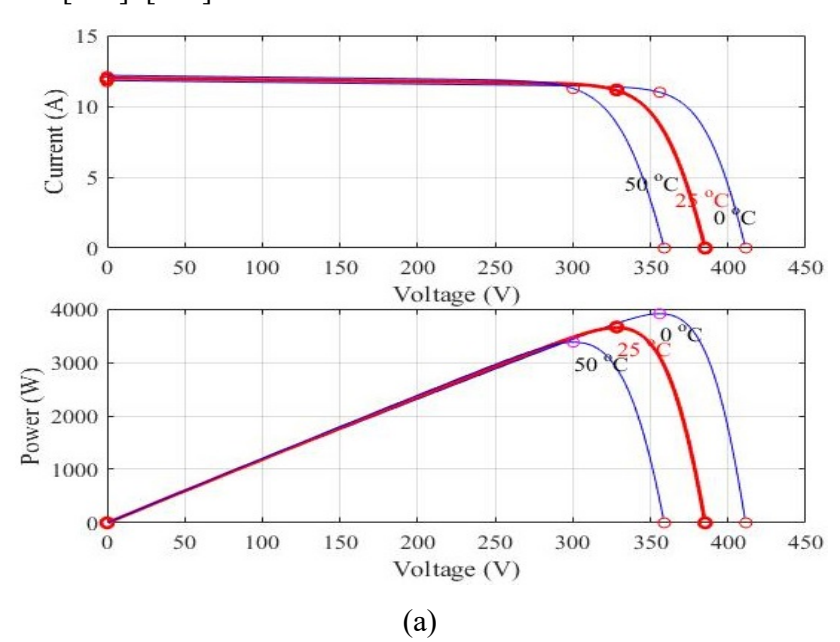
$$I_{o} = \frac{I_{\text{scref}}}{\exp \frac{V_{\text{ocref}}}{\alpha} - 1} \left(\frac{T_{c}}{T_{\text{cref}}}\right)^{3} \exp \left[\left(\frac{q \epsilon_{g}}{A k}\right) \left(\frac{1}{T_{\text{cref}}} - \frac{1}{T_{c}}\right)\right]$$
(3.6)

The open circuit voltage is represented as  $V_{ocref}$  of the PV and for silicon-based solar cells it can be defined as the energy band gap of 1.12ev. A single PV module produces a negligible amount of power. Consequently, in order to extract significant power, a PV string or array is required, composed of several modules interconnected in parallel ( $N_{pp}$ ) and series ( $N_{ss}$ ). Therefore, derived from the initial equation for PV cells, the following equation depicts a PV cell array. The PV array's new output current and voltage are now known as  $I_{photovoltaic}$  and  $V_{photovoltaic}$ , respectively.

$$I_{photovoltaic} = N_{pp}I_{ph} - I_{o} \left[ exp \left( \frac{V_{photovoltaic} + IR_{s} \left( \frac{N_{ss}}{N_{pp}} \right)}{\alpha} \right) - 1 \right] - \frac{V_{photovoltaic} + IR_{s} \left( \frac{N_{ss}}{N_{pp}} \right)}{R_{p} \left( \frac{N_{ss}}{N_{pp}} \right)}$$

$$(3.7)$$

The output current and voltage vary in line with the P-V and I-V curves based on environmental conditions. Figure 3.3(a) presents the I-V and P-V curves of an array at various temperatures (0°C, 25°C, and 50°C) under a constant solar insolation of 1000 W/m². We observe that as the temperature of the PV module decreases, both the output power and current increase. This graph illustrates the non-linear response of PV modules to variations in ambient conditions. The maximum power point is identified within these curves, and the peak output power of the PV module is observed. Figure 3.3(b) presents the P-V as well as I-V curves of a module under different solar insolation values of 200 W/m², 450 W/m², and 900 W/m² at a constant temperature of 25°C. From Figure 3.3 (b), it is observed that an increase in temperature led to an increase in both the power output and the output current of the solar system. Maximum Power Point Tracking, often known as MPPT, is utilized in order to achieve the best possible performance from the PV module, string, or array. A single-stage grid-connected PV system is able to create the voltage of DC-link through the use of the Maximum Power PT. In a two-stage grid-connected system, the module is required to function at MPPT [181]–[183].



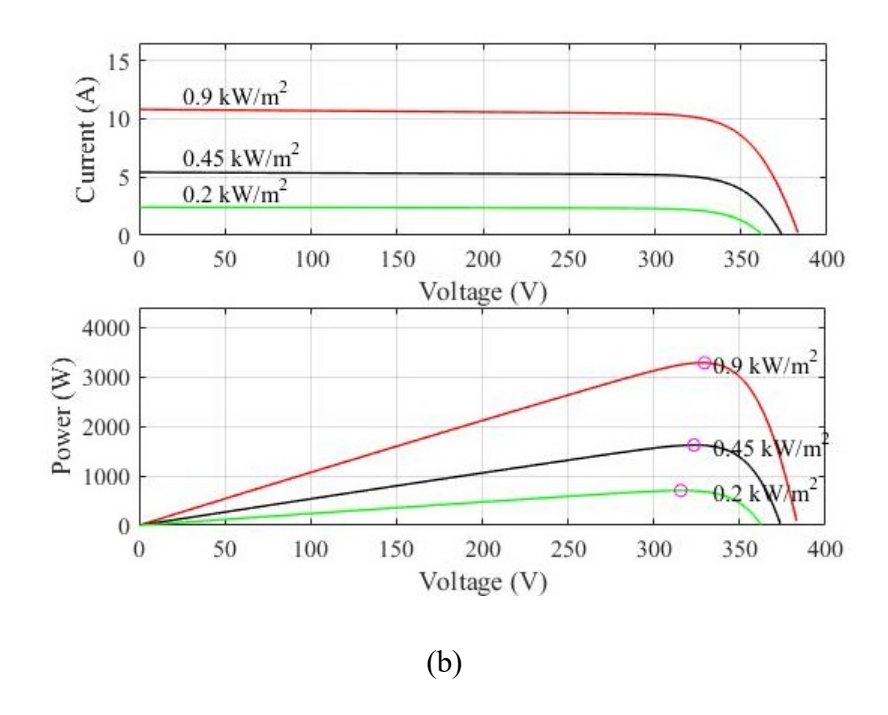


Fig. 3.3 I-V and P-V curve (a) at fixed solar insolation and different temperatures (b) I-V and P-V curve at fixed temperature and different solar insolation

### 3.2.1.2 Design of PV Array

The amount of power produced by an individual PV module is rather small. Depending on the specifications of current and voltage parameters, several PV modules can be interconnected in series or parallel to accommodate heightened power requirements. A PV array comprises a set of strings connected in parallel, whereas a PV string is constituted of modules linked in series. To augment the voltage, connect PV modules in series; to enhance the current, link them in parallel.

An essential part of single-stage PV system is the DC-DC converter. The minimum DC-link voltage ( $V_{dem}$ ) must be maintained above the output of the PV array and the reference DC-link value produced by the MPPT technique under all conditions. The minimum number of series-connected PV modules required can be calculated by equation 3.8.

$$N_{ss} = \frac{V_{dcm}}{V_{mp}} = \frac{325.22}{34.7} = 9.3 \tag{3.8}$$

Consequently, for the single-phase, single-stage grid-connected PV system, twelve modules have been assessed and connected in series. Table 3.2 presents its parameters.

Table 3.2: PV string parameters at STC for a single-stage grid-connected PV system

Parameters	Rating
No. of series modules	12
No. of parallel strings	1
Maximum Power $(P_{mp})$	3247.92 W
Open-circuit voltage $(V_{oc})$	528 V
Short-circuit current $(I_{sc})$	8.1 A
Voltage at maximum power point $(V_{mp})$	416.4 V
Current at maximum power point $(I_{mp})$	7.8 A

In a double-stage grid-connected solar system, the PV system's output is connected to the DC-link of the voltage source converter. This association is subsequently referenced in Table 3.2. These metrics were assessed under standard testing conditions. The idea to employ a boost converter arose from its ability to elevate voltage, along with its straightforward design and minimal component requirements. The limitation on the number of solar modules that may be connected in series has led to the preference for the double-stage system. The MPPT method utilizes the duty cycle input from the DC-DC boost converter as the output. Approximately fifty percent of that figure is the typical operating duty cycle for a DC-DC boost converter.

$$N_{ss} = \frac{V_{dcm}}{V_{mn}} \times 0.5 = \frac{325.22}{34.7} \times 0.5 = 4.65$$
 (3.9)

A duty cycle of around 0.5 for the boost converter is attained by connecting five modules in series inside this specific single-phase double-stage grid-connected solar system. To augment the power capacity, two parallel strings are employed, each including five modules. The attributes are delineated in Table 3.3.

Table 3.3: PV string parameters at STC for double-stage grid-connected PV system

Parameters	Rating
No. of series modules	5
No. of parallel strings	2
Total no. of PV modules	10
Maximum Power $(P_{mp})$	2706.6 W
Open-circuit voltage ( $V_{oc}$ )	220 V
Short-circuit current $(I_{sc})$	16.2 A
Voltage at maximum power point $(V_{mp})$	173.5 V
Current at maximum power point $(I_{mp})$	15.6 A

### 3.2.2 Calculation of DC-link Reference Voltage

Considering the voltage of the DC connection facilitates the injection of reactive power into the grid. Consequently, the voltage delivered to the grid must exceed the voltage provided to the DC link of a single-phase voltage source converter. The grid voltage magnitude may be determined using equation 3.10.

$$A_v = \sqrt{2}v_g \tag{3.10}$$

In this instance,  $v_g$  represents the grid voltage, while  $A_v$  denotes its magnitude. For simulation research, the advised supply voltage is 230V at 50Hz, whereas for actual implementation, it is 110V at 50Hz. Throughout the simulation, the DC connection reference voltage consider is

$$V_{dcref} > V_{dcm} = \sqrt{2}v_g = \sqrt{2} \times 230 = 325.27V$$
 (3.11)

The minimum DC-link voltage is shown as  $V_{\text{dcm}}$ . This indicates that 400V serves as the reference DC-link voltage.

### 3.2.3 DC-link Capacitor Design

The input grid voltage and load current significantly influence the DC-link voltage of the VSC. To sustain the voltage of the DC-link under dynamic conditions, the capacitance value must be adequately high. Equation 3.12 may be utilized to ascertain the capacitance of the DC connection.

$$C_{dc} = \frac{v_g h i_c \tau g}{\frac{1}{2} \left( V_{dcref}^2 - V_{dcm}^2 \right)} \tag{3.12}$$

The overloading factor is represented by h, and its value is considered as 1.2, the compensator or VSC current  $i_c$  25A, the gain constant g value is 0.3, the reference DC-link voltage is  $V_{dcref}$  value considered as 400V, and the minimum DC-link voltage is  $V_{dcm}$  has a value of 375.27V. The time constant is  $\tau = 0.02$  s, and g remains constant. Upon substituting these values into 3.12, the result is

$$C_{dc} = \frac{v_g h i_c \tau g}{\frac{1}{2} \left( v_{dcref}^2 - v_{dcm}^2 \right)} = 1527.6 \mu F \tag{3.13}$$

The simulation has been configured with an increased DC-link capacitor value,  $C_{dc} = 2000 \, \mu F$ .

### 3.2.4 Design of Interfacing Inductor

Current ripples can be eradicated by the utilization of an interface inductor. A larger inductor value enhances filtering but concurrently increases power loss. Thus, 3.14 is an essential formula for the accurate design of the filter inductor or interface ( $I_f$ ).

$$L_f = \frac{\sqrt{3}mV_{dcref}}{12hf_s\Delta i} \tag{3.14}$$

Here, mrepresents the modulation index, the DC link reference voltage is represented as  $V_{dcref}$ , the overloading factor is represented as h, switching frequency is represented as  $f_s$  and  $\Delta i$ represents the ripples in the current and is considered 5% of the maximum current. For simulation purposes its value is

$$L_f = \frac{\sqrt{3}mV_{dcref}}{12hf_s\Delta i} = \frac{\sqrt{3}\times1\times200}{12\times1.2\times10\times10^3\times1.5} = 1.6mH$$
 (3.15)

### 3.2.5 Design of DC-DC Boost Converter

A boost converter is employed by a DC-DC converter to elevate the input voltage. After these steps, the parameters of the boost converter have been engineered.

### 1. Duty cycle calculation (D)

$$D = 1 - \frac{V_{pv}}{V_0} \mu_b \tag{3.16}$$

Here,  $V_{pv}$ , D, and  $V_o$  represents input voltage, duty cycle and output input PV voltage respectively, whereas the converted efficiency is defined as  $\mu b$  and the efficiency considered as 95%.

$$D = 1 - \frac{V_{pv}}{V_o} \mu_b = 1 - \frac{173.5}{400} 0.95 \approx 0.6$$
 (3.17)

### 2. Design of inductor $(L_b)$

$$L_b \ge \frac{V_{pv(min)}D}{f_S\Delta I_{pv}} \tag{3.18}$$

Here,  $V_{pv(min)}$  is 173.5V, D = 0.6,  $f_s$  = switching frequency=5kHz and  $\Delta I_{pv}$  is the ripple current and it ranges from to 20% to 40%. Here,  $\Delta I_{pv}$  is considered 30% of PV current.

$$L_b \ge \frac{V_{pv(min)}D}{f_s\Delta I_{pv}} = \frac{173.5 \times 0.6}{5 \times 10^3 \times 0.3 \times 15.6} \approx 4.45 mH$$
 (3.19)

A little higher value of inductor (5.0 mH) is selected.

### 3. Design of output capacitance (C<sub>bo</sub>)

$$C_{bo} = \frac{I_{o(max)}D}{f_{c}\Delta V_{bo}} \tag{3.20}$$

Here,  $I_{o(max)}$  is 15.6 A and  $\Delta V_{bo}$  is 1% to 5% of  $V_{bo}$  and 2% ripple is considered here.

$$C_{bo} = \frac{I_{o(max)}^{D}}{f_s \Delta V_{bo}} = \frac{15.6 \times 0.6}{5 \times 10^3 \times 0.02 \times 400} = 234 \mu F$$
 (3.21)

The output capacitor value selected is  $400 \, \mu F$ .

#### 4. IGBT, Diode and Driver circuit

In simulation, an ideal IGBT and diode has been considered while in experimental setup Semikron make SKM50GAL12T4 (50A, 1200V) has been used. This IGBT switch has been integrated with diode also. PWM technique has been used for generating the pulses for IGBT.

The output of the DSP unit gives 5V signal so a suitable amplifying circuit has been used to amplify the signal to 15V. The IGBT pulses are generated using Semikron make Skyper32 Pro driver.

# 3.3 Design and Development of Three-Phase Grid-Connected Solar PV System

The system has three principal components: PV arrays, the alternating current grid, and PV inverters. PV inverters like the IGBT are essential to regulate the electricity supply to the AC power grid coming from the AC power grid.

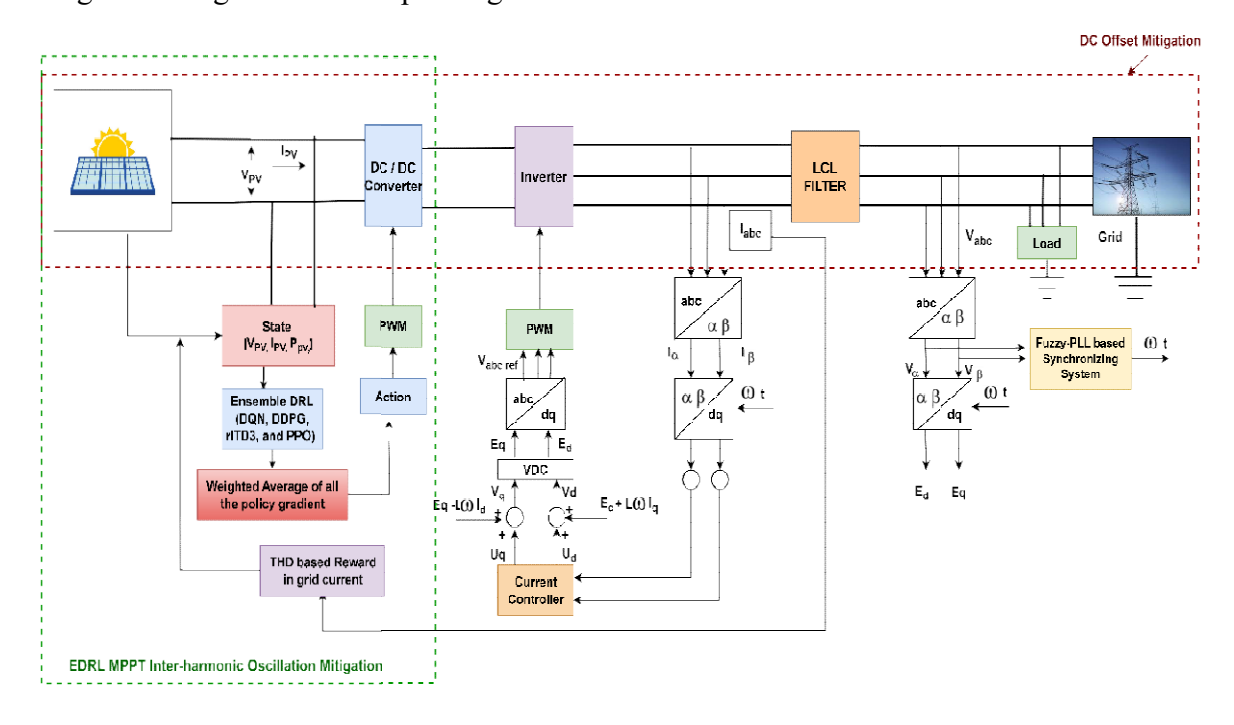


Fig. 3.4 System configuration of three-phase grid-connected PV system

The Ensembled DRL MPP approach utilises a signal of PWM tailored for a converter of boost, leveraging the THD Reward to improve the PV voltage profile while minimising harmonics of inner system components. Arrangements of the control panel are shown in Figure 3.4, demonstrating the standard configuration for three-phase solar-PV inverters connected to the grid. A three-phase converter connects a solar array, boasting a capacity of

250 kW, to a 25 kV electrical grid. A total of 88 threads constitute the solar array. Each string consists of seven Sun Power SPR-415E modules arranged in a series configuration.

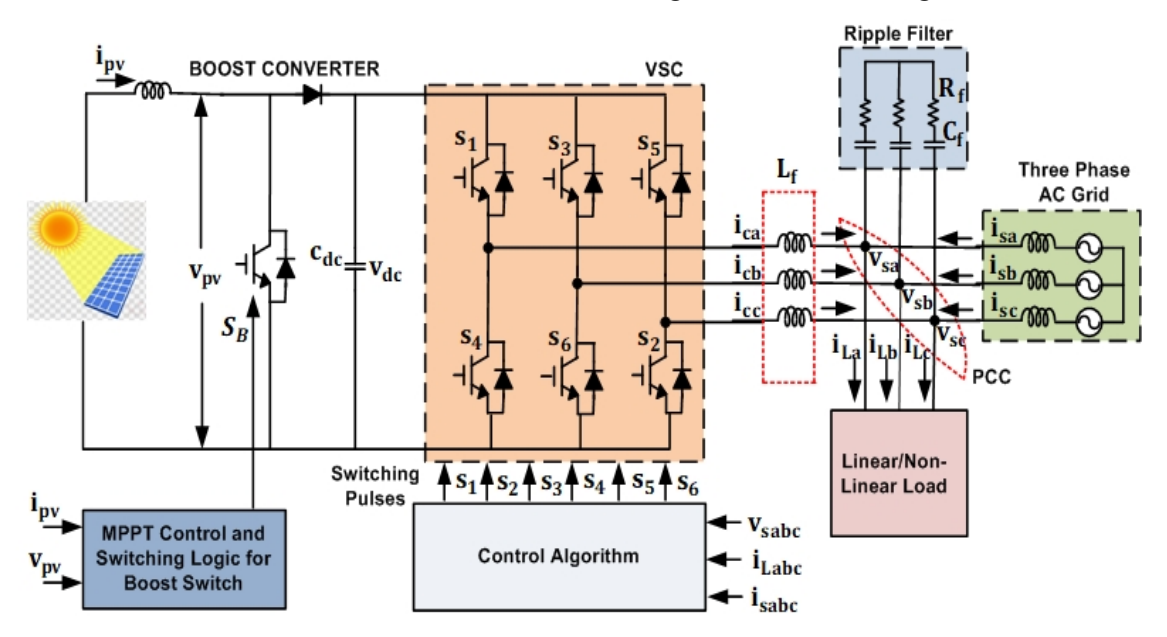


Fig. 3.5 Topology of three-phase grid-connected PV system

Fig. 3.5 presents a visual depiction of the system setup. This utility grid-connected solar PV system illustrates the use of a single stage solar PV array over a two stage system because of its inherent advantages. Local loads are powered by the utility grid, while power conversion and harmonic adjustment are made possible by the solar PV array's VSC connection. The PCC serves as a communication channel between the utility grid, non linear load and PV array. A CC-ROGI-FLL controller, which processes the voltage signal and current to produce VSC switching pulses, is used to accomplish the control. Compensation currents are given for harmonic compensation and power quality enhancement with the proper VSC switching. A first order high pass filter known as the ripple filter is employed in order to eliminate the noise. Additionally, the primary function of interfacing inductors is to lessen current ripples. The MPPT technique that is based on P&O allows solar PV arrays to operate at their highest operational efficiency.

Table 3.4 enumerates the pertinent system parameters. To optimize solar panel efficiency, MPPT is an essential technique. The strategy depends on two fundamental techniques: The

figure illustrates that interharmonics reduction is achieved by an EDRL-based MPPT method, while DC-offset elimination is performed using a COA-fuzzified PLL.

Table 3.4 The parameter setting of PV

Parameters	Values	Standard Units
PV arrays (series connected)	7	-
PV arrays (parallel	88	-
connected)		
Current of single PV array	6.09	A
Voltage of single PV array	85.3	V
Maximum power output	250	K watts
Operating Temperature	45	°C
Irradiation	680-1000	W/m <sup>2</sup>

Solar arrays, PV inverters, and an alternating current (AC) grid are the components that make up the system. When it comes to the management of the power transfer from solar panels to the electrical grid, PV inverters, and more especially the full-bridge inverter IGBT, play an essential role. A pulse width modulation (PWM) signal may be generated for a boost converter using the MPP based on ensemble DRL that uses the THD Reward approach. This results in an improvement in the profile of the voltage of the solar system and a reduction in the component with inner harmonics. The control setup that is usually used for three-phase solar inverters that are connected to the grid is shown in Figure 3.4. Two hundred and eighty parallel threads make up the solar array. Every string is made up of seven Sun Power SPR-415E modules that are installed in a series configuration. A list of the pertinent system parameters may be found in Table 3.4. When it comes to improving the power generation from solar panels, an MPPT algorithm is absolutely necessary.

### 3.3.1 Calculation of DC-link Reference Voltage

Taking into account the voltage of the DC connection allows for the injection of reactive power into the grid. Because of this, the DC-link voltage of a single-phase voltage source converter should not considerably exceed the voltage that is applied to the grid. One method for determining the voltage of the grid is to multiply the voltage by 3.22.

$$A_{v} = \frac{2\sqrt{2}V_{LL}}{\sqrt{3}m} \tag{3.22}$$

Where  $V_{LL}$  is the root-mean-square (RMS) grid voltage (line-to-line), and  $A_v$  is the magnitude of the grid voltage being measured. In this context, the modulation index is denoted by the letter m, and its value is considered as 1. According to the following equation, the DC link reference voltage can be derived by taking into consideration the supply voltage with the parameters of 415V ( $V_{ph}$ ) and a frequency of 50 Hz.

$$V_{dcref} > V_{dcm} = \frac{2\sqrt{2}V_{LL}}{\sqrt{3}m} = \frac{2\sqrt{2}\times415}{\sqrt{3}} = 677.67V$$
 (3.23)

Where,  $V_{dcref}$  and  $V_{dcm}$  are the reference and minimum DC link voltage. The DC reference voltage considered in this study is 800V.

### 3.3.2 Design of DC-link Capacitor

It's important to note that the DC-link voltage of the VSC is highly dependent on the input grid voltage and load current. In order to maintain DC-link voltage when dynamics are underway, the DC-link capacitance value must be sufficiently high. You can figure out the DC-link capacitance by plugging in 3.24.

$$C_{dc} = \frac{6v_{ph}hi_c\tau g}{v_{dcref}^2 - v_{dcm}^2} \tag{3.24}$$

Here,  $i_c$ , g,  $\tau$ ,  $V_{dcm}$ ,  $V_{dcref}$ , have the compensator current, gain constant, time constant, minimum DC link voltage, reference DC-link voltage, and overloading factor, respectively.

### 3.3.3 Design of Interfacing Inductor

It is possible to eliminate current ripples by using an interface inductor. While a greater inductor value improves filtering, it also increases loss. Therefore, the calculation of the filter inductor ( $I_f$ ) by 3.25 is an essential part of appropriate interface design.

$$L_f = \frac{\sqrt{3}mV_{dcref}}{12hf_s\Delta i} \tag{3.25}$$

Where,  $f_s$ , m, h, and  $V_{dcref}$  are the switching frequency, modulation index, overloading factor, and DC-link reference voltage respectively. Whereas, the current ripple at 5% of the maximum current is represented as  $\Delta i$ .

### 3.3.4 Design of PV Array

An electrical grid with twenty five kV connects to a solar array of two thousand and fifty kW via a three-phase converter. The solar array comprises 88 parallel threads. Each string consists of seven Sun Power SPR-415E modules arranged in series.

Table 3.5 The parameter setting of PV

Parameters	Values	Standard Units	
PV arrays (series connected)	7	-	
PV arrays (parallel	88	-	
connected)			
Current of single PV array	6.09	A	
Voltage of single PV array	85.3	V	
Maximum power output	250	K watts	
Operating Temperature	45	°C	
Irradiation	680-1000	$W/m^2$	

### 3.4 Summary

The design and development of grid-connected PV systems, both single-phase and three-phase, have been thoroughly covered in this chapter. There have been presented system configurations and design equations. PV arrays can be linked to single-phase or three-phase grid-connected PV systems in a single-phase or double-stage way. These system configurations will be used to the grid to offer active power injection, reactive power adjustment, and improved PQ in both experimental prototypes and simulations.

# **CHAPTER 4**

# IMPLEMENTATION OF ADVANCE CONTROL ALGORITHMS FOR SINGLE-PHASE GRIDCONNECTED SOLAR PV SYSTEM

### 4.1 General

A precise and accurate estimation of phase & frequency is crucial for the control and synchronization of the Solar-PV system. Hence, use of advanced control algorithms and synchronization techniques is mandatory. Out of several synchronization techniques discussed in literature PLLs and FLLs based synchronization are make popular. Some conventional and advanced control techniques for single-phase PLLs & FLLs are discussed in this chapter for computation of phase, frequency, amplitude and the synchronizing signals under uncertain conditions of PV and unbalanced load. The designed PLLs & FLLs are further applied for the PQ improvement and compensation of reactive power in the proposed system.

Various single-phase control techniques are examined under the intermittent condition of solar and unbalanced load in this chapter. These include 1φ-CBF-FLL, FOGI-FLL and APF-PLL. Their individual simulation results and experimental performances are examined under various operating scenarios.

# 4.2 1φ-CBF-FLL Control Approach

The primary goal of adaptive 1φ-CBF-FLL regulation in an SPV-based energy-producing system is eliminating harmonic currents while maintaining grid current balance under various load scenarios. Furthermore, it has been discovered that this 1φ-CBF-FLL control method rejects DC-offset and provides a good response with minimal steady-state error. Key advantages of the proposed 1φ-CBF-FLL scheme include: (1) rapid convergence behaviour, (2) effective suppression of harmonics and DC-offset components, and (3) ease of implementation.

### 4.2.1 Evaluation of 1φ -CBF-FLL

The asymmetrical frequency response of complex filters, which separates the components of both positive and negative sequences of unbalanced signals from one another, is one of their defining characteristics. This characteristic has led to the widespread use of sophisticated filters in many applications for three-phase signal control and processing, especially in the development of controllers and methods of synchronization for 3- $\phi$  power converters.

In [161], It is proposed to use CBF while developing a  $1\phi$  FLL. This concept is represented by the block layout known as  $1\phi$ -CBF-FLL, which is shown in Fig. 4.1(a). The single-phase signal  $i_L = I\cos(\theta)$  from its input may be seen as an unbalanced signal in  $\alpha\beta$  frame, which is the fundamental concept behind the construction of the  $1\phi$ -CBF-FLL as

$$2i_{L} = I \cos(\theta) + I \cos(-\theta) = i_{L\alpha}$$

$$0 = I \sin(\theta) + I \sin(-\theta) = i_{L\beta}$$
(4.1)

The positive sequence component is subsequently extracted through a CBF to eliminate the negative one. It is important to note that the 1- $\phi$  input may be calculated for phase, frequency, and amplitude using the in-phase and quadrature-phase versions provided by this positive sequence component. Finally, a first-order LPF processes the predicted frequency and feeds it back to the CBF so that it may adjust to variations in the frequency of the grid.

### 4.2.2 Examining 1φ -CBF-FLL

The 1 $\phi$ -CBF-FLL composition allows for any order and many implementation methods for the CBF. In this article, a second-order one is taken into consideration to keep the analysis simple. As seen in Fig. 4.1(b), the fundamental component of this CBF is a ROGI, which is represented in the Laplace domain as  $G_{ROGI}(s) = \frac{1}{s-i\omega}$ .

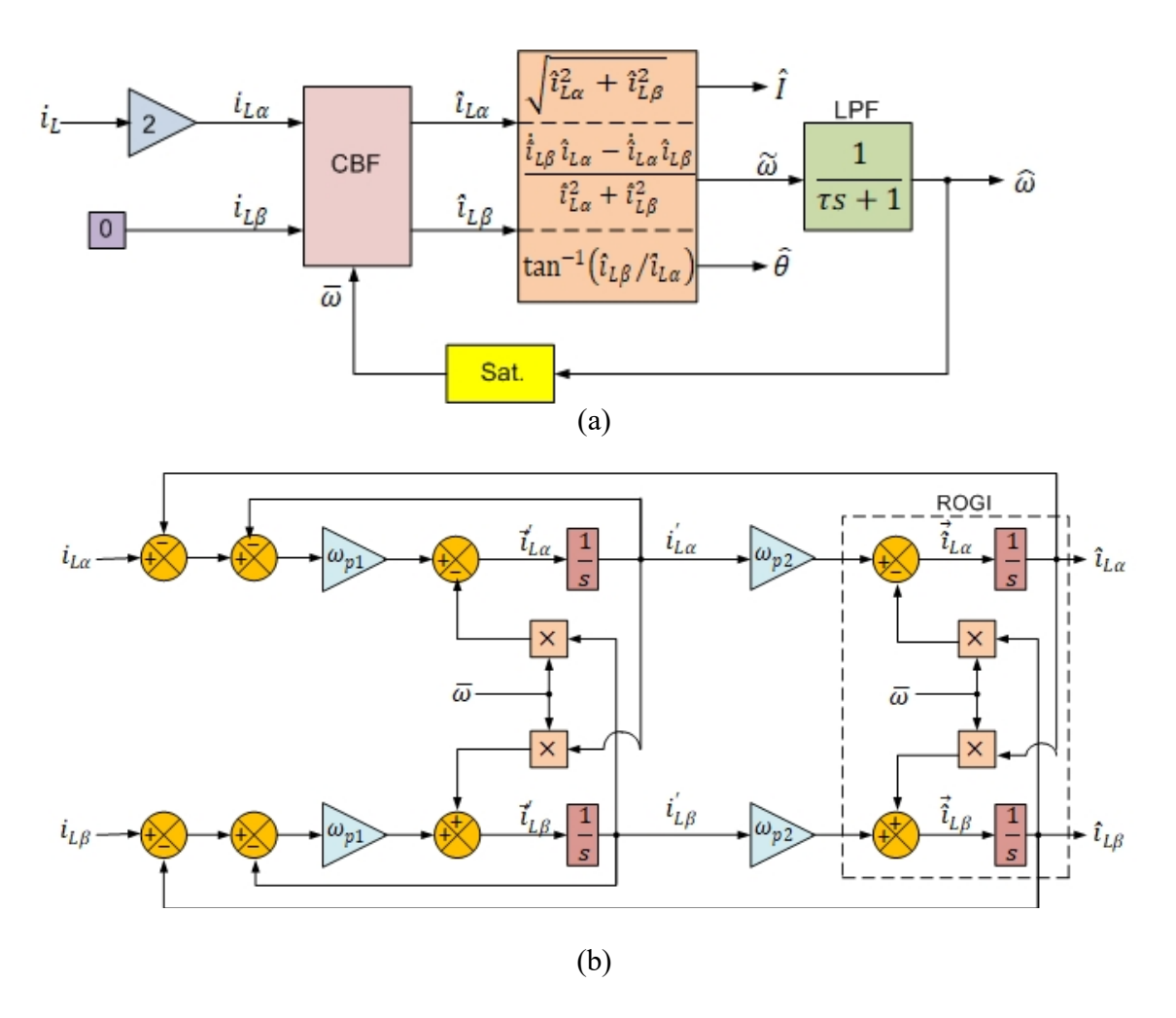


Fig. 4.1(a) 1φ -CBF-FLL configuration and (b) Second order CBF in the continuous time domain.

### 4.2.3 Modeling

Its tuning is rather challenging because its model has not yet been provided. Here, we demonstrate the small-signal modeling of this FLL in an attempt to make tuning more efficient.

We must ignore the negative-sequence component of input for  $1\phi$ -CBF-FLL to derive a small-signal model for it [equation (4.1)]. In this instance, the signals of  $\alpha\beta$  -axis of  $1\phi$ -CBF-FLL are written as

$$i_{L\alpha} = I\cos(\theta)$$
  
 $i_{L\beta} = I\sin(\theta)$  (4.2)

$$\hat{\iota}_{L\beta} = \hat{I}\sin(\hat{\theta}) \tag{4.3}$$

Additionally, we must ignore saturation in Fig. 4.1(a). In this instance,  $\overline{\omega} = \widehat{\omega}$ .

Using Fig. 4.1, we get

$$\vec{\hat{\theta}} = \frac{d}{dt} \left[ \tan^{-1} \left( \frac{\hat{i}_{L\beta}}{\hat{i}_{L\alpha}} \right) \right] = \frac{\vec{\hat{i}}_{L\beta}\hat{i}_{L\alpha} - \vec{\hat{i}}_{L\alpha}\hat{i}_{L\beta}}{\hat{i}_{L\alpha}^2 + \hat{i}_{L\beta}^2} = \overline{\omega}$$
(4.4)

$$\vec{\hat{\imath}}_{L\alpha} = \omega_{p2} i'_{L\alpha} - \overline{\omega} \hat{\imath}_{L\beta}$$

$$\vec{\hat{\imath}}_{L\beta} = \omega_{p2} i_{L\beta}' + \overline{\omega} \hat{\imath}_{L\alpha} \tag{4.5}$$

Substituting (4.5) into (4.4) gives

$$\vec{\hat{\theta}} = \overline{\omega} = \frac{\omega_{p2} \left[ i'_{L\beta} \hat{\imath}_{L\alpha} - i'_{L\alpha} \hat{\imath}_{L\beta} \right] + \overline{\omega} \left[ \hat{\imath}_{L\alpha}^2 + \hat{\imath}_{L\beta}^2 \right]}{\hat{\imath}_{L\alpha}^2 + \hat{\imath}_{L\beta}^2}$$

$$= \underbrace{\frac{\omega_{p2}}{\hat{\jmath}^2} \left[ i'_{L\beta} \hat{\imath}_{L\alpha} - i'_{L\alpha} \hat{\imath}_{L\beta} \right]}_{\mathcal{P}} + \overline{\omega}$$
(4.6)

Differentiate  $\vartheta$  in (4.6) with respect to time, we get

$$\vec{\vartheta} \approx \frac{\omega_{p2}}{\hat{t}^2} \left[ \vec{\imath}'_{L\beta} \hat{\imath}_{L\alpha} + i'_{L\beta} \hat{\imath}'_{L\alpha} - \vec{\imath}'_{L\alpha} \hat{\imath}_{L\beta} - i'_{L\alpha} \hat{\imath}'_{L\beta} \right]$$
(4.7)

Where

$$\vec{i}'_{L\alpha} = \omega_{p1} (i_{L\alpha} - \hat{i}_{L\alpha} - i'_{L\alpha}) - \overline{\omega} i'_{L\beta}$$

$$\vec{i}'_{L\beta} = \omega_{p1} (i_{L\beta} - \hat{i}_{L\beta} - i'_{L\beta}) - \overline{\omega} i'_{L\alpha}$$
(4.8)

Substituting (4.5) and (4.8) into (4.7) gives

$$\vec{\vartheta} \approx \frac{\omega_{p2}\omega_{p1}}{\hat{l}^2} \left[ i_{L\beta}\hat{i}_{L\alpha} - i_{L\alpha}\hat{i}_{L\beta} \right] + \omega_{p1} \underbrace{\frac{\omega_{p2}}{\hat{l}^2} \left[ i'_{L\alpha}\hat{i}_{L\beta} - i'_{L\beta}\hat{i}_{L\alpha} \right]}_{-\vartheta}$$
(4.9)

Considering (4.2) and (4.3), (4.9) can be rewritten as

$$\vec{\vartheta} \approx \frac{\omega_{p1}\omega_{p2}}{\hat{I}^2}I\hat{I}\sin(\theta - \hat{\theta}) - \omega_{p1}\,\vartheta$$

$$\approx \omega_{p1}\omega_{p2}(\theta - \hat{\theta}) - \omega_{p1}\,\vartheta$$
(4.10)

Based on (4.4), (4.6), (4.10), and Fig. 4.1(a), and defining,  $\theta = \theta_n + \Delta \theta$ ,  $\hat{\theta} = \theta_n + \Delta \hat{\theta}$ ,  $\overline{\omega} = \omega_n + \Delta \overline{\omega}$  where  $\theta_n = \int \omega_n dt$ , it is possible to design a 1 $\phi$ -CBF-FLL model as shown in Fig. 4.2(a). Recall that the unit of saturation was disregarded throughout the simulation process, meaning that  $\hat{\omega} = \overline{\omega}$  and, therefore,  $\Delta \hat{\omega} = \Delta \overline{\omega}$ . The block diagram algebra may be used to express this concept, as seen in Fig. 4.2(b).

Additional comments on a few 1 $\phi$ -CBF-FLL difficulties are given in this section. The 1 $\phi$ -CBF-FLL has an offset in frequency in the first problem, and previously described double-frequency errors in the second problem. Presume that the second-order CBF  $\alpha\beta$ -axis outputs from Fig. 4.3 as

$$\hat{\imath}_{L\alpha}(n) = I\cos(n\omega T_s)$$

$$\hat{\imath}_{L\beta}(n) = I\sin(n\omega T_s) \tag{4.11}$$

Where, n represents the current sample and I and  $\omega$  stand for grid voltage amplitude and angular frequency. It is also considered that I and  $\omega$  are constants for simplicity. The predicted frequency  $\widetilde{\omega}$  from Fig. 4.3 can be expressed in this way:

$$\widetilde{\omega}(n) = \frac{\hat{\iota}_{L\alpha}(n-1)\hat{\iota}_{L\beta}(n) - \hat{\iota}_{L\beta}(n-1)\hat{\iota}_{L\alpha}(n)}{T_{s}[\hat{\iota}_{L\alpha}^{2}(n) + \hat{\iota}_{L\beta}^{2}(n)]}$$

$$= \frac{I^{2}[\cos((n-1)\omega T_{s})\sin(n\omega T_{s}) - \sin((n-1)\omega T_{s})\sin(n\omega T_{s})]}{T_{s}I^{2}[\cos^{2}(n\omega T_{s}) + \sin^{2}(n\omega T_{s})]}$$

$$= \frac{\sin(\omega T_{s})}{T_{s}} = \omega - \frac{\omega^{3}T_{s}^{2}}{3!} + \frac{\omega^{5}T_{s}^{4}}{5!} - \cdots$$
(4.12)

It is evident from equation (4.12) that the predicted frequency of 1φ-CBF-FLL has an offset error. In cases where the sample frequency is high, this inaccuracy is minimal. The existence of dual-frequency oscillatory errors in 1φ-CBF-FLL calculated values is the second problem. It was previously mentioned that because progressively limiting the FLL bandwidth causes its dynamic reaction to become very sluggish, it would not be a smart strategy to mitigate these oscillatory problems. As mentioned in [122], raising the CBF order is another course of action. Getting a model for 1φ-CBF-FLL configuration might be an issue in this situation, especially if 1φ-CBF-FLL order is quite high. Thankfully, there is a distinct relationship between the CBF structures of the 1φ-CBF-FLL model. This fact has already been shown in the situation of second-order CBF (in Figs. 4.1(b) and 4.2(a)). It is quite simple to tune the controlling parameters by using the given systematic technique after the small signal model has been generated.

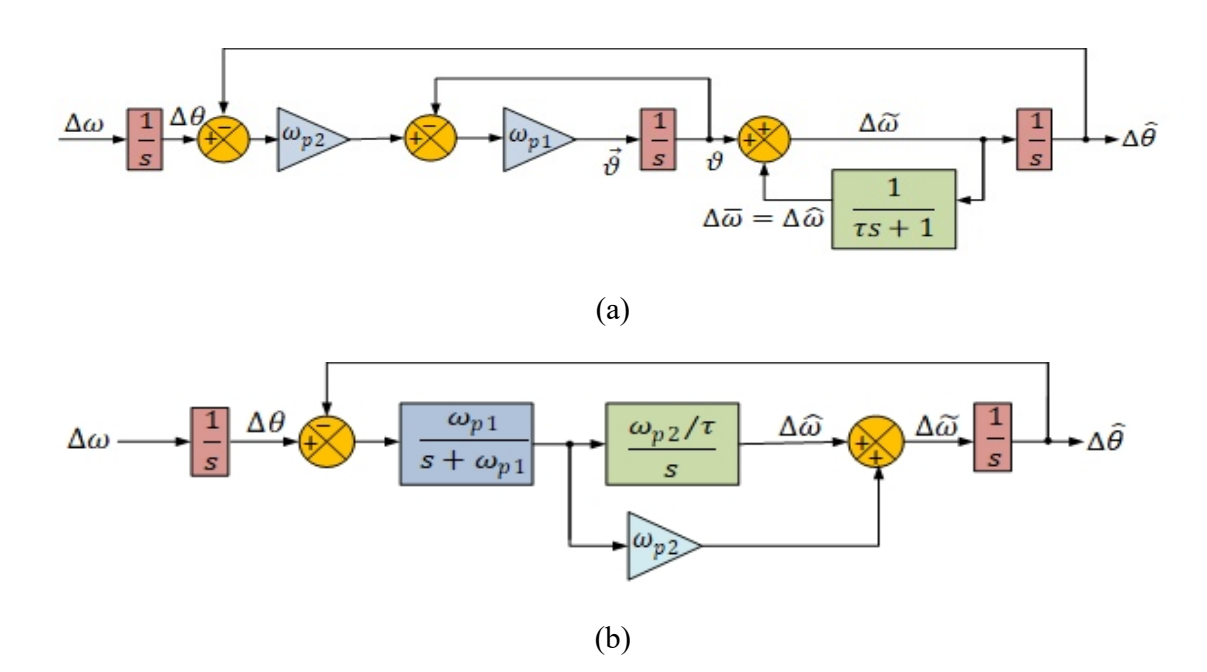


Fig. 4.1(a) Model of 1φ-CBF-FLL (b) Its alternate depiction.

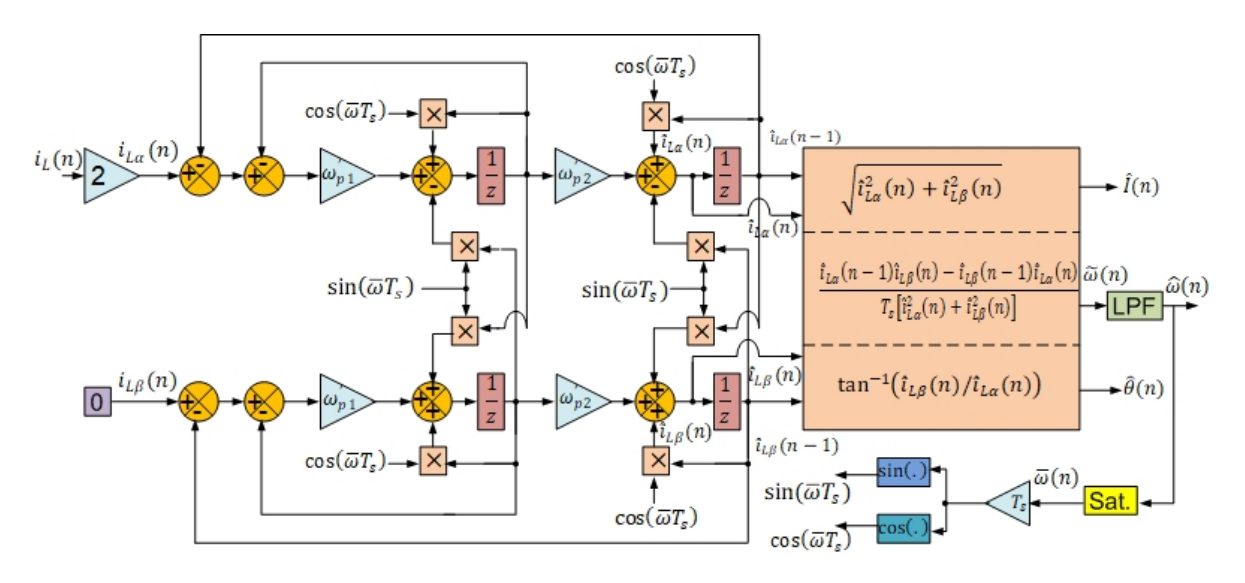


Fig. 4.3 Digital model of 1φ-CBF-FLL

### 4.2.4 Calculation of Fundamental Load Current Component

The amplitude of the load current is determined using the  $1\phi$ -CBF-FLL control technique. Fig. 4.3 displays the block diagram representation used to determine the load current amplitude. The in-phase and quadrature signals are used to determine the load current magnitude ( $I_{fL}$ ). There are virtually no waves in the projected amount of the load current,

therefore an extra filter is not necessary. Once the calculation of load current is completed, all conventional techniques often use an extra filter. This is yet another benefit of the suggested method. To separate the  $\alpha\beta$  components of the distorted load current and get the fundamental load component, the suggested 1 $\phi$ -CBF-FLL method is utilized.

$$I_{fL} = \sqrt{i_{L\alpha}^2 + i_{L\beta}^2}$$
 (4.13)

### 4.2.5 Estimation of Reference Current

The reference current  $(i_g^*)$  can be determined after computing the DC loss component  $(I_{DC})$ , load current component  $(I_{fL})$  and synchronization signal  $(\sin \theta)$ . By multiplying the predicted net current by the synchronizing signal, one may estimate the reference grid current. The net current  $(I_{net})$  is formed by summing  $I_{fL}$  and  $I_{DC}$  as given in equation (4.14).

$$I_{net} = I_{fL} + I_{DC} (4.14)$$

The reference current  $i_q^*$  is estimated as

$$i_a^* = I_{net} \sin \theta \tag{4.15}$$

### 4.2.6 Simulation Results

In the proposed work 1-φ Grid-Tied Solar PV (GTSPV) system is modelled and simulated. The system operates under a 230 V, 50 Hz supply and is tested with both linear and non-linear loads. A control strategy based on the 1φ-CBF-FLL is designed to extract the fundamental component of the load connected to the system. The simulation-based results in case of different operating conditions are displayed in the figure.

### 4.2.6.1 Dynamic Behaviour of System Under Solar Irradiance Variations

Fig. 4.4(a) and (b) illustrate the dynamic performance of the GTSPV system in response to changes in solar irradiance. The irradiance level increases from 500 w/m² to 1000 w/m² at t=1.3 sec. As depicted in Fig. 4.4(a), this increase results in a corresponding rise in both the PV current and output power. Meanwhile, Fig. 4.4(b) shows a reduction in grid current as the irradiance level rises. Despite the presence of an unbalanced load and irradiance fluctuations, the 1φ-CBF-FLL -based control strategy effectively maintains stability by regulating the compensator current, grid voltage, and DC-link voltage.

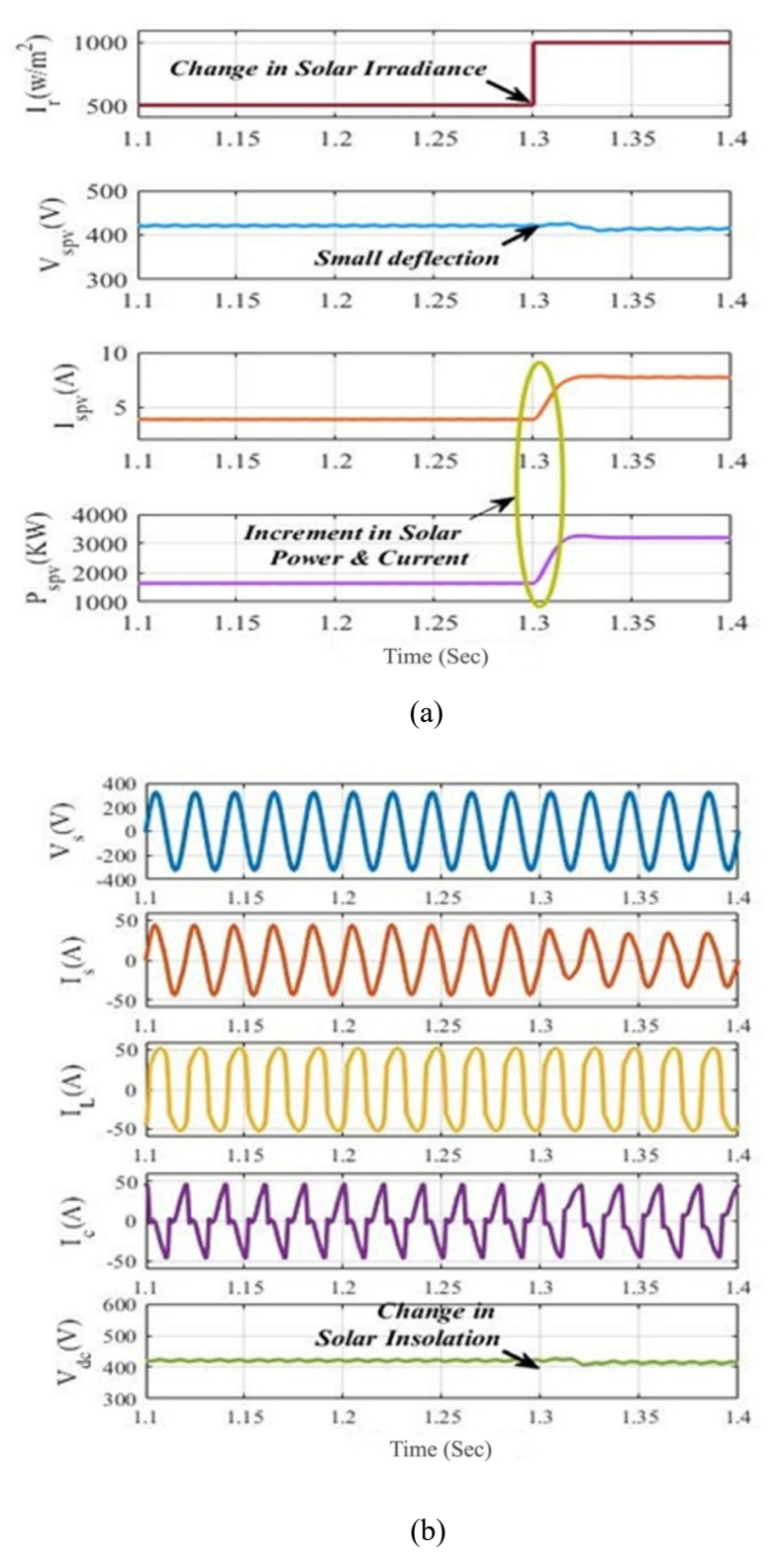
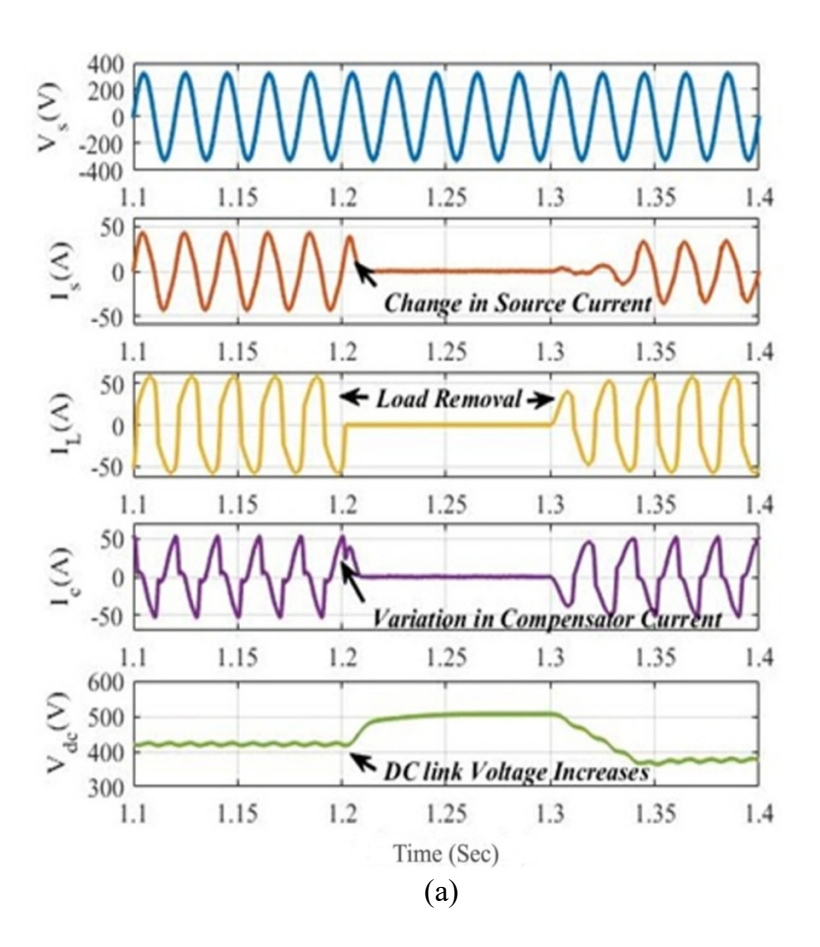


Fig. 4.4(a) & (b) Dynamic response of GTSPV in case of change in solar irradiance

### 4.2.6.2 Dynamic Behaviour of System During Load Removal/Insertion

The dynamic behaviour of the GTSPV system under load removal/insertion is illustrated in Fig. 4.5(a) and Fig. 4.5(b). At t=1.2, the load is disconnected, and it is reconnected at t=1.3. During the disconnection interval, the compensator current, load current, and source current reduce to zero. Despite this, the proposed control strategy effectively sustains the source voltage, and an increase in the DC-link voltage is observed, as depicted in Fig. 4.5(a). In Fig. 4.5(b), the system experiences load insertion between t=1.2-1.3 s, whereas the load is absent during the intervals t=1.1-1.2 s and t=1.3-1.4 s. During these time intervals of load removal all current components—compensator, load, and source become zero. Whereas, the controller successfully regulates the source voltage and maintains stability of the DC-link voltage throughout these transitions.



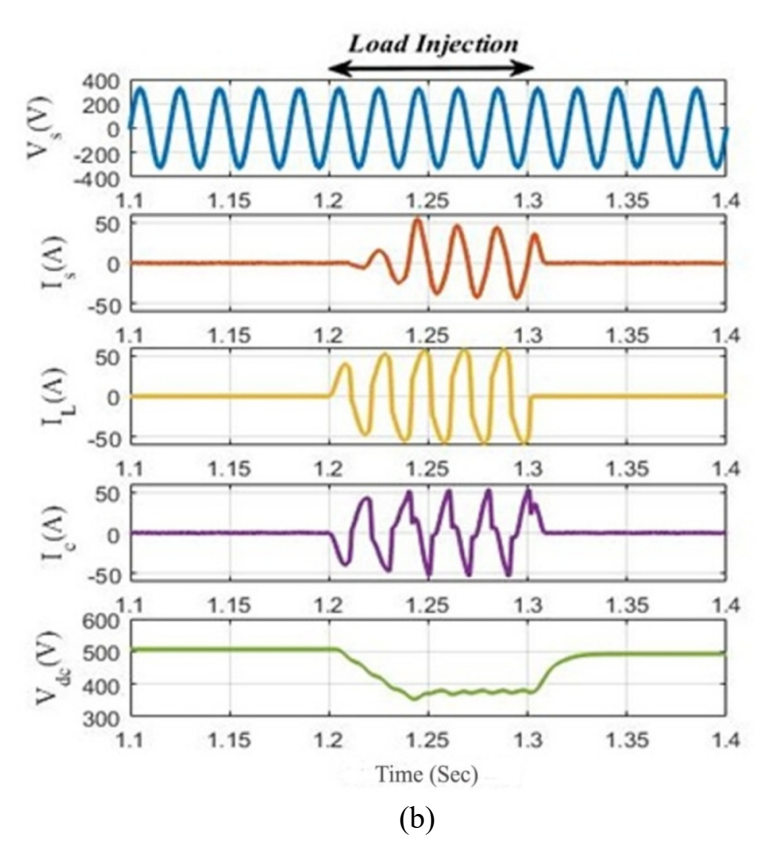


Fig. 4.5(a) & (b) Dynamic response of GTSV in case of load removal/insertion

### 4.2.6.3 Dynamic Behaviour of System in Case of Load Variation

In Starting both the linear and non-linear loads are connected to the system and the irradiance level of PV is kept constant. At t=1.2 s the linear load is disconnected therefore load demand of the system goes down. When the load varies, there is some disturbance in the DC link voltage, but controller action controls it. At t=1.3 sec linear load is again connected and initial values of the system conditions are reinstated as in Fig. 4.6.

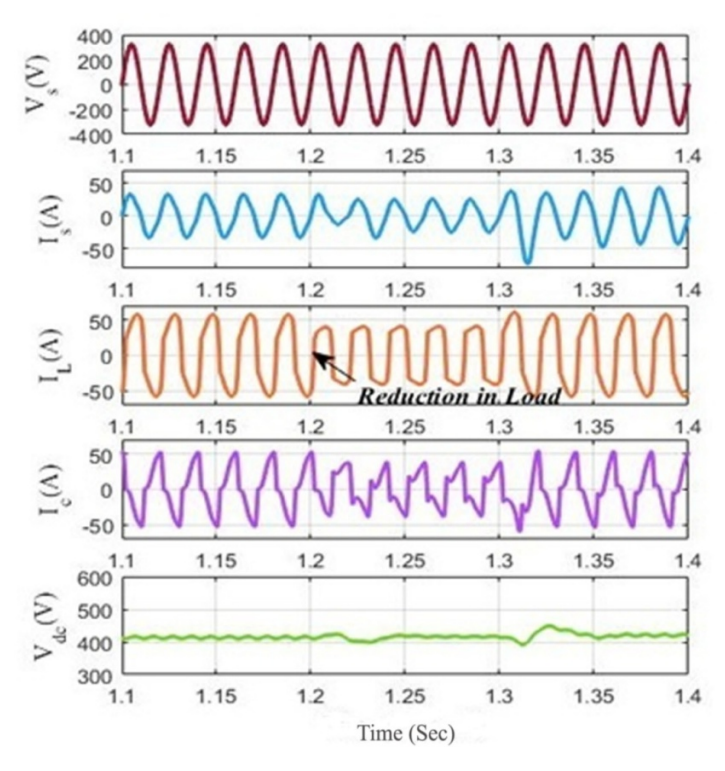
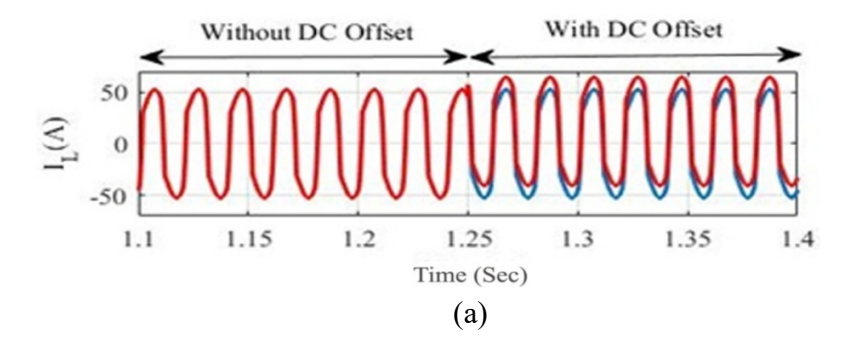


Fig. 4.6 Dynamic response of GTSPV system in case of change in load

### 4.2.6.4 Performance of the System in Case of DC-Offset Condition

Fig. 4.7(a) & (b) display the execution of the proposed system with DC-offset conditions. Fig. 4.7(a) shows the load current of the system with and without the insertion of the DC-offset. In this at t=1.25 sec response of the system under 25% DC-offset is shown. In this case, the proposed controller maintains the source current sinusoidal and stable the DC link voltage under DC-offset and non-linear load conditions as shown in Fig. 4.7(b). In this condition of insertion of DC-offset under non-linear load condition the proposed controller maintains the source current, compensator current and voltage of the DC link.



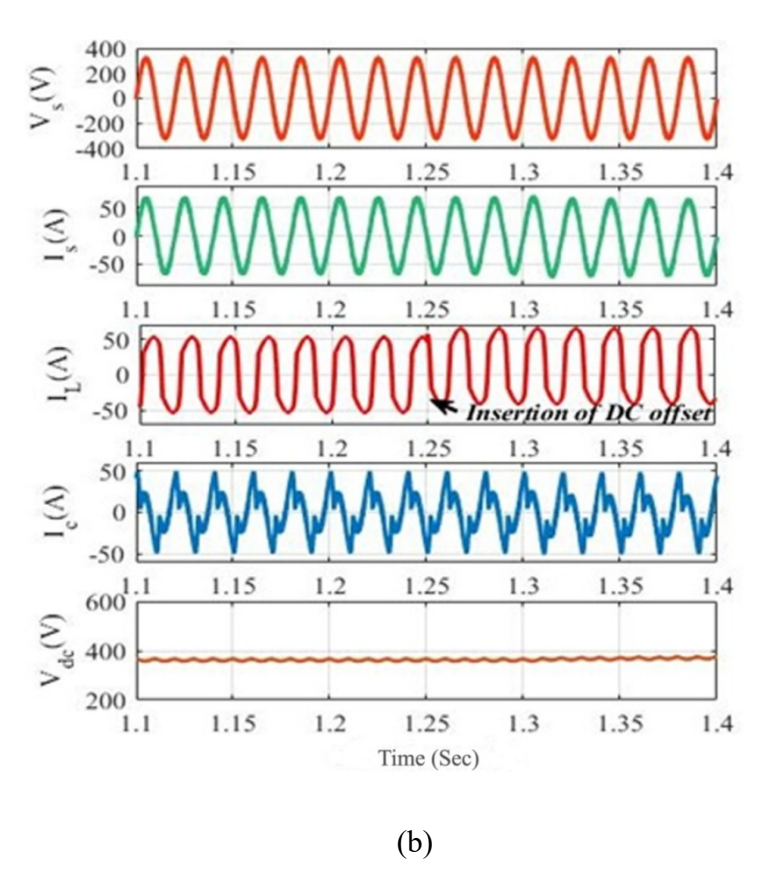


Fig. 4.7 (a) & (b) Performance of GTSPV system in case of DC-offset condition

### 4.2.6.5 Harmonics Analysis

Fig. 4.8(a)-(c) shows the THD of load current  $(i_L)$ , source current  $(i_S)$ , and source voltage  $(v_S)$  of the 1- $\phi$  GTSPV under unbalanced load conditions. The analysis reveals THD values of 24.54% for  $i_L$ , 4.02% for  $i_S$ , and 3.21% for  $v_S$ .Under nonlinear load scenarios, the proposed VSC control strategy effectively mitigates harmonics while sustaining grid voltage stability. Notably, the THD values for both source current and voltage are fewer than 5%, which are within permissible bounds and satisfy IEEE-519 requirements.

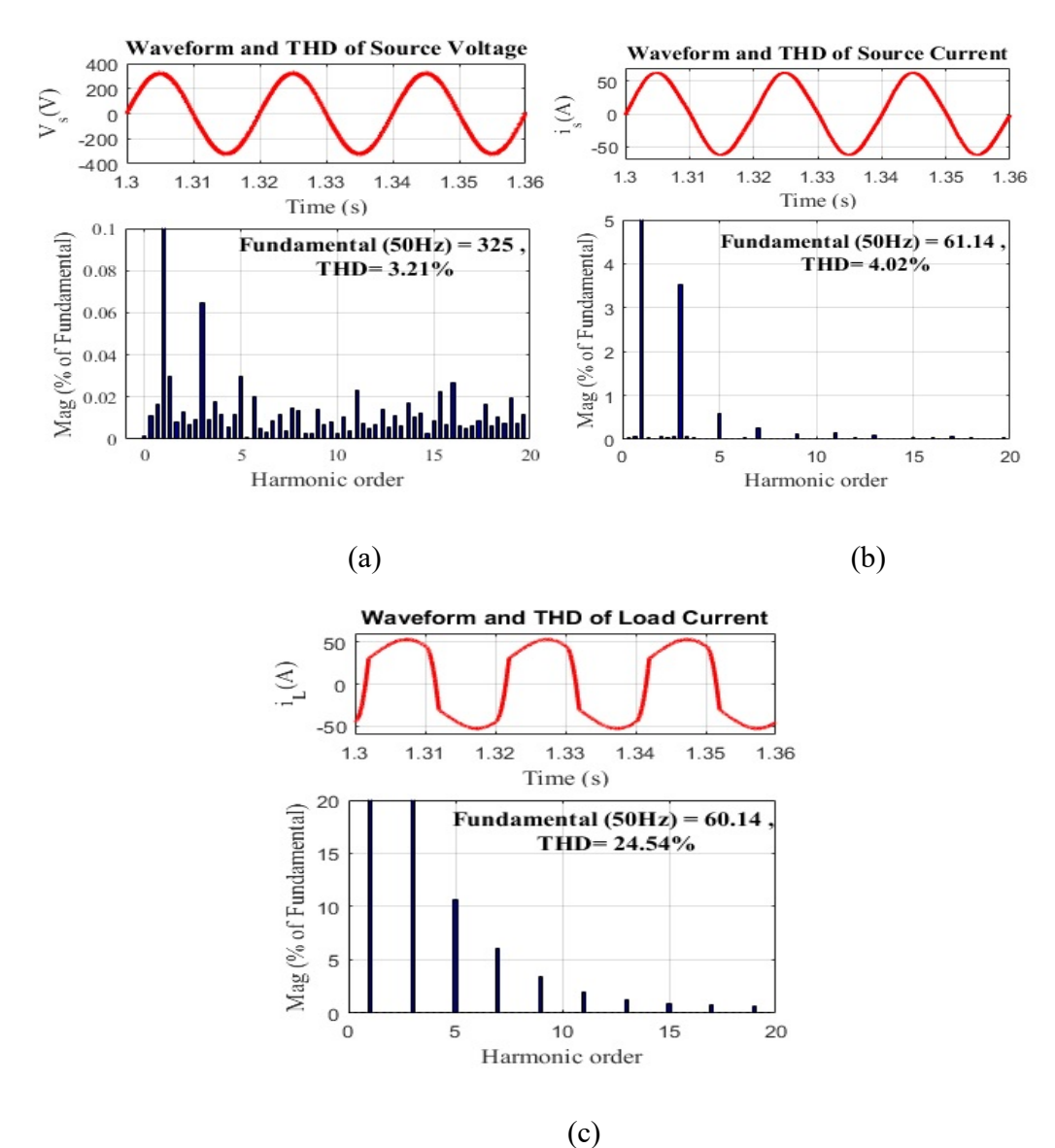


Fig. 4.8(a)-(c) Harmonics analysis of 1-φ GTSPV system

### 4.2.6.6 Performance Comparison

Fig.4.9 illustrates an analysis of the comparison of the proposed controller (1 $\phi$ -CBF-FLL) with a few control techniques. The figure presents a comparison of all three techniques that are being discussed, based on their ability to extract the fundamental component of the load current. The suggested control strategy has a faster response and less oscillation as compared to the other two control strategies. The THDs of  $i_s$  are 4.76% and 4.58% for SOGI-FLL and LKF-FLL respectively, whereas the THD of  $i_s$  is 4.02% for the proposed 1 $\phi$ -CBF-FLL.

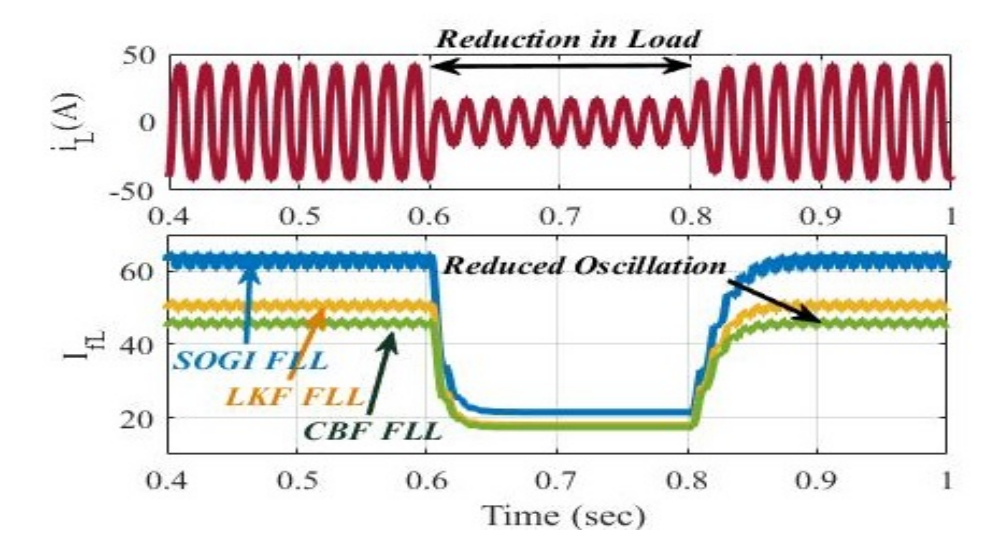


Fig. 4.9 Comparative performance of proposed 1φ-CBF-FLL with LKF-FLL and SOGI-FLL.

Table 4.1: Performance overview of various controllers

Features	SOGI-	LKF-FLL	Proposed
	FLL		1φ-CBF-
			FLL
Oscillation	Less	Less	Less
DC-Offset Rejection	Good	Good	Better
THD of Grid Current	4.76%	4.58%	4.02%
Steady State Performance	Good	Good	Better
Dynamic Performance	Good	Good	Better
Grid Synchronization	Yes	Yes	Yes

Table 4.1 shows the comparison of suggested 1φ-CBF-FLL controller with a few control techniques. The comparison table shown demonstrates the effectiveness of the suggested control strategy in relation to many properties, including grid current THD and DC-offset rejection. Results indicate that the suggested scheme performs better than existing control algorithms, including SOGI-FLL and linear Kalman filter-based frequency-locked loop (LKF-FLL) in case of change in solar insolation and unbalanced non-linear load.

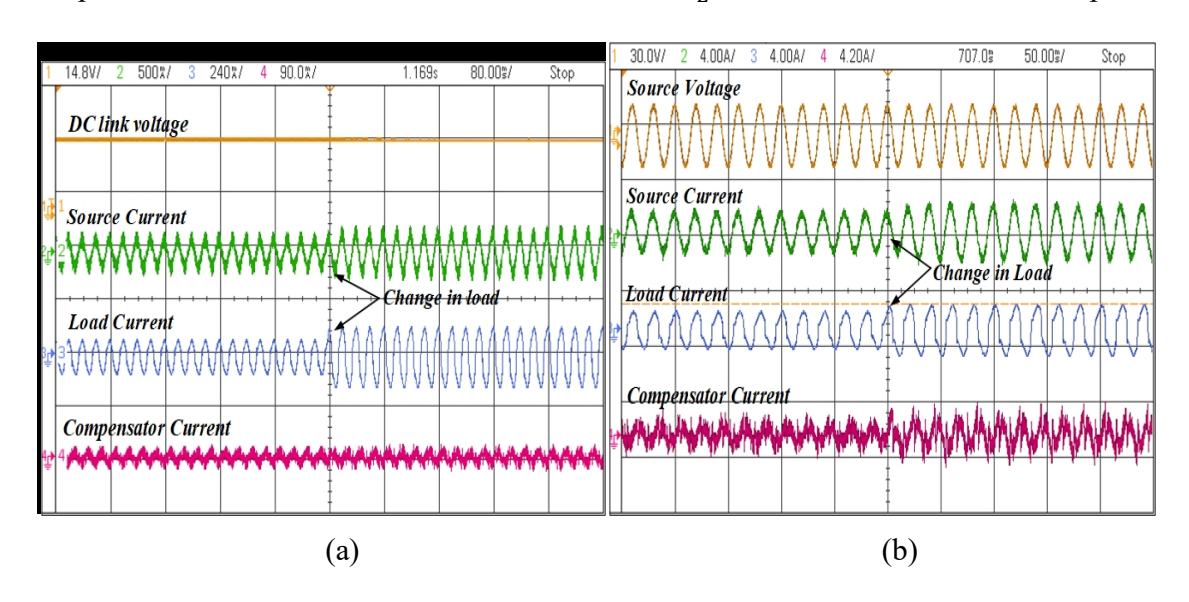
### 4.2.7 Test Results

A hardware prototype of the proposed system is developed in the lab to experimentally validate the simulation outcomes. The setup operates using an AC supply that is 110 V and 50 Hz. Additionally, the nonlinear load on the DC side of the rectifier is modelled as an RL load

in the prototype hardware. To provide compensatory currents through interacting inductors, a DSTATCOM is attached at the CPI. The DSP dSPACE1104 board is interfaced and attached to several sensors for measuring current and voltage are LA-25P for current and LV-25P for voltage. The DSTATCOM receives switching pulses from DSP to properly manage the system. To record different hardware dynamic outcomes, a DSO is employed. Using a power analyzer (HIOKI PQ3100), the experimental findings of harmonics, current and voltage are recorded.

### 4.2.7.1 Dynamic Behaviour of System Under Load Variation

The system's transient behaviour in response to load variations is illustrated in Fig. 4.10(a)–(d). If the load varies, the following parameters are shown: DC link voltage  $(v_{dc})$ , compensator current  $(i_c)$ , load current  $(i_L)$ , source current  $(i_s)$ , and source voltage  $(v_s)$ . The waveforms of  $v_s$ ,  $v_{dc}$ ,  $i_s$ ,  $i_L$  and  $i_C$  under load change conditions are shown in Fig. 4.10(a)–(b). These graphs depict how the system reacts to an increase in load as the  $i_L$  rises. The  $v_{dc}$  is constant, and  $v_s$ ,  $i_s$ , and  $i_L$  all have the same phase in their waveforms. The plots of  $v_s$ ,  $i_s$ ,  $i_L$  and  $v_{dc}$  in case of load-varying conditions are shown in Fig. 4.10(c). The  $i_s$  remains sinusoidal and phase-aligned with the  $v_s$  following correction. In Fig. 4.10(d). plots of fundamental component,  $i_L$ ,  $v_s$ , and  $i_s$  are displayed, illustrating system performance when  $i_L$  drops. The waveform demonstrates how the shift in  $i_L$  modifies the fundamental component.



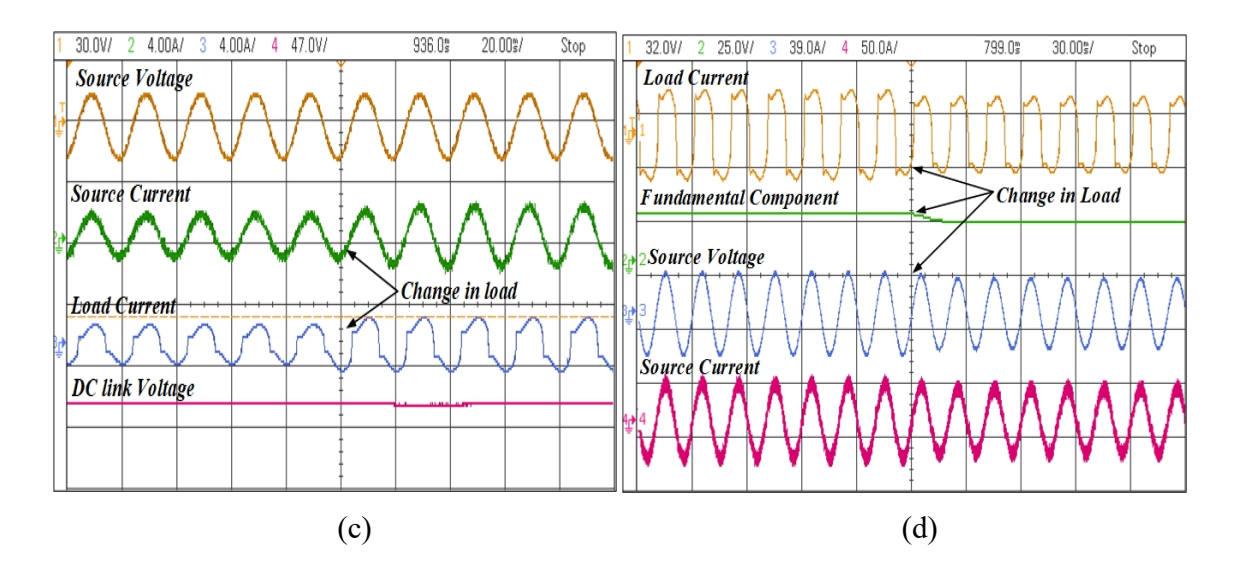


Fig. 4.10 (a)-(d) Dynamic response of the proposed system in case of change in load

### 4.2.7.2 Harmonics Analysis

Even when the grid is under the influence of a highly nonlinear load, the THD of  $v_s$  and  $i_s$  of the proposed system are consistently well under the allowed limit of 5%. The THDs of the  $v_s$  and  $i_s$  in the 1 $\phi$ -CBF-FLL control technique are 2.12% and 4.46%, respectively, as shown in Fig. 4.11(a), below the IEEE 519 standard threshold of 5%. The non-linear  $i_L$  has a THD of 29.77%, as seen in Fig. 4.11(b).

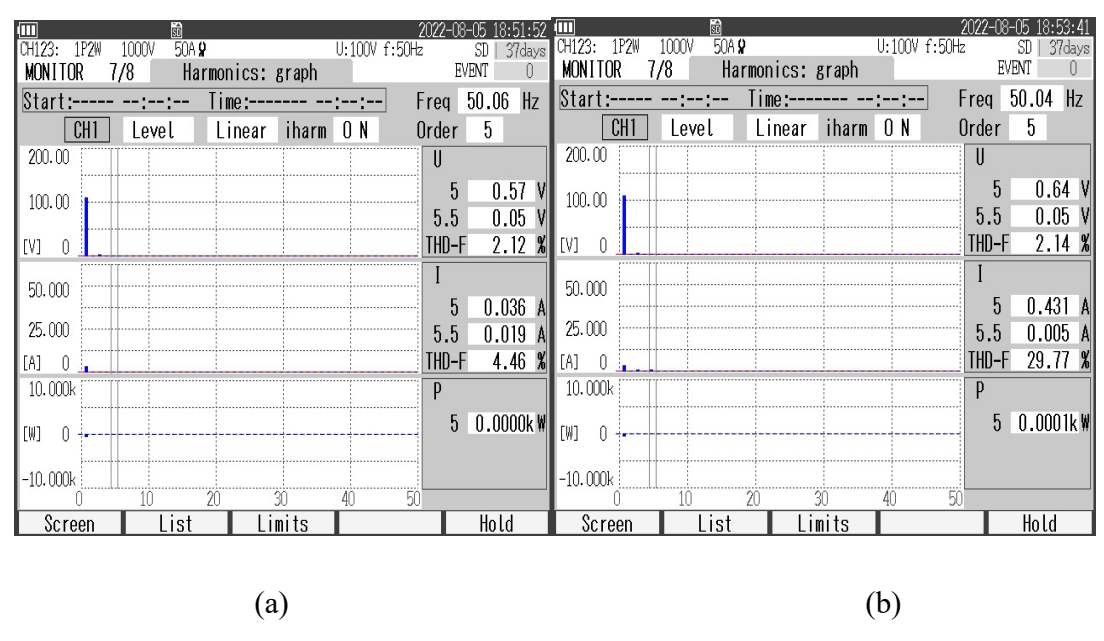


Fig. 4.11 (a) & (b) Harmonic spectra of the proposed system

### 4.3 APF-PLL Control Approach

Fig. 4.12 depicts the complete control architecture, which includes both the MPPT and VSC switching mechanisms. The VSC switching algorithm generates control pulses to achieve goals such as load regulation, power factor correction, reactive power compensation, and increased power penetration in the distribution grid. These control pulses are coordinated with the MPPT algorithm, which adjusts the solar PV arrays to keep the desired DC-bus voltage level.

### 4.3.1 Modeling

Considering that the single-phase input signal of APF-PLL is,

$$v(t) = V_1 \cos(\theta_1) \tag{4.16}$$

Where  $\theta_1$  and  $V_1$  are the angle and voltage, respectively. The  $\alpha\beta$ -axis input of the APF-PLL can be demonstrated as

$$v_{\alpha}(t) = V_1 \cos(\theta_1)$$

$$v_{\beta}(t) = V_1 \sin(\theta_1)$$
(4.17)

Considering (4.17), the  $\alpha\beta$ -axis output of the APF-PLL can be considered as

$$\hat{v}_{\alpha 1}(t) = \hat{V}_1 \cos(\hat{\theta}_1)$$

$$\hat{v}_{\beta 1}(t) = \hat{V}_1 \sin(\hat{\theta}_1)$$
(4.18)

Where  $\hat{V}_1$  and  $\hat{\theta}_1$  are estimations of  $V_1$  and  $\theta_1$ , respectively.

### 4.3.2 Phase Estimation Dynamics:

Using (4.18), the phase angle can be expressed as

$$\hat{\theta}_1 = \tan^{-1} \frac{\hat{v}_{\beta 1}(t)}{\hat{v}_{\alpha 1}(t)} \tag{4.19}$$

Differentiating equation (4.19), we get

$$\frac{d\hat{\theta}_1}{dt} = \frac{\hat{v}_{\alpha 1}(t)\frac{d\hat{v}_{\beta 1}(t)}{dt} - \hat{v}_{\beta 1}(t)\frac{d\hat{v}_{\alpha 1}(t)}{dt}}{\hat{v}_{\alpha 1}^2(t) + \hat{v}_{\beta 1}^2(t)}$$
(4.20)

Where

$$\frac{d\hat{v}_{\alpha 1}(t)}{dt} = \frac{1}{2} \left[ \frac{dv_{\alpha}(t)}{dt} - \frac{dv_{\alpha}'(t)}{dt} \right]$$

$$\frac{d\hat{v}_{\alpha 1}(t)}{dt} = \frac{1}{2} \left[ \frac{dv_{\alpha}(t)}{dt} + \frac{dv_{\beta}(t)}{dt} - \widetilde{\omega} \left\{ v_{\beta}(t) + 2\widetilde{v}_{\alpha 1}(t) - v_{\alpha}(t) \right\} \right]$$
(4.21)

$$\frac{d\tilde{v}_{\beta 1}(t)}{dt} = \frac{1}{2} \left[ \frac{dv_{\beta}(t)}{dt} - \frac{dv_{\beta}'(t)}{dt} \right]$$

$$\frac{d\tilde{v}_{\beta_1}(t)}{dt} = \frac{1}{2} \left[ \frac{dv_{\beta}(t)}{dt} - \frac{dv_{\alpha}(t)}{dt} + \widetilde{\omega} \left\{ v_{\alpha}(t) - 2\widetilde{v}_{\beta_1}(t) + v_{\beta}(t) \right\} \right] \tag{4.22}$$

Put (4.21) and (4.22) into (4.20), and we get

$$\frac{d\tilde{\theta}_{1}}{dt} = \frac{1}{2\tilde{v}_{1}^{2}} \left[ \left( \tilde{v}_{\alpha 1}(t) \frac{dv_{\beta}(t)}{dt} - \tilde{v}_{\beta 1}(t) \frac{dv_{\alpha}(t)}{dt} \right) + \tilde{\omega} \left( \tilde{v}_{\alpha 1}(t) v_{\alpha}(t) + \tilde{v}_{\beta 1}(t) v_{\beta}(t) \right) + \tilde{\omega} \left( \tilde{v}_{\alpha 1}(t) v_{\beta}(t) - \tilde{v}_{\beta 1}(t) v_{\alpha}(t) \right) - \left( \tilde{v}_{\alpha 1}(t) \frac{dv_{\alpha}(t)}{dt} + \tilde{v}_{\beta 1}(t) \frac{dv_{\beta}(t)}{dt} \right) \right]$$
(4.23)

Put (4.17) and (4.18) into (4.23), and we get

$$\frac{d\tilde{\theta}_{1}}{dt} = \frac{1}{2} \left[ \left( \frac{d\theta_{1}}{dt} + \widetilde{\omega} + \frac{1}{V_{1}} \frac{dV_{1}}{dt} \right) \frac{V_{1}}{\widetilde{V}_{1}} \sin(\theta_{1} - \widetilde{\theta}_{1}) + \left( \frac{d\theta_{1}}{dt} + \widetilde{\omega} - \frac{1}{V_{1}} \frac{dV_{1}}{dt} \right) \frac{V_{1}}{\widetilde{V}_{1}} \cos(\theta_{1} - \widetilde{\theta}_{1}) \right] (4.24)$$

$$\frac{d\tilde{\theta}_1}{dt} = \omega_n + \frac{d\Delta\tilde{\theta}_1}{dt} \tag{4.24a}$$

$$\frac{1}{V_1}\frac{dV_1}{dt} = \frac{1}{V_2 + \Delta V_1}\frac{d\Delta V_1}{dt} = \frac{1}{V_2}\frac{1}{1 + \Delta V_1/V_2}\frac{d\Delta V_1}{dt} \approx \frac{1}{V_2}\frac{d\Delta V_1}{dt} - \frac{1}{V_2}\Delta V_1\frac{d\Delta V_1}{dt} \approx \frac{1}{V_2}\frac{d\Delta V_1}{dt}$$
(4.24b)

$$\frac{d\theta_1}{dt} + \widetilde{\omega} = 2\omega_n + \frac{d\Delta\theta_1}{dt} + \Delta\widetilde{\omega}$$
 (4.24c)

$$\frac{V_1}{\tilde{V}_1} = \frac{V_n + \Delta V_1}{V_n + \Delta \tilde{V}_1} = \frac{1 + \Delta V_1 / V_n}{1 + \Delta \tilde{V}_1 / V_n}$$

$$\approx (1 + \Delta V_1 / V_n) (1 - \Delta \tilde{V}_1 / V_n)$$

$$= 1 + \Delta V_1 / V_n - \Delta \tilde{V}_1 / V_n - \Delta V_1 \Delta \tilde{V}_1 / V_n^2$$

$$\approx 1 + \Delta V_1 / V_n - \Delta \tilde{V}_1 / V_n$$
(4.24d)

$$\sin(\theta_1 - \tilde{\theta}_1) \approx (\Delta \theta_1 - \Delta \tilde{\theta}_1) \tag{4.24e}$$

$$\cos(\theta_1 - \tilde{\theta}_1) \approx 1 \tag{4.24f}$$

By putting (4.24) into (4.23) and we get

$$\frac{d\Delta\tilde{\theta}_1}{dt} \approx \omega_n \left(\Delta\theta_1 - \Delta\tilde{\theta}_1\right) + \frac{\omega_n}{V_n} \left(\Delta V_1 - \Delta\tilde{V}_1\right) + \frac{1}{2} \frac{d\Delta\theta_1}{dt} - \frac{1}{2V_n} \frac{d\Delta V_1}{dt} + \frac{1}{2} \Delta\tilde{\omega}$$
(4.25)

### 4.3.3 Amplitude Estimation Dynamics:

Using (4.28), the amplitude can be expressed as

$$\tilde{V}_1 = \sqrt{\tilde{v}_{\alpha 1}^2(t) + \tilde{v}_{\beta 1}^2(t)} \tag{4.26}$$

Differentiating the above equation, we get

$$\frac{d\tilde{V}_1}{dt} = \frac{\tilde{v}_{\alpha 1}(t)\frac{d\tilde{v}_{\alpha 1}(t)}{dt} + \tilde{v}_{\beta 1}(t)\frac{d\tilde{v}_{\beta 1}(t)}{dt}}{\tilde{V}_1}$$
(4.27)

Put the value of (4.21) and (4.22) into (4.27), and we get

$$\frac{d\tilde{v}_{1}}{dt} = \frac{1}{2\tilde{v}_{1}} \left[ \left( \tilde{v}_{\alpha 1}(t) \frac{dv_{\alpha}(t)}{dt} + \tilde{v}_{\beta 1}(t) \frac{dv_{\beta}(t)}{dt} \right) - \tilde{\omega} \left( \tilde{v}_{\alpha 1}(t) v_{\beta}(t) - \tilde{v}_{\beta 1}(t) v_{\alpha}(t) \right) - 2\tilde{\omega} \left( \tilde{v}_{\alpha 1}^{2}(t) + \tilde{v}_{\beta 1}(t) v_{\beta}(t) \right) + \left( \tilde{v}_{\alpha 1}(t) \frac{dv_{\beta}(t)}{dt} - \tilde{v}_{\beta 1}(t) \frac{dv_{\alpha}(t)}{dt} \right) \right]$$
(4.28)

Put the value of (4.17) and (4.18) into (4.28), and we get

$$\frac{d\widetilde{V}_{1}}{dt} = \frac{1}{2} \left[ \left( \frac{d\theta_{1}}{dt} + \widetilde{\omega} + \frac{1}{V_{1}} \frac{dV_{1}}{dt} \right) V_{1} \cos(\theta_{1} - \widetilde{\theta}_{1}) - \left( \frac{d\theta_{1}}{dt} + \widetilde{\omega} - \frac{1}{V_{1}} \frac{dV_{1}}{dt} \right) V_{1} \sin(\theta_{1} - \widetilde{\theta}_{1}) - 2\widetilde{\omega} \, \widetilde{V}_{1} \right]$$

$$(4.29)$$

Considering (4.24), (4.29) can be approximated by

$$\frac{d\Delta \tilde{V}_1}{dt} \approx \omega_n \left( \Delta V_1 - \Delta \tilde{V}_1 \right) - \omega_n V_n \left( \Delta \theta_1 - \Delta \tilde{\theta}_1 \right) + \frac{1}{2} \frac{d\Delta V_1}{dt} + \frac{V_n}{2} \frac{d\Delta \theta_1}{dt} - \frac{V_n}{2} \Delta \tag{4.30}$$

Using (4.25) and (4.30) the proposed can be constructed, and illustrated in Fig. 2.

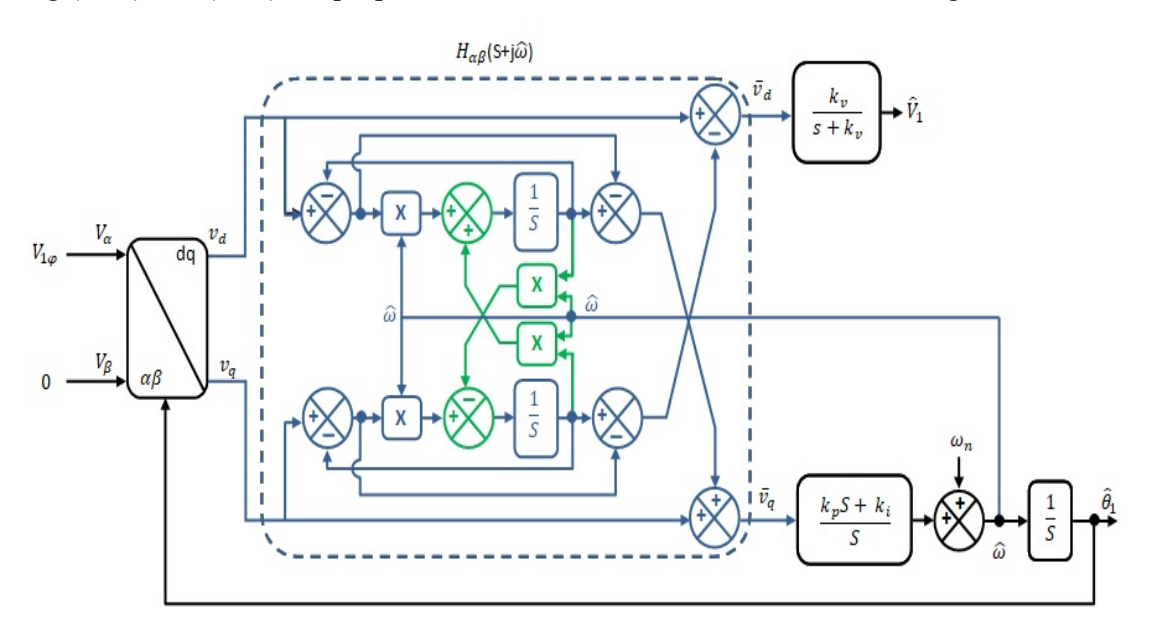


Fig. 4.12. APF-PLL control algorithm

### 4.3.4 Results and Discussion

A single-phase grid-connected PV system is constructed in this proposed study. The APF-PLL-based control strategy is designed to extract the fundamental component of the nonlinear load current. The P&O algorithm is utilized for maximum power extraction from the PV array. System performance is evaluated under various operating conditions, including load imbalance and fluctuations in solar irradiance.

## 4.3.4.1 Steady-State Performance of the Proposed System Under Constant Solar Irradiance

Fig. 4.13 illustrates the steady-state behaviour of a single-phase GCSPV system supplying a balanced nonlinear load under constant solar irradiance. The system's key parameters are analyzed in the steady-state regime. Under nonlinear load conditions, the proposed control strategy implemented through the VSC provides effective power delivery, achieves load balancing, and harmonic suppression in addition to improving overall PQ.

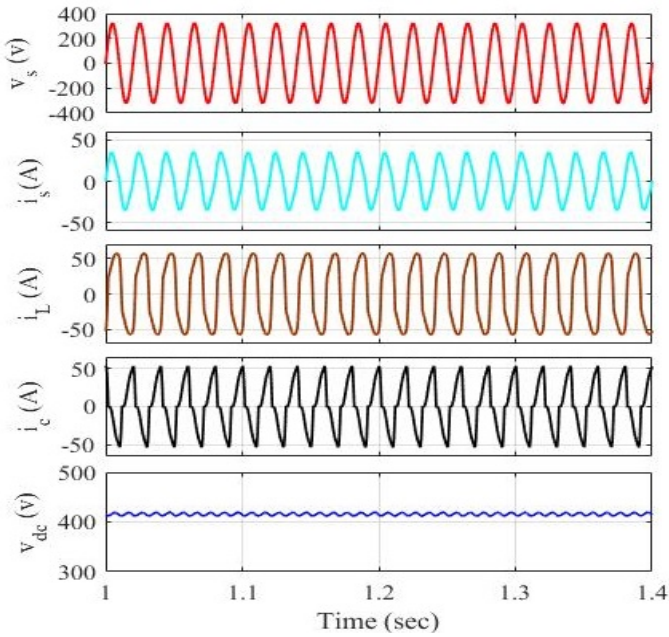


Fig. 4.13 Steady-state performance of the proposed system under constant solar irradiance given to a balanced load

### 4.3.4.2 Dynamic Response of the Proposed System to Solar Irradiance Variations

Fig. 4.14 shows the dynamic performance of the GCSPV system under varying solar irradiance conditions. At t = 1.2 seconds, the solar irradiance level rises from 450 W/m<sup>2</sup> to 900 W/m<sup>2</sup>. As depicted in Fig. 4.14(b), this change results in a corresponding decrease in the grid current. Despite variations in unbalanced load and solar irradiance, an APF-PLL-based control framework with VSC regulates dc-link voltage, compensator current, and grid voltage.

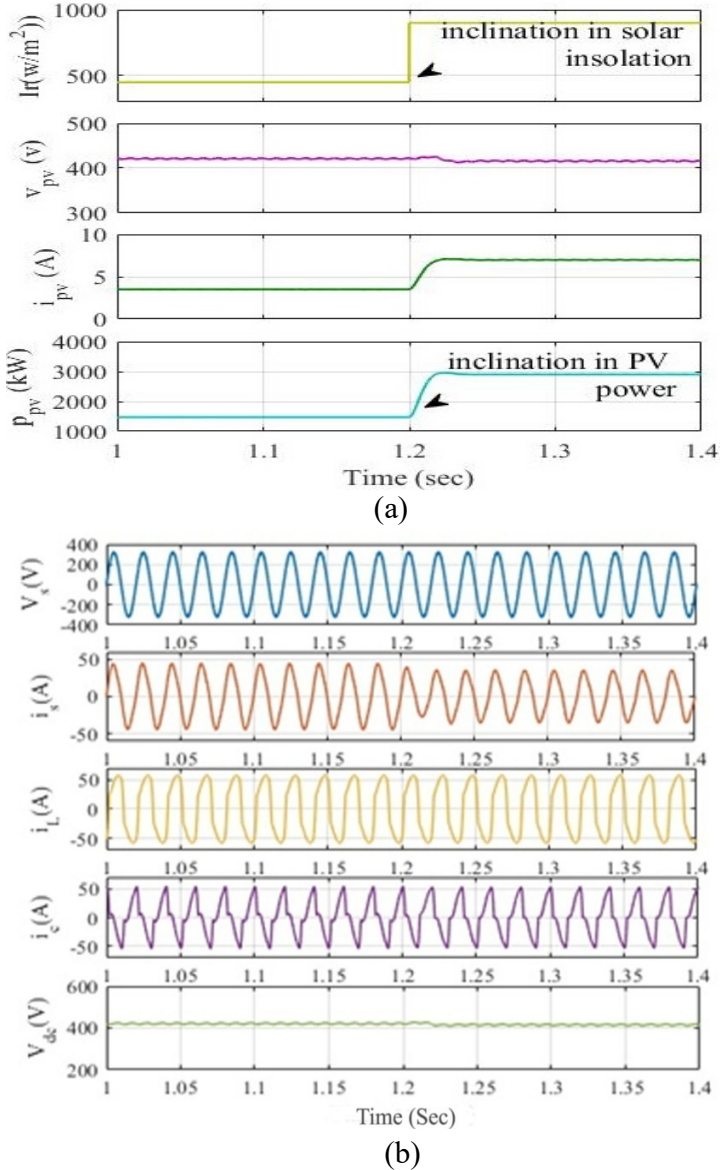


Fig. 4.14 (a) and (b) Dynamic output of proposed system in case of variation in solar irradiance

### 4.3.4.3 Dynamic Response of the Proposed System Under Load Variation

Fig. 4.15 illustrates the dynamic behaviour of a -phase GCSPV system operating under load variation while supplying an unbalanced nonlinear load. At t=1.1s, the load is disconnected, and it is reconnected at t=1.3s. During the load disconnection period, reductions are observed in the source current, load current, and compensator current. Despite the load variation, the controller effectively sustains a stable source voltage and concurrently regulates the DC-link voltage upward throughout the transient event.

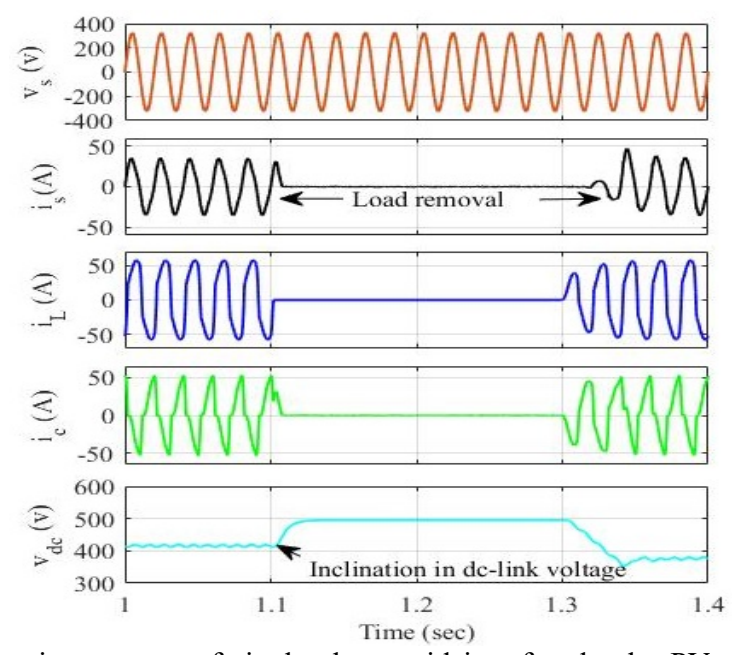


Fig. 4.15 Dynamic response of single-phase grid interfaced solar-PV system under load variation.

### 4.3.4.4 Power Curve Under Different Loading Conditions

Fig. 4.16 depicts the power response of a grid-connected solar PV system under various operating conditions, including constant and fluctuating solar irradiance, as well as unbalanced load. When solar irradiance and load are constant, the system produces a steady power output of 5.5 kW. A dynamic increase in irradiance from 450 W/m² to 900 W/m² at t = 1.3 s leads to a power increase from 5.5 kW to 7 kW. When irradiance decreases from 900 W/m² to 450 W/m² at the same timestamp, power output drops from 7 kW to 5.5 kW. Load removal between t = 1.1 s and t = 1.3 s increases power, while load insertion reduces it. Throughout all test conditions, the source voltage follows a sinusoidal waveform, and both

voltage and current harmonic distortions are less than 5%, ensuring compliance with the IEEE 519 standard.

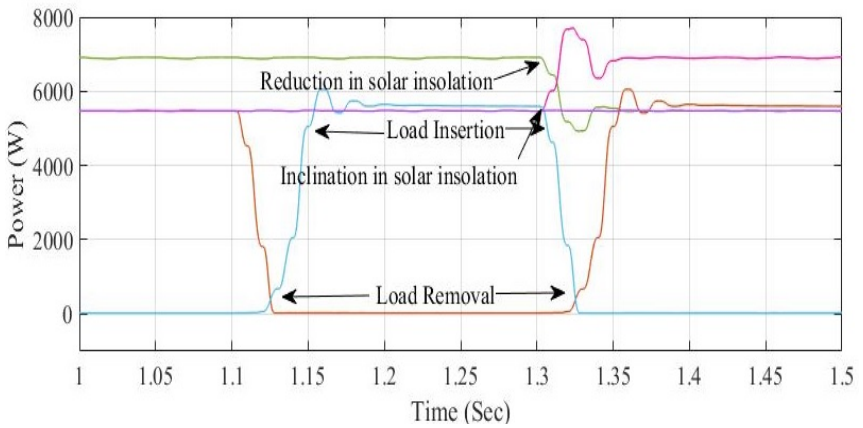
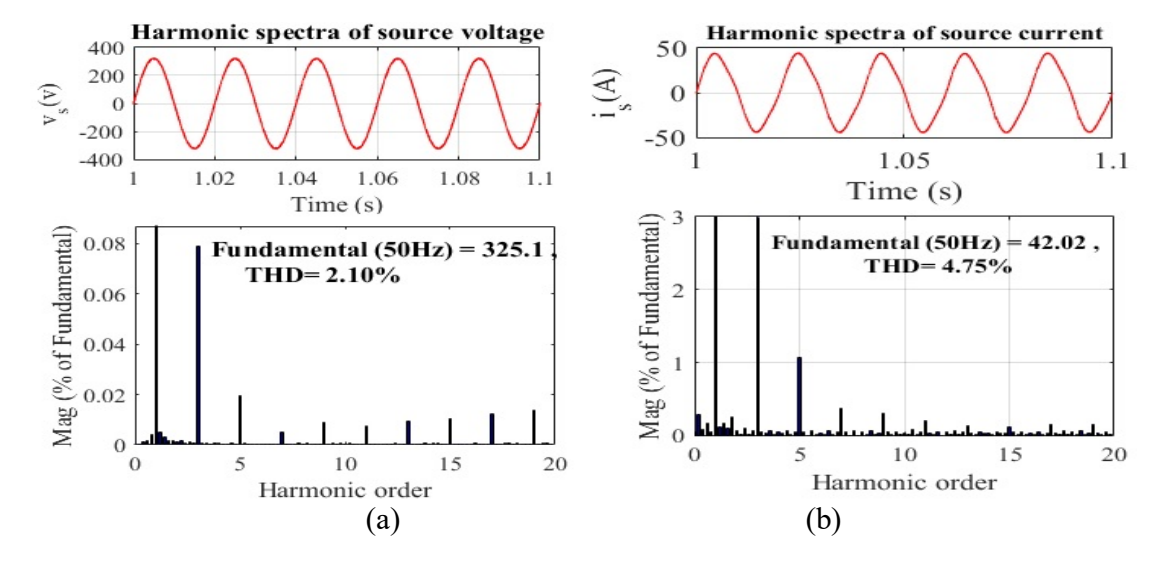


Fig. 4.16 Power curve under varying load conditions

### 4.3.4.5 Harmonic Analysis

Fig. 4.17(a)–(c) illustrates the THD observed in the load current, source current, and source voltage of the single-phase GCSPV system when operating under nonlinear load conditions.



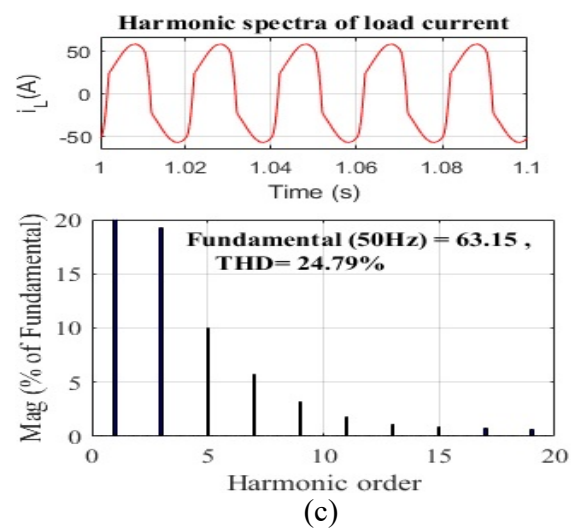


Fig. 4.17 (a)-(c) Harmonic analysis of (a) source voltage (b) source current, and (c) load current

The THD values observed for the load current, source current, and source voltage are 24.79%, 4.75%, and 2.1%, respectively. Under nonlinear loading conditions, the proposed VSC control effectively mitigates harmonics while preserving the quality of the source voltage. The source current and voltage THDs levels remain below the 5% threshold, thereby complying with the IEEE 519 standard.

### 4.3.4.6 Comparative Performance

Table-4.2 presents a performance comparison between the proposed APF-PLL control strategy and conventional control algorithms. The results indicate that the proposed method offers enhanced stability and effectively minimizes oscillations, particularly under varying solar insolation and dynamic load conditions.

Table-4.2 Performance comparison between the proposed APF-PLL and conventional control schemes

Features	SOGI-	EPLL	Proposed
	FLL		APF-PLL
Oscillations	Less	Less	Less
THD of Grid Current	4.87%	4.96%	4.75%
Stability	Good	Good	Better
Grid Synchronization	Yes	Yes	Yes

### 4.4 FOGI-FLL Control Approach

Fig. 4.18 illustrates the overall structure of the control algorithm. The maximum available power from solar PV arrays is transferred using the MPPT algorithm to maintain the desired DC bus voltage level, even in the face of changing weather conditions. A VSC switching algorithm generates the gating signals necessary for the VSC to carry out a number of functions, such as enhancement of power injection into the distribution system, achieving unity power factor activity, load adjusting, and compensating for reactive power. The control scheme utilizes inputs such as line voltages at the PCC, the amplitude of the primary load currents, feed-forward, loss components, and gating pulses to synthesize the in-phase unit templates for the IGBTs within the VSC [184].

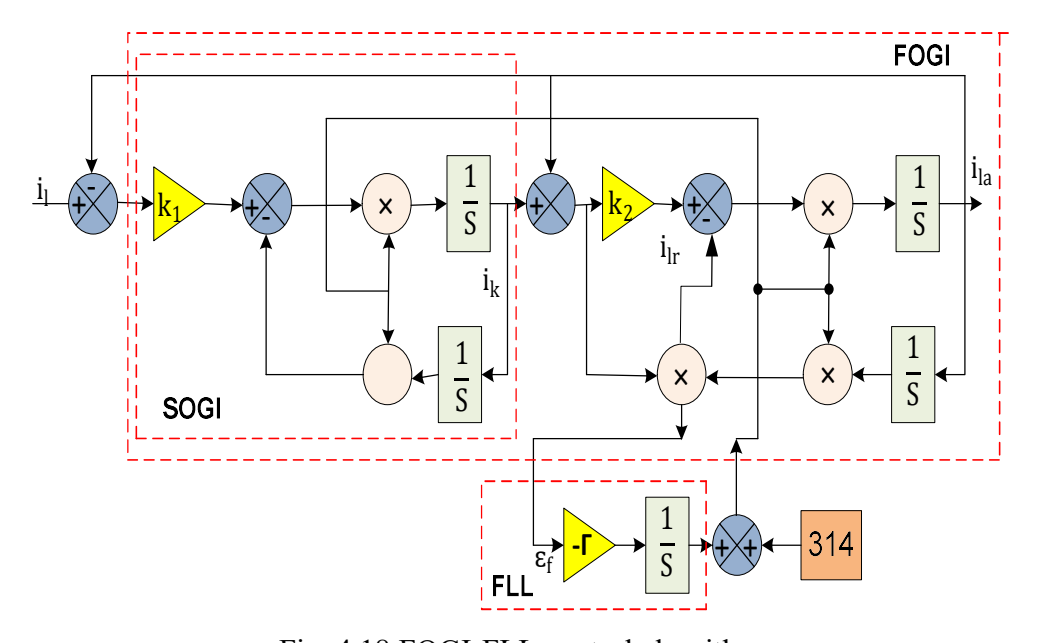


Fig. 4.18 FOGI-FLL control algorithm

### 4.4.1 MPPT Control

To ensure maximum power extraction, the system utilizes a P&O-based MPPT method. The control signal generated by the P&O algorithm regulates the duty cycle of the DC-DC boost converter, thereby maintaining the PV array at its MPP. The corresponding duty ratio is determined as follows,

$$D = 1 - \frac{V_{pv}^*}{V_{dc}} \tag{4.31}$$

Here,  $V_{dc}$  is voltage at DC link, and  $V_{pv}^*$  is the MPPT control output.

# 4.4.2 Estimation of the Peak Value of the Fundamental Load Current Component

Fig. 4.18 illustrates the basic structure of FOGI-FLL. Compared to SOGI-FLL, FOGI-FLL has better DC-offsets separation capacity and exhibits enhanced performance in consonant sifting skills. The lack of frequency evaluation has led to a decline in SOGI execution due to variations in frequency. The load current transmittance for the basic component that is in phase is provided as,

$$i_{la}(s) = \frac{K_1 K_2 \omega^2 s^1}{(s^2 + K_2 \omega s + \omega^2)(s^2 + \omega^2) + K_1 K_2 \omega^2 s^2} i_l(s)$$
(4.32)

Where,  $i_l$  represents load current and  $\omega$  is estimated frequency of the system. The load current transmittance corresponding to the quadrature fundamental component can be expressed as described in [184],

$$i_{lr}(s) = \frac{K_1 K_2 \omega^3 s^1}{(s^2 + K_2 \omega s + \omega^2)(s^2 + w^2) + K_1 K_2 \omega^2 s^2} i_l(s)$$
(4.33)

$$\dot{\omega} = -\Gamma((i_k - i_{la}) \times i_{lr}) \tag{4.34}$$

Where,  $i_k$  represents the intermediate control signal of FOGI-FLL and  $\Gamma$  is a constant. The peak magnitude and phase angle of the fundamental component of the load current are determined using equations 4.32 and 4.33, as outlined in [180].

$$I_{fl} = \sqrt{i_{la}^2 + i_{lr}^2} \tag{4.35}$$

$$\emptyset = \tan^{-1} \frac{i_{lr}}{i_{la}} \tag{4.36}$$

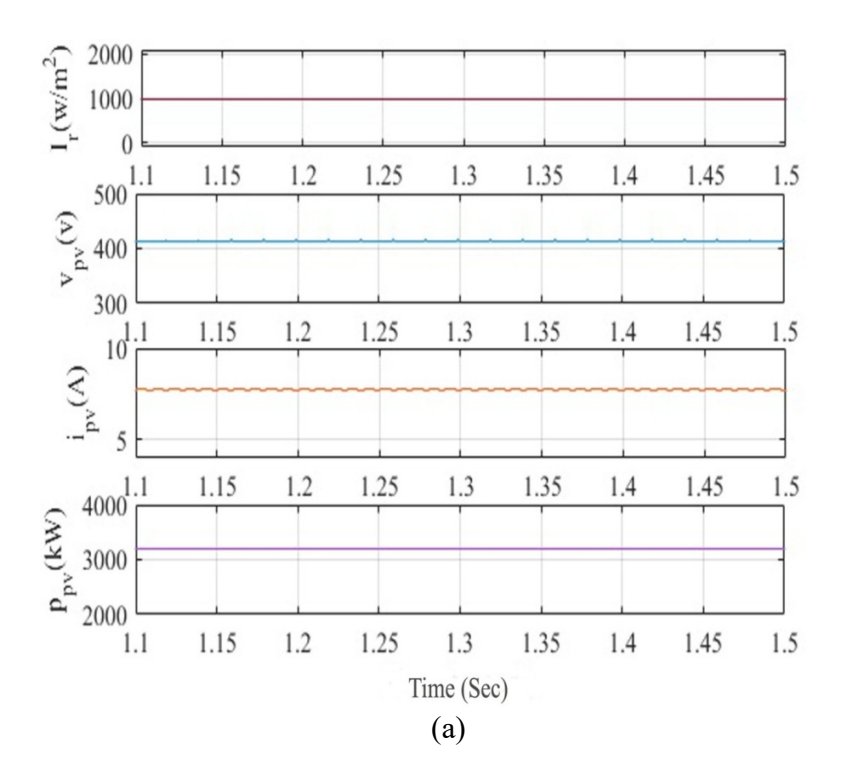
### 4.4.3 Simulation Results

This work proposes to interface a GCSPV system. VSC, nonlinear load, and a 5kW SPV are all included in the recommended system. The proposed configuration employs FOGI-FLL control with VSC to achieve active/reactive power correction, harmonic elimination, and enhance overall system power delivery of the recommended system. An imbalanced load and variations in solar insolation are two examples of the parameters that are used to analyse the simulated outcomes. Simulation results include waveforms of grid voltage

and current, load and compensator currents, as well as PV-side parameters such as DC-link voltage, PV voltage, current, and power.

## 4.4.3.1 Static Response of the Suggested System Under Fixed Solar Irradiance and Load

Fig. 4.19 illustrates the static behaviour of a single-phase GCSPV system supplying a balanced nonlinear load under constant solar irradiance. Specifically, Fig. 4.19(a) shows the solar irradiance maintained at 1000 W/m². Under these conditions, the PV power, PV current, and PV voltage are 3.1kW, 7.02A, and 400V, respectively. The steady state response of the DC voltage is investigated, together with the source current and voltage, load and compensator current, and so on. The control strategy implemented effectively extracts the fundamental component of the load current across a range of operating conditions. Furthermore, under nonlinear load situations, the recommended VSC-based control demonstrates load balancing, power support, harmonic suppression, and an overall improvement in PQ.



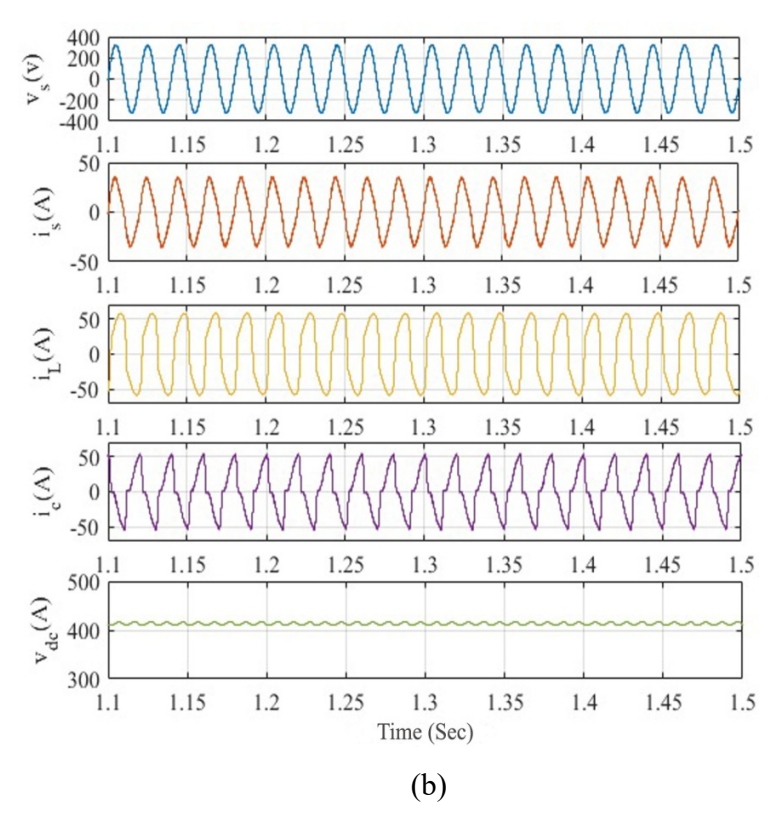


Fig. 4.19 Steady-state performance of the proposed system under constant solar irradiance supplying a balanced nonlinear load.

## 4.4.3.2 Performance Evaluation of the Proposed System Under Varying Solar Irradiance Conditions

The dynamic behaviour of the GCSPV system under sun insolation varies is shown in Fig. 4.20. The solar insolation decreases to 450 w/m² at t=1.8s from 900 w/m². Changes in solar insolation result in a drop in solar irradiance, PV power, voltage, and current. As illustrated in Fig. 4.20(b), the grid current increases in response to the decline in solar insolation. Despite these variations and the presence of an unbalanced load, the proposed controller, integrated with a VSC, effectively regulates the compensating current, DC-link and grid voltage under dynamic operating conditions.

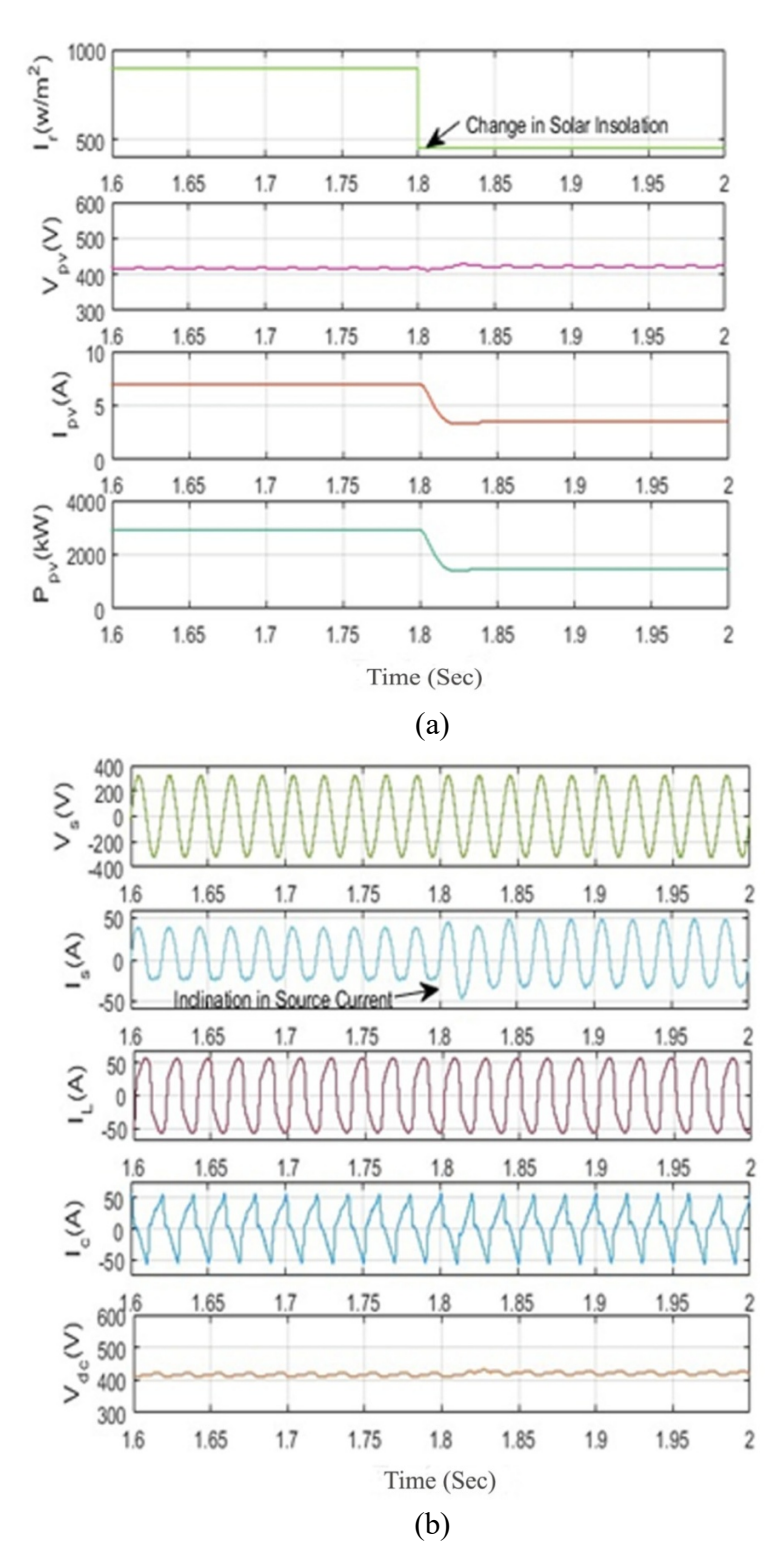


Fig. 4.20 (a) & (b) Performance response of the GCSPV system under varying levels of solar irradiance.

## 4.4.3.3 Effective Response of Suggested System Under Constant Solar Irradiance with Unbalanced Load Conditions

Fig. 4.21 illustrates the dynamic performance of the single-phase GCSPV system under an unbalanced nonlinear load at a constant solar irradiance level. At t=1.2s, the load is disconnected, and at t=1.4s, it is reconnected. The compensator, load and source current are all decrease while the load is being removed. Throughout the duration of the load removal, the controller raises the dc link voltage while maintaining a constant source voltage.

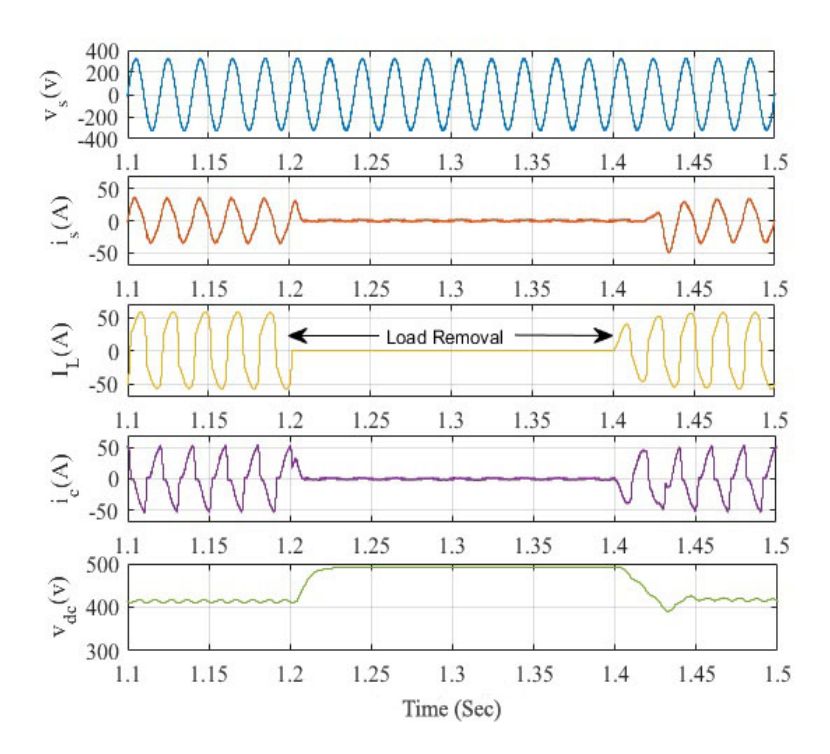


Fig. 4.21 Effective response of the system under fixed solar irradiance with unbalanced load conditions.

### 4.4.3.4 Harmonics Analysis of Suggested System

Fig. 4.22 illustrates the THD observed in the load current, grid current and voltage for a PV system interfaced with the grid under nonlinear load conditions. The measured THD values for the grid load, current, and voltage are 24.81%, 4.69%, and 1.99%, respectively. The proposed VSC control strategy effectively mitigates harmonic distortion in the presence of nonlinear loads while preserving grid voltage quality. The grid-side THD values remain below 5%, thus comply with IEEE-519 standards.

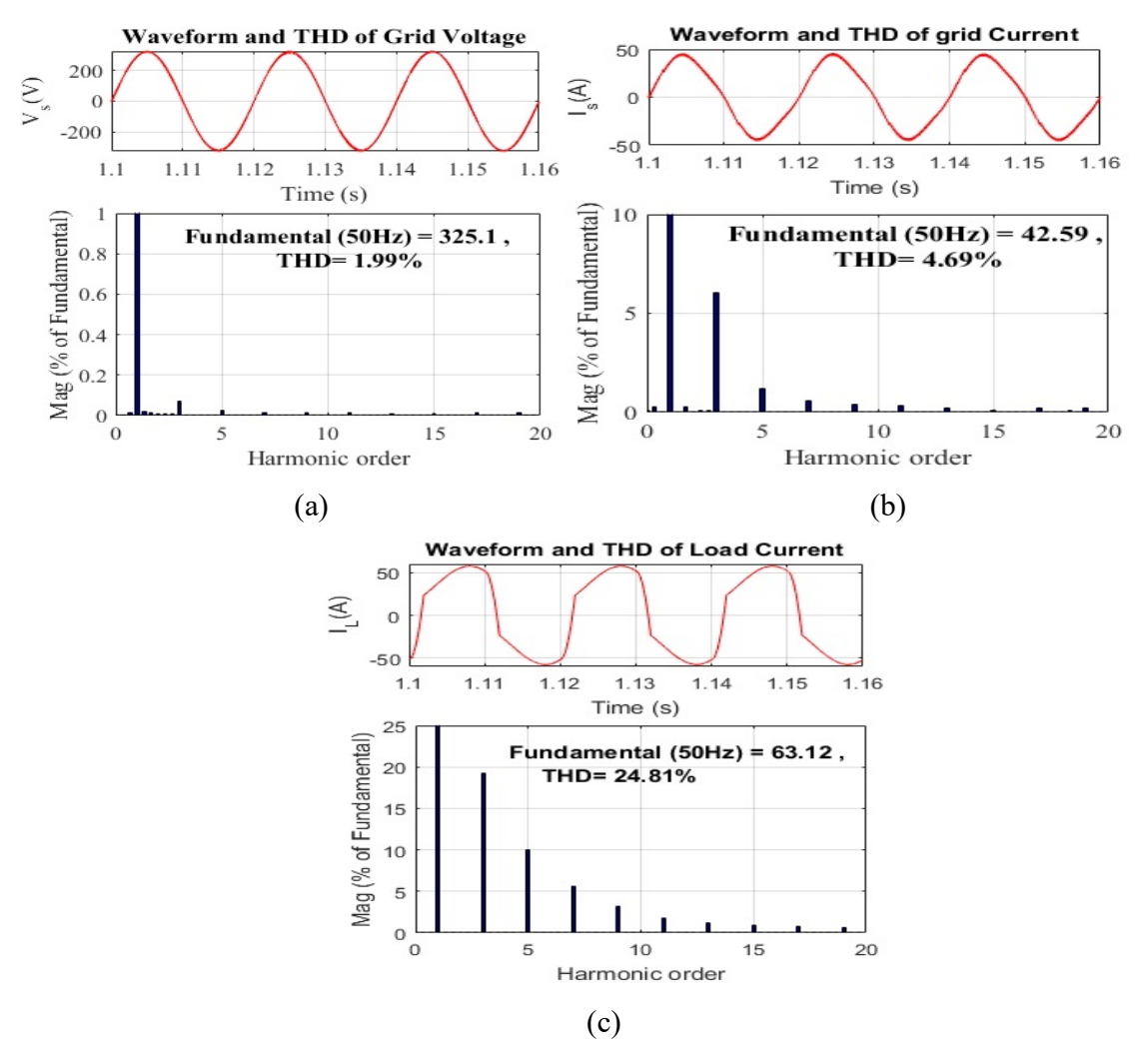


Fig. 4.22 THD performance of GCSPV system operating under nonlinear load conditions.

### 4.5 Summary

In this chapter, control strategies based on 1φ-CBF-FLL, FOGI-FLL and APF-PLL have been developed and implemented for a single-phase grid-connected Solar PV system. The effectiveness of all the above-said algorithms has been evaluated through simulation. The performance approves the above control algorithms with VSC and provides power compensation, harmonics abatement, DC-Offset reduction and voltage & frequency stabilization of the proposed system. The PQ has been improved under intermittency circumstances of solar and nonlinear load. Further, the MPPT technique (P&O) gives their better performance during the intermittent condition of solar power.

## **CHAPTER 5**

## STUDY OF CONTROL METHODOLOGIES FOR THREE-PHASE GRID-CONNECTED SOLAR PV SYSTEM

### 5.1 General

A3-PV Solar grid system has been proposed in this chapter which helps in improving the power quality of the system under non-linear demand scenarios. Both pristine and contaminated grid scenarios were employed to evaluate the proposed technique. To mitigate harmonics, several methodologies are employed, including the CC-ROGI-FLL control technique, an MPPT utilizing EDRL for inter-harmonic elimination, and a PLL integrated with a Novel COA for DC-offset correction. The first component of the approach is the ensemble deep reinforcement learning (DRL), which improves the maximum PPT process. Combining ensemble policy gradients with reinforcement learning is the strategy that is being explored here. Identifying the maximum PP of a solar PV may be accomplished through the employment of NN architecture designs that are tailored to the application. Through the utilization of weighted averaging, these agencies work together and share their information. Both the accuracy of the MPPT process and the diversity of the research are improved as a result of this. This ensemble strategy improves efficiency by reducing the impacts of interharmonics, which hurt the system and lower the quality of the electricity.

To mitigate the impacts of inter-harmonic oscillation, the voltage of DC-Link reference is established along system working utilizing the EDRL MPPT methodology. The EDRL controller employs a THD-based reward and punishment scheme to regulate the DC-link voltage,  $V_{\rm dc}$ . Electrical disruption that may occur in power networks between intervals that are inhabited by non-integer harmonics are interharmonics. These are between the usual integer harmonic frequencies. Instabilities in the power system, non-linear loads, voltage variations, and partial shedding are all potential causes of interharmonics As a result of the

predominance of non-linear loads, the grid may be able to absorb distorted currents, which is an important factor to take into account. There is a manifestation of vacuum distortion at the system bus whenever frequency-variable currents travel across the impedances of the power distribution system. For the purpose of mitigating the impacts of DC-offset, this technique makes use of a PLL as well as a COA-fuzzified PLL. In order to properly regulate grid current in real-time, the COA-fuzzified-PLL system makes use of a complex control method known as the COA. As soon as a DC-offset is identified in the current waveform, real-time corrections are implemented in order to reduce the amount of distortions that occur. When COA optimization is used to enhance the parameters of the membership functions, fuzzy logic controllers work at their most efficient level. When it comes to determining and removing DC-offset in a solar system that is linked to the grid, the COA-improved PLL is an effective method. The use of this method reduces the possibility of power quality problems and guarantees that the system will continue to be completely synced with the grid. The fundamental purpose of this technology is to improve the quality of solar PV systems of grid. This will be accomplished by optimizing energy extraction, raising power quality, and effectively resolving DC-offset and interharmonics.

The CC-ROGI-FLL removes or rejects disturbances prior to the FLL control loop while preserving proper dynamic behaviour. By significantly lowering the ripple magnitude in the fundamental load current, a CC-ROGI-FLL control method improves the capacity to remove harmonics. When compared to present controls, a CC-ROGI-FLL can effectively assess the amount of the fundamental load current component, resulting in better noise elimination and improved convergence with fewer oscillations. The proposed control provides power support, balancing of load, harmonic lessening and a reduction in the system's PQ issues under changing insolation and unbalanced load situations. The suggested system total harmonic distortions (THDs) at PCC are in limit with the IEEE-519 standard for source voltages and currents. To maximise power output from a solar PV system during periods of intermittent solar insolation, a P&O control algorithm is utilised.

### 5.2 CC-ROGI-FLL Control Approach

In the proposed system, control methods provide active and reactive power balance during load fluctuations, harmonic abatement, and voltage stabilization. When CC-ROGI-FLL control is used, the system operates with less oscillation and a quick dynamic return. Additionally, it extracts the fundamental load current component under various load and RES scenarios. The proposed system control structure is illustrated in Figure 5.1. A P&O based MPPT technique is created and put into practice to maximize power output from the SPV system under various solar energy circumstances.

### **5.2.1 P&O-Based MPPT Control**

The MPP voltage of PV during a change in insolation is extracted using the suggested P&O approach. The duty ratio is calculated using the measured DC-link voltage and the PV output voltage from the proposed MPPT technique. The steps for the P&O-based MPPT technique are as follows.

$$(if \Delta P_{pv} > 0) then \Delta P_{pv}(s) = P_{pv}(s) - P_{pv}(s - 1)$$
(5.1)

$$(if \Delta P_{pv}(s) > \Delta P_{pv})$$
 then  $v_{s \text{ new}}(s-1) = v_{sold} + \Delta v_{pv}$  (5.2)

(if 
$$\Delta P_{pv} < \Delta P_{pvold}$$
) then  $v_{s \text{ new}} = v_{s \text{ old}} - \Delta v_{pv}$  (5.3)

Where, the variations in SPV voltage and power are represented by  $(\Delta v_{pv})$  and  $(\Delta P_{pv})$ . The PV array's maximum power is denoted by  $(v_{s new})$ , while the step size for the PV voltage  $(v_{pv})$  is represented by  $(\Delta v_{pv})$ .

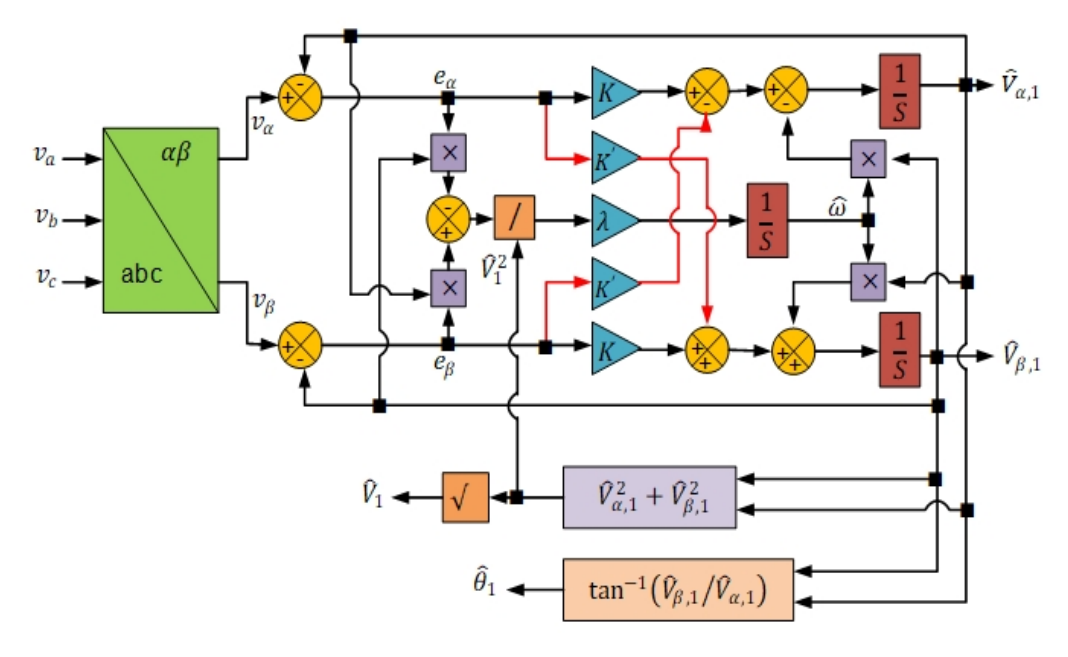


Fig. 5.1 CC-ROGI-FLL control algorithm

### 5.2.2 CC-ROGI –FLL Control Approach for VSC

This section presents the CC-ROGI-FLL small-signal modeling to make analysis easier. In order to do this, a few presumptions, definitions, and fundamental equations explaining the CC-ROGI-FLL dynamics are initially provided.

The signals at the  $\alpha\beta$ -axis of its input and output may be regarded as

$$v_{\alpha} = V_1 \cos(\theta_1), v_{\beta} = V_1 \sin(\theta_1) \tag{5.4}$$

$$\hat{v}_{\alpha,1} = \hat{V}_1 \cos(\hat{\theta}_1), \, \hat{v}_{\beta,1} = \hat{V}_1 \sin(\hat{\theta}_1) \tag{5.5}$$

Where  $\theta_1$  and  $V_1$  are the phase angle and amplitude of the grid voltage basic component, respectively, and  $\hat{V}_1$  and  $\hat{\theta}_1$ , as stated above, are estimates of these parameters. The estimated and actual numbers are thought to be quite near to one another.

For the small-signal modeling of the CC-ROGI-FLL, the following definitions are also provided:  $\Delta$  represents a minor perturbation, and nstands for the nominal value.

$$\omega = \omega_n + \Delta \omega$$

$$V_1 = V_n + \Delta V_1$$

$$\theta_1 = \theta_n + \Delta \theta_1$$

$$\hat{\omega} = \omega_n + \Delta \hat{\omega}$$

$$\hat{V}_1 = V_n + \Delta \hat{V}_1$$

$$\hat{\theta}_1 = \theta_n + \Delta \hat{\theta}_1 \tag{5.6}$$

The CC-ROGI-FLL dynamics are described by the following equations, which are also readily found from Fig. 5.1:

$$\frac{d\hat{v}_{\alpha,1}}{dt} = -\hat{\omega}\hat{v}_{\beta,1} + K(v_{\alpha} - \hat{v}_{\alpha,1}) - K'(v_{\beta} - \hat{v}_{\beta,1})$$

$$(5.7)$$

$$\frac{d\hat{v}_{\beta,1}}{dt} = \widehat{\omega}\widehat{v}_{\alpha,1} + K(v_{\beta} - \widehat{v}_{\beta,1}) + K'(v_{\alpha} - \widehat{v}_{\alpha,1})$$

$$(5.8)$$

$$\frac{d\hat{\omega}}{dt} = \frac{\lambda}{\hat{V}_1^2} \left[ \hat{v}_{\alpha,1} \left( v_{\beta} - \hat{v}_{\beta,1} \right) - \hat{v}_{\beta,1} \left( v_{\alpha} - \hat{v}_{\alpha,1} \right) \right] = \frac{\lambda}{\hat{V}_1^2} \left[ \hat{v}_{\alpha,1} v_{\beta} - \hat{v}_{\beta,1} v_{\alpha} \right]$$

$$(5.9)$$

$$\hat{\theta}_1 = \tan^{-1}(\hat{v}_{\beta,1}/\hat{v}_{\alpha,1}) \tag{5.10}$$

$$\hat{V}_1 = \sqrt{\hat{V}_{\alpha,1}^2 + \hat{V}_{\beta,1}^2} \tag{5.11}$$

### **5.2.3 Simulation Results**

The grid-connected PV system is comprehensively simulated, considering load imbalances and the intermittent nature of RESs during the system design. The core component is intended to be extracted from the load attached to the system using a control strategy based on CC-ROGI-FLL. The graphic shows the results of simulation based calculations for various operating situations.

#### **5.2.3.1** Response in Case of Steady State Condition

Figure 5.2 demonstrates the system's performance when the nonlinear load is powered by constant solar irradiation, maintained at 1000 W/m². The steady-state behavior of the DC voltage is analyzed, focusing on the source voltage, source current, load current, compensator current, and voltage. The proposed control method effectively extracts the fundamental component of the load current across various operating conditions. Furthermore, the recommended control provides load balancing, harmonic suppression, and power support under nonlinear load circumstances, all of which enhance overall power quality.

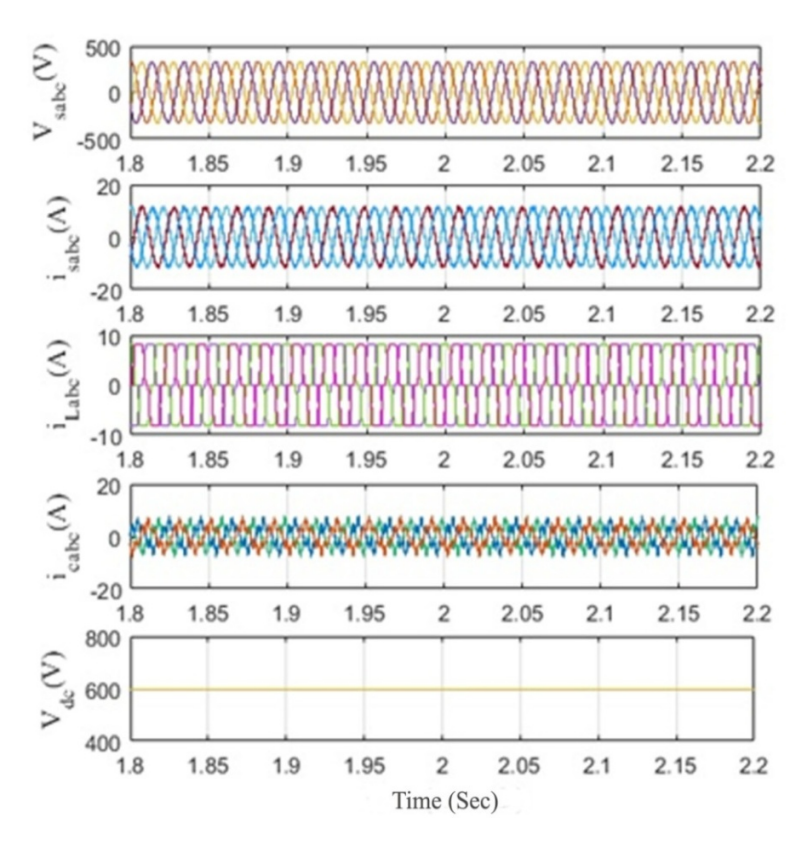
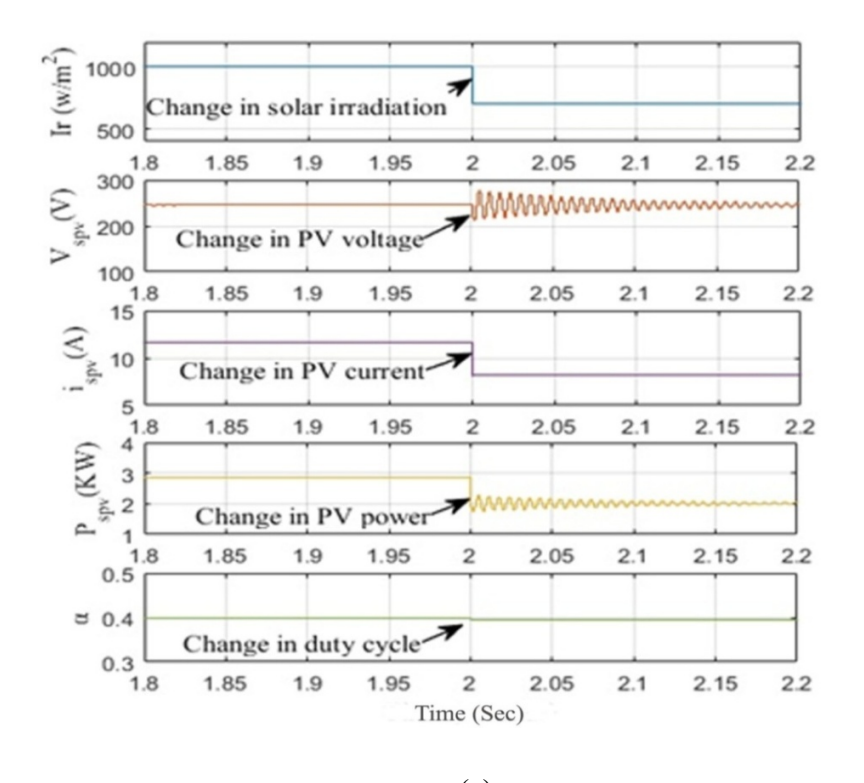


Fig. 5.2 Response at steady state condition

### 5.2.3.2 Response in Case of Varying Solar Insolation

Figure 5.3(a) and (b) show how the systems function dynamically when supplied with a constant nonlinear load at varying solar insolation. This one has a set temperature of 25 °C and a constant load while the solar insolation decreases from 975 w/m<sup>2</sup> to 675 w/m<sup>2</sup> at t=2s. As the solar insolation decreases, the PV current drops from 12.5A to 8.26A, the PV power (also known as solar power) drops from 2.7kW to 1.9kW, and the duty cycle likewise decreases (see Figure 5.3(a)). Figure 5.3(b) illustrates how the proposed controller effectively regulates the source voltage after a brief deviation caused by the abrupt shift in solar insolation at t=2s. The abrupt shift in solar insolation at t = 2s leads to a reduction in both the source and compensator currents. When solar insolation suddenly changes, a CC-ROGI-FLL-based controller keeps the system frequency steady.



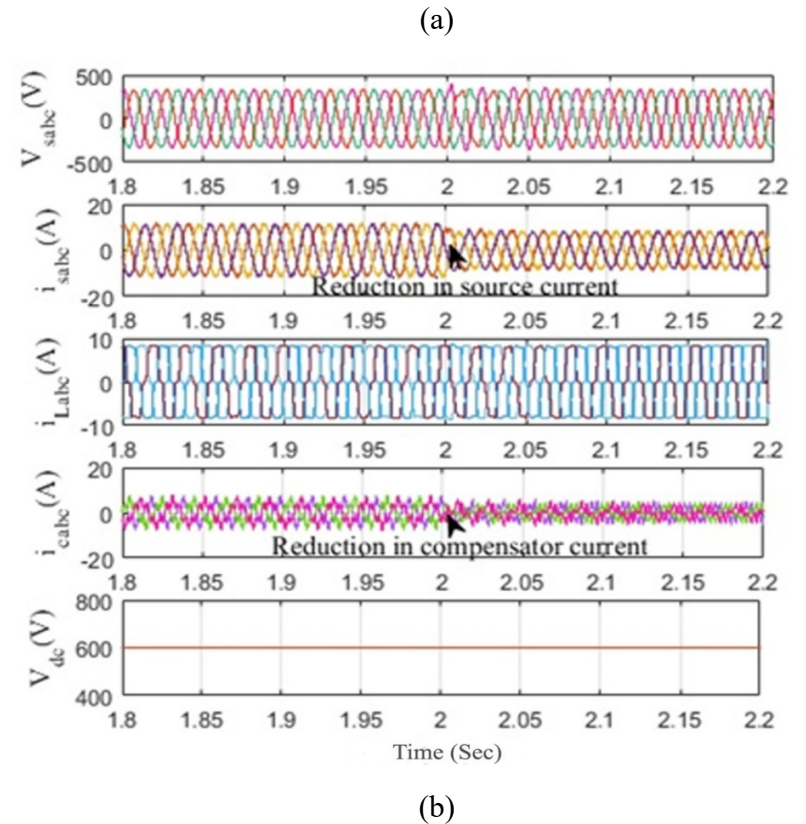


Fig. 5.3(a) and (b) Response in case of varying insolation

### 5.2.3.3 Response in Case of Unbalanced Load

Figure 5.4 depicts the constant solar insolation response of the system that supplies the distorted, unbalanced load. Phase "a" load is removed between t=1.9 and t=2.1 seconds. The system load current decreases and the compensation current increases during the abrupt shift in load. The abrupt drop in demand causes the system's total produced power to rise. As the load suddenly shifts from 1.9s to 2.1s, a controller based on CC-ROGI-FLL effectively stabilizes the system's frequency, ensuring the current and voltage at the PCC remain steady.

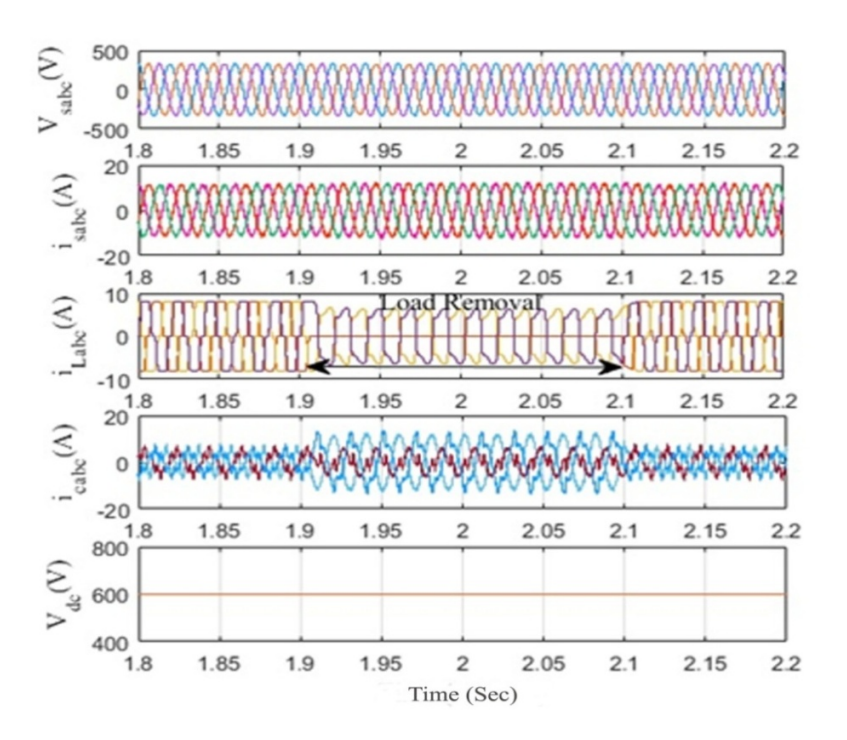


Fig. 5.4 Response in case of unbalanced load

### 5.2.3.4 Harmonic Analysis

Fig. 5.5(a)–(c) depicts harmonics analysis of the system. The research demonstrates that the load current, source current and source voltage have 24.08%, 3.85% and 1.73% of THDs respectively. The PCI currents are sinusoidal and have the least amount of harmonic distortion in steady state. The suggested VSC control provides harmonic correction under nonlinear load circumstances while preserving grid voltage. Less than 5% THDs for source voltage and current fall within allowable limitations and meet IEEE-519 standards.

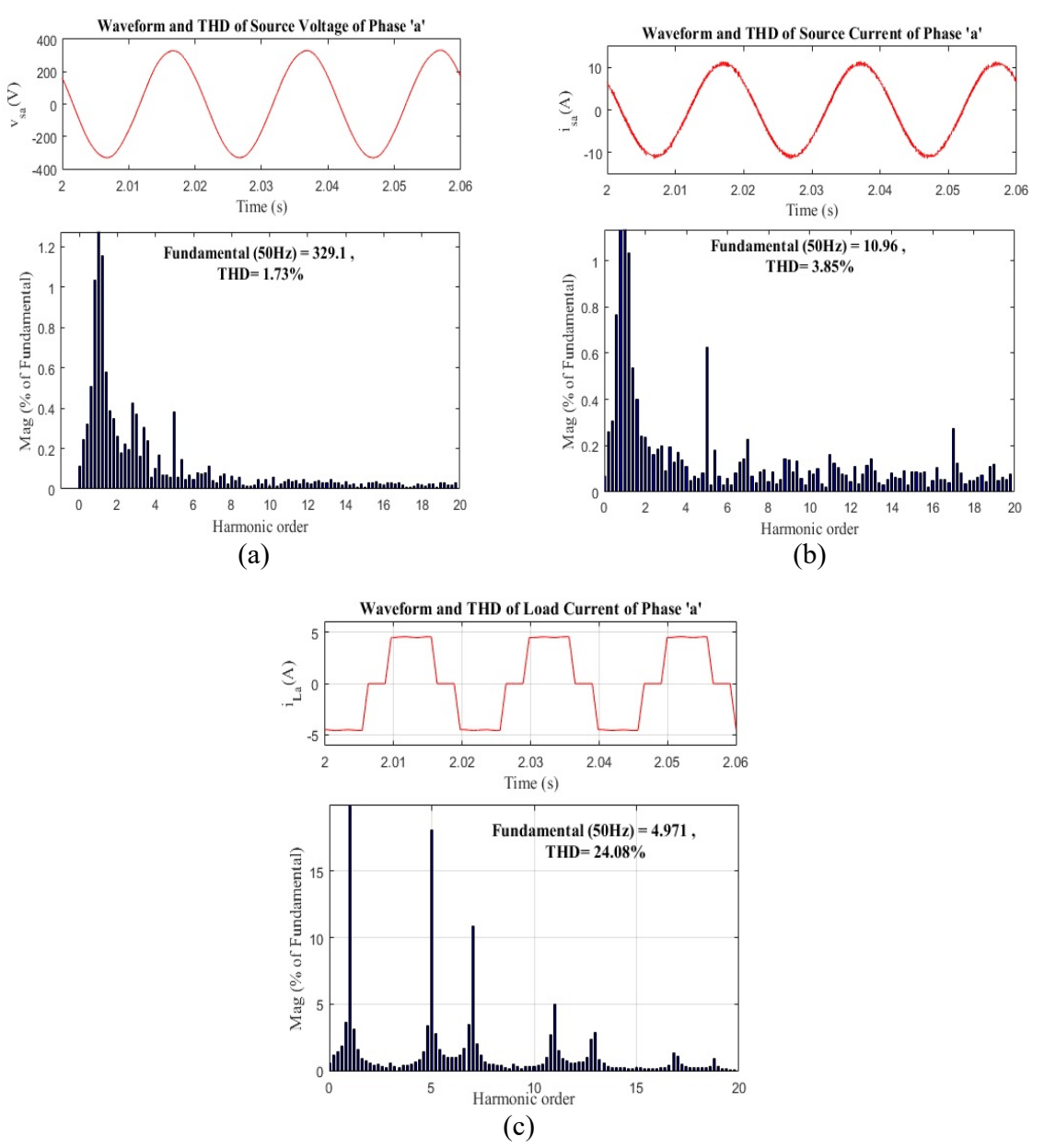


Fig. 5.5(a)-(c) Harmonic analysis

### 5.3 Interharmonic Mitigation via EDRL-MPPT

This research enhances power extraction from solar panels with a novel approach known as EDRLs. This system maximizes the harvesting of power by monitoring the solar array greatest power point and incorporating these techniques. MPPT plays a vital role in enhancing the efficiency of solar systems. The main goal is to improve the efficiency of these systems by continuously fine-tuning the operating point of the PV array to reach peak energy output. A reward system based on total harmonic distortion is utilised, and a consistent reference DC voltage is maintained at the DC connection. This is carried out to guarantee the successful fulfilment of the power extraction process. This method has the ability to diminish interharmonics and improve quality of power, making it one of its essential features. The EDRL-MPPT utilises the discrete (DQN, PPO) and continuous (DDPG and rlTD3) frameworks to illustrate system analogies. Figure 5.6 presents a visual representation of the EDRL.

The four main elements of DRL consist of the action space U, the function for reward r, and the space of state X [185]. The MPPT focuses on maximising power extraction from solar panels to improve the power output by ensuring the operating voltage that aligns with their MPP. Engaging with the environment helps the agent gain understanding about it. The proposed system moves from its present state  $x \in X$  to the subsequent state x(t+1) by performing an action  $x \in X$ . The THD reward acts as a quantifiable measure of the agent's actions or decisions, providing the agent with insights about its effectiveness. The motivation acts as a cue to concentrate on the attainable objective or the best resolution. The main goal of the reinforcement learning approach is to determine the best policy  $x \in X$  based on the given criteria.

$$J^* = \text{maximum}_{\pi} J_{\pi} = \text{max}_{\pi} \text{imum} E_{\pi} \{ r_t \mid x_t = x \}$$
 (5.12)

The cumulative expected reward associated with a specific policy  $\pi$  is denoted by the symbol  $J_{\pi}$ . For a given policy  $\pi$ , the expected cumulative reward, or value function over a specified time interval,  $V^{\pi}(x)$ , is defined as  $x^{\pi} = \{x_t\}_{t=1}^{t=n}$ , where  $k^{\pi} = \{k_t\}_{t=1}^{t=n}$  denotes the state values, and t = 1-n indicates the agent's action sequence.

### **5.3.1** State Space

The design for MPPT space of state issues involves analyzing the program of the MPP on the PV curve along the conditions of climates. The direct current voltage, PV current, and power of the coupling control the reinforcement learning process. The variables in the state-space are represented by the vector X, which is a sub space of  $X \in [V_{PV}, I_{PV}, P_{PV}, \Delta P_{PV}, \Delta P_{PV}, \Delta V_{DC}].X$  is the variable that controls the duty cycle selection within the interval [0,1]. Where,  $V_{DC}$  is the reference coupling voltage, and  $\Delta V_{DC}$  is the difference between the observed. Whereas, the divergence of PV power is represented as  $\Delta P_{PV}$ .

### **5.3.2** Action Space

In most instances, the MPPT issue is connected to a discrete action space. The method that was described earlier is not only practical in terms of its computing efficiency, but it also guarantees a high level of accuracy and functions as an effective educational instrument. There is a set duty cycle that the EDRL-MPPT agent operates according to. Assuming a discrete action space, the duty cycle  $D_c$  is determined by a sequence of operations that fall within the interval  $D_c$ =[0,1], with a precision of 0.01. This process yields a matrix with 100 distinct potential outcomes.

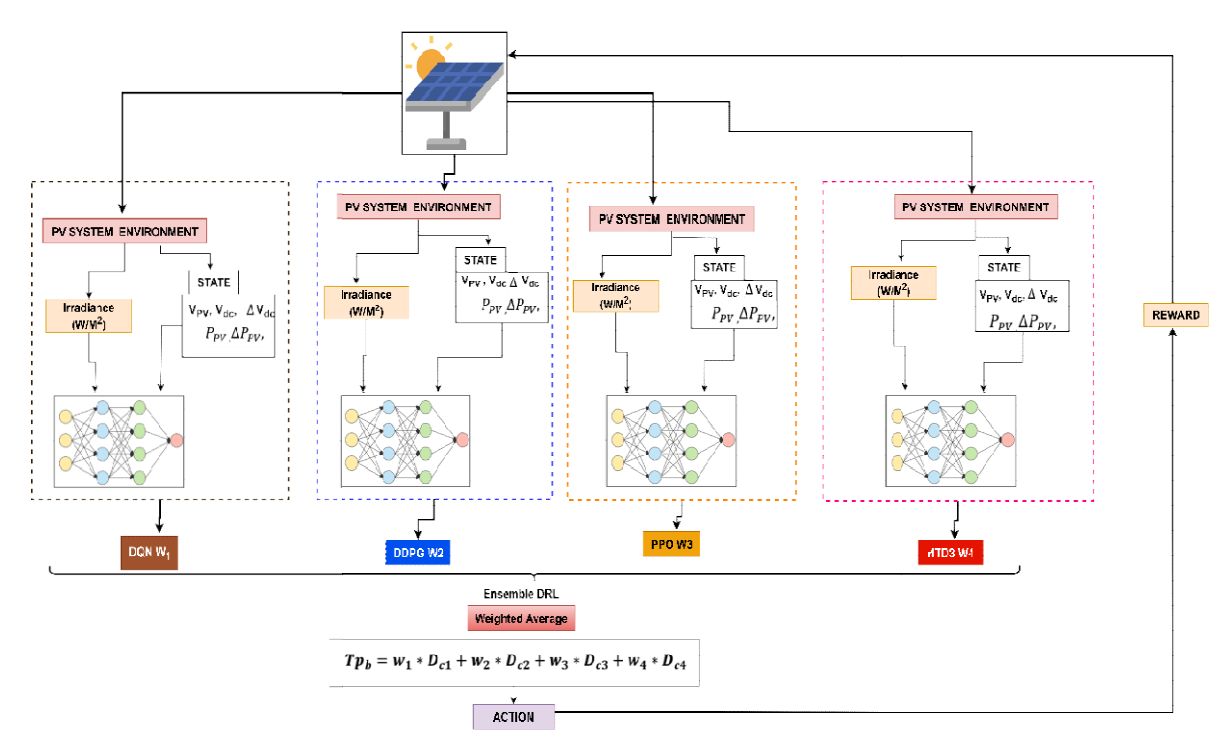


Fig 5.6. Three-phase grid-connected PV system using ensembled DRL for MPPT control

### 5.3.3 Reward

When an agent successfully completes an activity, they receive a reward. The reward signals were designed to reduce the overall distortion in the grid current harmonics. Overall, Distortions harmonics serve as an important measure that assesses the degree of THD as grid current waveform, highlighting its significance in the evaluation of power supply quality. Utilising THD as a driving force in EDRL allows agents to improve the effectiveness of control and operations of systems. This greatly aids in lowering THD while ensuring a stable electricity supply to the grid. The agents can work together to assess various control techniques, configurations, and switching procedures aimed at minimizing THD through the ensemble methodology. The group of agents can improve the quality of the solar system connected to grid power and reduce harmonic distortion by working together and using mistakes as chances to learn.

In three-phase PV systems connected to the grid, the THD of the grid current is used to assess the harmonic distortion found within the current's wavelength. This system allows for the implementation of a DRL incentive function that integrates THD to promote the reduction of harmonic distortions.

The current of grid in the THD can be expressed as:

$$THD = \sqrt{\left(\frac{l_{rms}}{l_1}\right)^2} \times 100 \tag{5.13}$$

Where  $I_1$  denotes the fundamental current component, and  $I_{rms}$  refers to each specific harmonic current component. The objective is to reduce the THD value by integrating it into the DRL reward function. One approach is to provide the THD with negative incentives that are proportional to their value. A description of the reward for THD is provided as follows.:

$$Reward = -K \times THD \tag{5.14}$$

While K serves as a constant which is scaling that regulates the influence of THD on the calculation of rewards. The objective of the DRL agent is to reduce harmonic distortions by acquiring rules that minimize THD values and implementing this reward function.

The proposed EDRL technique enhances the resilience and efficiency of the learning system by integrating a cohort of collaborative DRL models. A weighted ensemble technique in deep reinforcement learning entails training many deep reinforcement learning models, each with a distinct weight. A decision-making process employing weighted averaging or a similar aggregation method utilizing specified weights is implemented to consolidate the model's outputs. The weights may be constantly changed based on the model's quality, the conflicts between exploration and exploitation, and other pertinent aspects. This method aims to use the distinct talents and experience of each agent by allocating varying weights according to their confidence or performance levels. The weighted average DRL methodology is shown. This algorithm is the inaugural one. This research deployed four distinct neural network agents: rlTD3, DDPG, PPO, and DQN. To train each agent separately, we employed several architectures, exploration strategies, and parameter combinations, which will be elaborated upon in the subsequent paragraphs. Reinforcement learning techniques enable agents to engage with their environment, get rewards, and modify their strategies based on the outcomes of these interactions. Upon the completion of training for all four DRL models, the produced policy is employed to ascertain the cycle of operation, denoted as Dc. According to Equation (5.15), the overall probability may be expressed as the weighted average of the cycles comes from each distinct DRL. The sign Tp<sub>b</sub> denotes this.

$$Tp_b = w_1 * D_{c1} + w_2 * D_{c2} + w_3 * D_{c3} + w_4 * D_{c4}$$
(5.15)

The weights  $w_1$ ,  $w_2$ ,  $w_3$ , and  $w_4$  are the weights of DRL models proposed above. These weights are represented according to their respective values. In addition, the operational cycle is represented by the letters  $D_{c1}$ ,  $D_{c2}$ ,  $D_{c3}$ , and  $D_{c4}$ , this is the case for each and every DRL model. The training and saving of the models is accomplished by using the algorithms shown in [186]. The work in [186] is the source of the approach that was utilized in order to extract the outcomes based on average weight process of DRLs. Every model is subjected to the technique, yielding  $D_{c1}$ ,  $D_{c2}$ ,  $D_{c3}$ , and  $D_{c4}$ . Equation (5.15) yields the final weighted average action. The proposed model structure is illustrated in Fig 5.6.

In this context, the weights  $w_1$ ,  $w_2$ ,  $w_3$ , and  $w_4$  denote the discrete, continuous, rITD3, and discrete components of DQN, DDPG, and PPO, respectively. Each DRL model is characterized by its respective duty cycle, represented as  $D_{c1}$ ,  $D_{c2}$ ,  $D_{c3}$ , and  $D_{c4}$ . The models are trained and stored utilizing the algorithms PPO, rITD3 (continuous), DDPG (discrete), and DQN (discrete)[186]. The findings of the weighted average DRL method are based on the research cited as [186]. Upon executing the procedure on each model, the results obtained are  $D_{c1}$ ,  $D_{c2}$ ,  $D_{c3}$ , and  $D_{c4}$ . Utilize equation (5.15) to calculate the final weighted average. Figure 5.6 illustrates the proposed model structure.

#### Algorithm 1: EDRL THD Reward MPPT PV Control

- 1. Establish a connection to the solar PV array SunPower SPR-415E.
- 2. Determine the magnitude of the current and voltage that results from a short circuit and open circuit
- 3. Calculate the maximum power for  $N_S = 7$  (PV's in series) and  $N_p = 88$  (PV's in parallel) using  $P_{npp} = (N_S \times V_{mpp}) \times (N_P \times I_{mpp})$
- 4. Choose the DC-link voltage.
- 5. Set the EDRL agent's initial state, action, and reward.
- 6. State-space  $X = |V_{PV}, I_{PV}, P_{PV}, \Delta P_{PV}, \int \Delta P_{PV}|$
- 7. Action space U = (0,1]
- 8. Update duty cycle  $D_c$
- 9. calculate: e(t) and  $\Delta e(t)$
- 10. Pass the error and  $\Delta e(t)$  through
- 11. Provides these values to the network DQN, PPO, TD3, and DDPG
- 12. Initialize / Load Q,  $\alpha$  learning rate, and  $\gamma$  discount factor.
- 13. for j = 1to Mdo
- 14. Get initial state  $x_0$
- 15. for t = 1 to T do
- 16. Select action  $u_t$  from the set defined
- 17. Execute the action  $u_t$
- 18. Get a new state  $x_{t+1}$  and reward r
- 19. Store the transition  $(x_t, u_t, u_{t+1}, u_{t+1})$
- 20. IF |R| > N
- 21. Update the network using weighted average EDRL:
- 22. end if
- 23. Set  $x_t = x_{t+1}$
- 24. end for
- 25. end for

This investigation makes use of an EDRL approach to evaluate the behaviours of four different models, and it does so by employing a weighted average of those behaviours. With regard to the models, there are two that operate in an action space with continuous manner and discrete. It is anticipated that the following section will give further information concerning these models. A representation of the typical episode reward during the EDRL training process is shown in Figure 5.3.

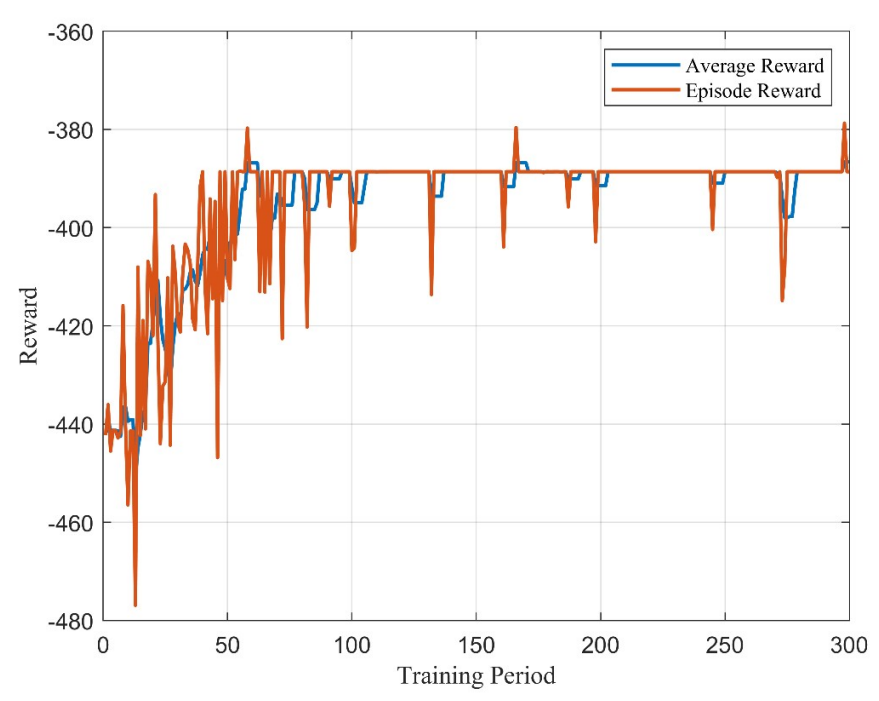


Fig 5.7. EDRL reward allocation per episode

#### 5.3.4 DQN (Discrete)

To handle a discrete action space, DQN and its variant, double Q-learning, are frequently used [187], [188], [189], [190]. According to the reference, choosing a policy to apply in DQN is dependent on determining which course of action would yield the most possible reward for the current condition. The main issue brought up in DQN is its tendency to overestimate Q-values, which makes it difficult to come up with the best plan of action. To mitigate this, policy-based methods have proven effective in managing DQN-related complexities. Algorithms such as DDPG and PPO exhibit adaptability across both continuous and discrete action domains. In this work, rather than implementing a continuous version of DQN, we adopt a DDPG-based framework tailored to discrete actions. This approach enables the model to compute a behavior policy by averaging over multiple actions with appropriate weighting.

State-action pairings are stored in DQN as  $\langle S_t, A_t, S_{t+1}, A_{t+1} \rangle$ .  $S_{t+1}, A_{t+1}$ . The states and actions at t+1 are  $S_{t+1}, A_{t+1}$ . DQN offers incredibly disassociated historical event data.

Weight loss function ( $\theta$ ):

$$L_i(\theta_i) = \mathbb{E}_{S, A \sim \rho(\cdot)}[(yS_i - Q(S, A; \theta_i))^2]$$
(5.16)

Equation (5.16) defines the loss function where  $y_i$  is the target value and  $Q(S, A; \theta_i)$  represents the current estimate of the action-value function parameterized by  $\theta_i$ . In the preceding iteration, the weights were  $\theta_{i-1}$ , and the corresponding target  $y_i$  computed as:

$$y_i = \mathbb{E}_{S' \sim \varepsilon}[r + \gamma \max_{A'} Q(S', A'; \theta_{i-1})]$$
(5.17)

Substituting the target  $y_i$  from Equation (5.17) into the loss function in Equation (5.16), the stochastic gradient descent is then applied to update the parameters accordingly.

$$\nabla_{\theta_i} L_i(\theta_i) = \mathbb{E}_{S, A \sim \rho(.)} [(r + \gamma \max_{A'} Q(S', A'; \theta_{i-1}) - Q(S, A; \theta_i)) \nabla_{\theta_i} Q(S, A; \theta_i)]$$
 (5.18)

The reward is represented by r, while the discount factor is denoted by the variable  $\gamma$ . The computing process executes a total of M iterations. Depending on the selected action, the agent picks a specific group of data tuples. The execution of tasks is performed in accordance with the formulation outlined in Equation (5.18). The outcome of the reward depends on the actions of the agent, which can result in either positive or negative consequences.

#### 5.3.5 DDPG (Continuous)

The DDPG model falls under the category of policy-based methods that may be used with discrete or continuous action spaces. The current method is suggested as a means of resolving issues with the DQN and lessening the effects of densely coupled NNs. The method outlined in [191]has proven effective in handling settings with continuous action spaces. As such, it is ideal for the contemporary environment of academic research.

There are two separate parts to the DDPG architecture: the critic and the actor. The actor is indicated by the symbol  $\mu(S|\theta^{\mu})$ ). An notation for the critic representation is  $(S,A|\theta^{Q})$ ).

The policy function represented by  $\theta^{\mu}$  and the Q represented by  $\theta^{Q}$  are both incorporated into the gradient update. The performers and critic share information with one another during every training cycle. The actor and critic networks in Deep Deterministic Policy Gradient (DDPG) soft update networks are represented by the notations  $\mu(S|\theta^{\mu'})$  and  $(S,A|\theta^{Q'})$ , respectively.

According to the nomenclature used in the text, the Target Q network is denoted by  $\theta^{Q'}$  and the Target policy network by  $\theta^{\mu'}$ . The policy function with direction,  $\theta^{\mu}$ , is often written as  $J(\theta^{\mu})$ ,, and its gradient is usually written as follows:

$$\frac{\partial J(\theta^{\mu})}{\partial \theta^{\mu}} = E[\nabla_{\mu(S)}Q(S, \mu(S|\theta^{\mu})|\theta^{Q})\nabla_{\theta^{\mu}}\mu(S|\theta^{\mu})]$$
(5.19)

In the DDPG framework, the critic network is trained to minimize the Mean Square Error (MSE) between predicted and target Q-values with respect to the taken action. Consequently, the corresponding loss function is formulated as

$$(\theta^{Q}) = E[(Q_{target} - Q_{predict})^{2}]$$
(5.20)

Where, 
$$Q_{target} = r + \gamma Q(S_{t+1}\mu(S_{t+1}|\theta^{\mu'})|\theta^{Q'})$$
 and  $Q_{predict} = Q(S,A|\theta^{Q})$ 

The target networks are updated every time and step by using soft updates, in contrast to the DQN technique.

#### 5.3.6 PPO (Discrete)

One essential part of the weighted ensemble technique used here is the PPO calculation. As noted in prior literature[191], it is an approach that constrains policy updates to ensure stability and consistency across successive policies. This is done to make sure the policies are in line with one another. This method can be effectively utilized in both discrete and continuous action spaces. For the action space for discrete issue with an on-policy framework, the scope of policy updates during execution is inherently limited. Using the critic network in accordance with the advantage function, the effectiveness of a selected action is assessed. The advantage function is given by equation (5.18).

$$\hat{A}_t = \delta_t + (\lambda_\gamma)\delta_{t+1} + \dots + (\lambda_\gamma^{T-t+1})\delta_{T-1}$$
(5.21)

$$\delta_t = r_t + \gamma V_{\pi}(S_{t+1}) - V_{\pi}(S_t) \tag{5.22}$$

The state-value function, represented by  $V_{\pi}(S)$  in Equation (5.19), is a representation.

$$V_{\pi}(S) = \mathbb{E}_{\pi}[\sum_{k=0}^{\infty} \gamma^{k} \, r_{t+k+1} | S_{t} = S]$$
 (5.23)

The policy under optimization is represented as  $\pi_{\theta}$ , while the policy used for environmental sampling is marked as  $\pi_{\theta old}$ . PPO ensures training process stability by using

the clipped surrogate goal to set boundary limits on the policy updates. A transformation is applied to the target function used in PPO, as shown in Equation (5.24).

$$J_{\theta} \approx \sum_{(S_{t}, A_{t})} \min\left(\frac{\pi_{\theta}(A_{t}/S_{t})}{\pi_{\theta old}} \hat{A}_{t}, clip\left(\frac{\pi_{\theta}(A_{t}/S_{t})}{\pi_{\theta old}}, 1 - \epsilon, 1 + \epsilon\right) \hat{A}_{t}$$
(5.24)

#### 5.3.7 rlTD3 Twin-Delayed DDPG (Continuous)

An actor-critic structure called TD3 combines value function on the current policy with action as a policy function. TD3 requires an ongoing area for action [192]. Value function overestimation is eliminated by TD3, the improved DDPG technique. Mitigating overestimation of the value function enhances precision and lowers variability. Every two steps, TD3's delayed actor network updates to ensure stability and effectiveness throughout training. When the action is chosen, targets are calculated using clipped noise. The model is resilient in all circumstances (continuous action space) when it has a high action value. While TD3 uses two Q-functions, delays policy updates to maintain stability, and smoothes the target policy, DDPG overestimates the Q-function. The targeted action policy  $\mu_{\theta targ}$ , is updated for DDPG as shown by equation (5.25).

$$A'(S') = clip(\mu_{\theta targ}(S') + clip(\in, -c, c), A_{Low}, A_{High}), \in \mathcal{N}(0, \sigma)$$

$$(5.25)$$

The resulting actions A are ensured to remain within the acceptable bounds, i.e.,  $A_{Low} \le A \le A_{High}$ 

Equation (5.26) defines the target value in the clipped double Q-learning mechanism:

$$y(r, S', d) = r + \gamma(1 - d) \min_{i=1,2} Q_{\phi_{i,targ}}(S', A'(S'))$$
(5.26)

The policy is optimized by maximizing the first Q-function as shown below:

$$\max_{\theta} \mathbb{E}[Q_{\phi_1}(S, \mu_{\theta}(S))] \tag{5.27}$$

The Q-network parameters are updated using a one-step gradient descent approach, as given by:

$$\nabla_{\phi_i} \frac{1}{|B|} \sum_{(S,A,r,S',d)} (Q_{\phi_1}(S,A) - y(r,S',d))^2 , \text{ for } i = 1,2$$
 (5.28)

Correspondingly, the policy parameters are updated via a single-step gradient ascent procedure:

$$\nabla_{\phi_i} \frac{1}{|B|} \sum_{S \in B} Q_{\phi_1}(S, \mu_{\theta}(S)) \tag{5.29}$$

## 5.4 DC-Offset Mitigation Using Improved PLL

There is usually a DC-offset voltage module included in the output of a PV inverter. A number of variables, including differences in current sensing and other modules contribute to this occurrence. As discussed in [3], the sense of such an offset in the grid voltage can lead to erroneous estimations of grid voltage amplitude and frequency. Two factors influence the produced ripple amplitude: the power grid's basic frequency and the proportion of the offset value. Therefore, the grid parameter estimate process is essentially impossible when there is an offset in the observed grid voltage. In order to mitigate induced offset, an innovative technique is presented here. Figure 3 illustrates how the suggested strategy uses a COA Fuzzified-PLL-based controller. The Proportional-Integral (PI) controller was swapped out for a FLC, forming the Fuzzified-PLL. To optimize the fuzzy inference system, scaling factors and rule base, the Coati Optimization techniques are used. In order to address the ambiguity and imprecision related to DC-offset, fuzzification is used, which turns the input signals into fuzzy sets.

A VCO is used in the procedure, and its phase is adjusted until the two signals align phasewise. The operational efficiency of PLLs can be negatively impacted by a range of issues, including noise, non-linearities, and sudden shocks [109]. These restrictions are somewhat addressed by the PLL architecture's incorporation of fuzzy logic. Each phase angle leap is followed by changes in the angular phase angle( $\Delta\theta$ ). In order to handle both rapid and subtle changes, phase angle change is applied. In a typical PLL device, the fuzzy controller is inserted between the low-pass filter and the phase detector in the suggested model.

In conventional PLL systems, Clarke's transformation is applied. It is then further transformed using Park's transformation to the dq rotating frame, as seen in Fig 1. The PLL framework's current control mechanism is the subject of the recommended adjustment. A fuzzy logic controller is introduced, which takes as input the error between the reference and measured current components,  $I_d$  and  $I_q$ . The Fuzzified-PLL modelling architecture is shown in the equation. The three-phase voltage magnitudes are represented by the variables  $V_a$ ,  $V_b$ , and  $V_c$ .

$$\begin{bmatrix} V_a \\ V_b \\ V_c \end{bmatrix} = \begin{bmatrix} V_m \cos \theta \\ V_m \cos(\theta - 2\pi/3) \\ V_m \cos(\theta + 2\pi/3) \end{bmatrix}$$
(5.30)

The Clarke transformation is applied to convert the signals into the stationary frame signals  $V_{\alpha}$  and  $V_{\beta}$ , and the Park transformation is applied to convert these signals into the dq frame.

$$\begin{bmatrix} V_{\alpha} \\ V_{\beta} \end{bmatrix} = \frac{2}{3} \begin{bmatrix} 1 & -\frac{1}{2} & -\frac{1}{2} \\ 0 & -\sqrt{3}/2 & \sqrt{3}/2 \end{bmatrix} V_{\alpha} V_{b} V_{c}$$
 (5.31)

$$\begin{bmatrix} V_d \\ V_q \end{bmatrix} = \begin{bmatrix} \cos \theta^* & -\sin \theta^* \\ \sin \theta^* & \cos \theta^* \end{bmatrix} \begin{bmatrix} V_\alpha \\ V_\beta \end{bmatrix}$$
 (5.32)

$$V_d = V_{\alpha} cos\theta^* - V_{\beta} sin\theta^* \approx V_{d,Offset} + V_m$$
 (5.33)

$$V_q = V_{\alpha} sin\theta^* + V_{\beta} cos\theta^* \approx V_{q,offset} - V_{me}$$
 (5.34)

The magnitude of the predicted angle, the input angle, and the voltage are represented by the symbols  $\theta^*$ ,  $\theta$ , and V respectively. e represents the phase angle error. The primary goal of the suggested controller is to remove the DC-offset present in the synchronous d and q-axis components, which are represented by the equations  $V_{d,offset}$  and  $V_{q,offset}$  respectively.

The fuzzy logic controller determines appropriate control actions by interpreting input variables through predefined fuzzy sets and a structured rule base, enhanced with optimized parameters. These control signals dynamically adjust the parameters of the PLL to effectively suppress the DC-offset component. The fuzzy control mechanism operates in three core stages: fuzzification, inference, and defuzzification. During fuzzification, numerical inputs are transformed into linguistic variables represented by fuzzy sets. The efficacy of the optimized fuzzy-PLL is assessed based on its capability to minimize DC-offset and enhance PQ.

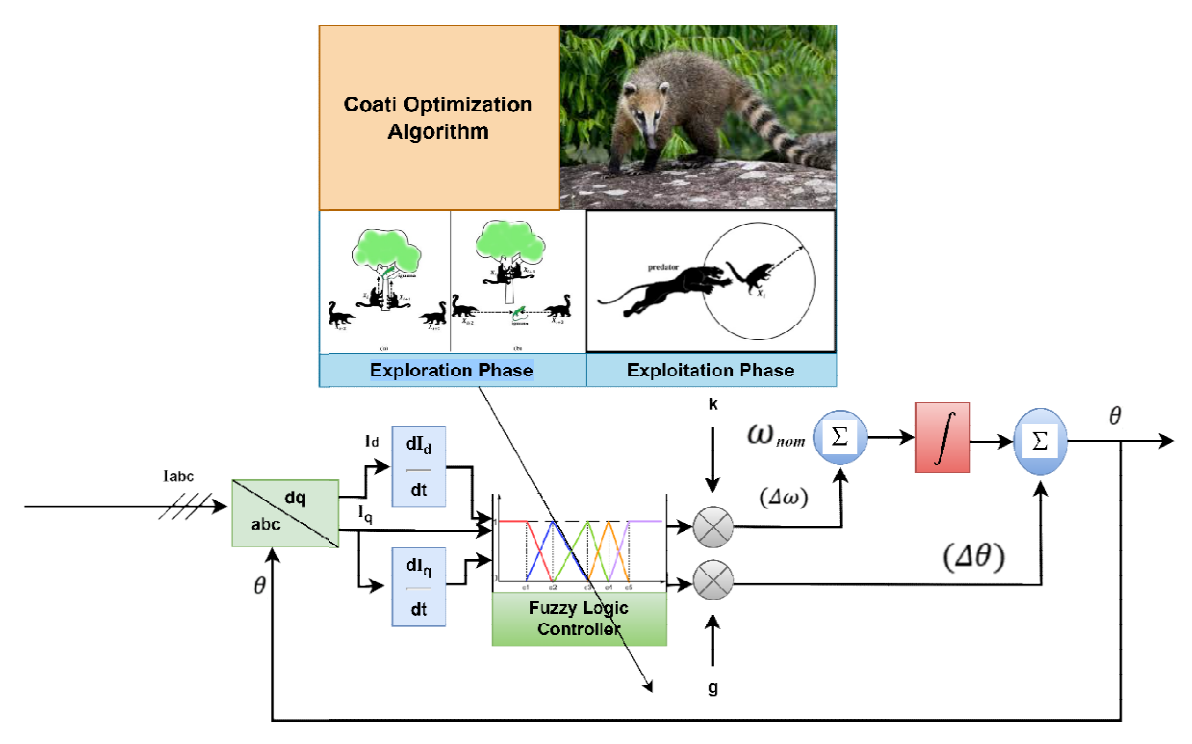


Fig 5.8. COA Fuzzified-PLL based Controller

Fuzzified-PLL parameter optimization is done using the Novel Coati Optimization technique. A detailed model of a fuzzy PLL is shown in Fig 5.8. Among the many benefits of the global optimization COA technique are its excellent research and search process balance, its capacity to tackle high-dimensional, complicated issues in a variety of disciplines, its lack of control parameters, and its efficient handling of optimization applications. The COA method must be used to optimize 18 locations of the membership functions given the presence of one output and two inputs. The controller under investigation uses linguistic variables to determine the error and error rate: positive big (PB), medium positive (PM), small positive (PS), zero (ZE), small negative (NS), negative medium (NM), and negative large (NB) Their matching memberships serve as a means of distinguishing these factors.

For every coati, the research consists of changing eighteen membership function points. Based on the error that results, a fuzzified-PLL system is then assessed. Two inputs have membership ranges of [-10 to 10] and [-1 to 1], whereas one output has a membership range of [-10 to 10]. Throughout the simulation, the aforementioned ranges don't change and stay unchanged. It's also important to remember that every membership function has two sites of

intersection with other membership functions. Table 5.1 offers convincing proof for this claim.

Table 5.1 Controller range Triangular (Tri) or Trapezoida (TZ)

Range parameters	Functions
$[x(5), x(6), 0.032, \infty]$	TZ
[x(4),x(5),x(6)]	TR
[0,x(4),x(5)]	TR
$[-\infty, -0.032, x(1), x(2)]$	TZ
[x(1),x(2),x(3)]	TR
[x(2), x(3), 0]	TR
[x(3),0,x(4)]	TR

With the information in Table 5.1, it is easy to predict the most common values. When dealing with a single variable, the tuning procedure calls for modifying four distinct values. Nevertheless, the total number of values that need to adjusted rises to 18 when working with three variables. There are several limitations that need to be taken into account while modifying these values.

There are several restrictions on the problem, which are shown in Table 5.2 mandate that each value meet the predetermined conditions for inequality:

Table 5.2. Fuzzy Controller constraints

<b>Boundary Condition</b>	Input		
-1 to 1	Phase angle output $\Delta\theta$		
-10 to 10	Change in Error $\Delta E$		
-0.032 to 0.032	Error E		
x(1) < x(2) < x(3)	Order		

After making changes to the fuzzy controller membership function values, the model is run with the updated values. The goal function value will be represented by the THD, which will be the aim to be minimized.

$$objective function = minTHD$$
 (5.35)

Detailed versions of the above-mentioned formulas for phase angle changes are shown in Table 5.3. The derivative of the grid voltage q-axis component is also considered an input to the FLC. Fuzzy Logic Controllers (FLCs) outputs must be multiplied by two variables in order to include variables with different ranges. The variables k and g represent the parameters shown in Fig. 5.3. A detailed model of a fuzzy PLL is shown in Figure 5.3.

Table 5.3 Fuzzy rule for output variable  $\Delta\theta$ 

Δθ	NB	NM	NS	ZE	PS	PM	PB
NB	NB	NB	NB	NM	NM	NS	ZE
NM	NB	NB	NM	NM	NS	ZE	PS
NS	NB	NM	NM	NS	ZE	PS	PM
ZE	NM	NM	NS	ZE	PS	PM	PM
PS	NM	NS	ZE	PS	PM	PM	PB
PM	NS	ZE	PS	PM	PM	PB	PB
PB	ZE	PS	PM	PM	PB	PB	PB

Using coati optimization, the fuzzy controller settings are adjusted. The parameters' overall form changes as a result of the tuning process, which modifies the parameters' initial values. The numbers depicted in Fig. 5.9. The improved fuzzy logic membership functions, which now cover a wider range, are shown in (a) through (c). These changes have been made to make it easier to use the coati optimization technique to identify the least mistake.

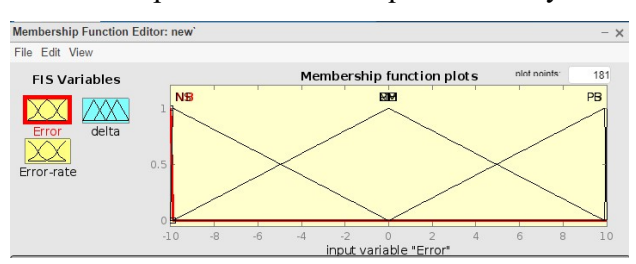


Fig 5.9 (a): Function of Membership for input E optimized using the Coati algorithm

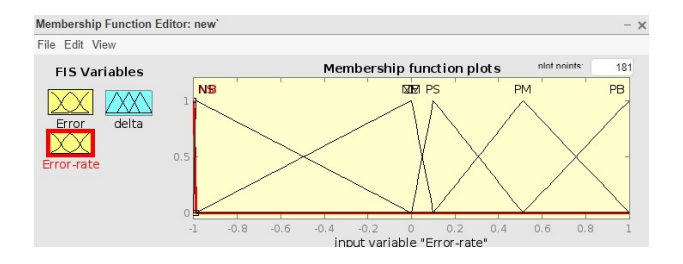


Fig 5.9 (b): Function of Membership for input  $\Delta E$  optimized using the Coati algorithm

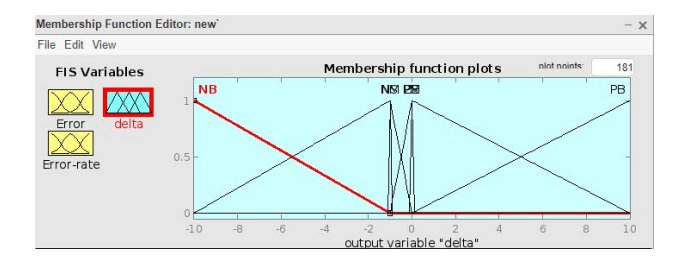


Fig 5.9 (c): Membership function for input  $\Delta\theta$  optimized using the Coati algorithm

#### 5.5 Simulation Results

We have simulated and assessed the efficacy of the COA-Fuzzified PLL synchronization strategy and the suggested EDRL-MPPT algorithm aimed at mitigating interharmonics. Three separate examples have been run through the simulation, as follows:

- The PV inverter operates under constant solar irradiance, representing a steady-state MPPT condition at its rated capacity of 250 kW. Under this condition, significant inter-harmonic distortion is typically observed. This scenario investigates the effect of interharmonics when utilizing the conventional P&O MPPT algorithm in conjunction with a traditional PLL-based synchronization method in a grid-connected three-phase PV system.
- In this scenario, the improved MPPT method is applied along with the conventional PLL synchronization approach to assess its effectiveness in reducing interharmonics within a grid-connected three-phase PV system.
- This case addresses the occurrence of offset due to sudden load variations. To mitigate
  the disturbances introduced by such offsets, the combination of the EDRL-MPPT
  method and the proposed synchronization strategy is proposed.

One significant source of interharmonics in grid current arises from the transient behavior of the DC-link voltage controller, particularly under partial shedding conditions, as discussed earlier. Maintaining a stable DC-link voltage during operation is essential for mitigating interharmonic distortion in PV inverters. To address this, an EDRL-MPPT strategy is employed, facilitating improved voltage regulation. In this study, a reward mechanism based on the THD of the grid current is integrated into the EDRL framework, guiding the agent to select actions that minimize harmonic distortion. This approach effectively suppresses

interharmonic components. Figure 5.10 compares the performance of conventional P&O MPPT with the proposed method stability and interharmonic suppression in the output waveform.

In the traditional scenario, the reference DC-link voltage (also known as the PV voltage) is determined during operation using an MPPT technique, such as P&O, in order to maximize power extraction from the solar system. A PLL controller is then used by the dc-link voltage controller to regulate the  $V_{dc}$ . The current is managed by this controller. Figure 5.10 shows the result, represented as  $(V_{dc})$ , that was achieved by utilizing the standard phase-locked loop control method in conjunction with the typical MPPT methodology. In the first case, the MPPT procedure was assessed using the P&O approach. It is noteworthy; nevertheless, that the injected grid current associated with this process exhibits a far larger degree of distortion, as Figure 5.11 shows. Another way to see the difference in waveform is to look at a magnified plot with a range of 0.1 to 0.2 seconds.

As shown in Fig. 5.12, the frequency spectrum under the P&O algorithm exhibits a THD of 8.90%. To address the issue of a rise in harmonics, an EDRL-MPPT scheme is introduced. This method leverages a distortion-sensitive reward-punishment mechanism to actively minimize harmonic disturbances in the grid current. Furthermore, the proposed system integrates PLL synchronization to ensure improved dynamic response and stability.

Figure 5.10 shows the response of system to a quick decrease in irradiance from 1000 W/m<sup>2</sup> to complete darkness (0 W/m<sup>2</sup>) under load conditions. Compared to a typical MPPT, the EDRL-MPPT maintains a steady dc voltage output with reduced waveform distortion. Solar irradiance significantly decreased to a value of 0 W/m<sup>2</sup> at intervals of 0.55 to 1 sec.

The grid current waveform corresponding to the proposed EDRL-MPPT system is depicted in Figure 5.11. The magnitude of the dominant frequency component within the grid current is illustrated in Figure 5.12. A detailed spectral analysis of the output current (refer to Figure 5.12) indicates a substantial reduction in the amplitude of inter-harmonic components. In this scenario, the calculated THD is 7.069%. Additionally, Figure 5.13 demonstrates that the angular frequency exhibits less damping in comparison to the conventional approach. The integration of the proposed algorithm with a Phase Lock mechanism effectively reduces inter-

harmonic content. A comparative analysis between the phase error produced by the EDRL-MPPT and that of a standard PLL-based P&O MPPT method is performed under nominal operating conditions. As shown in Figure 5.14, the proposed is capable of generating accurate control signals, enabling precise phase angle tracking of the grid signal and minimizing the deviation of phase relative to the reference waveform.

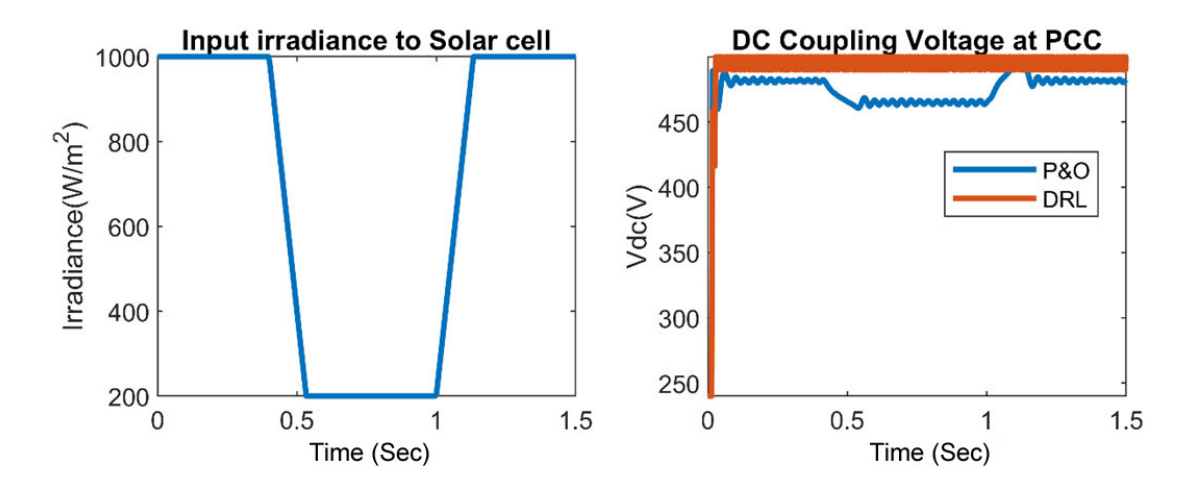


Fig 5.10 The DC-coupled voltage output obtained by the P&O and EDRL methods.

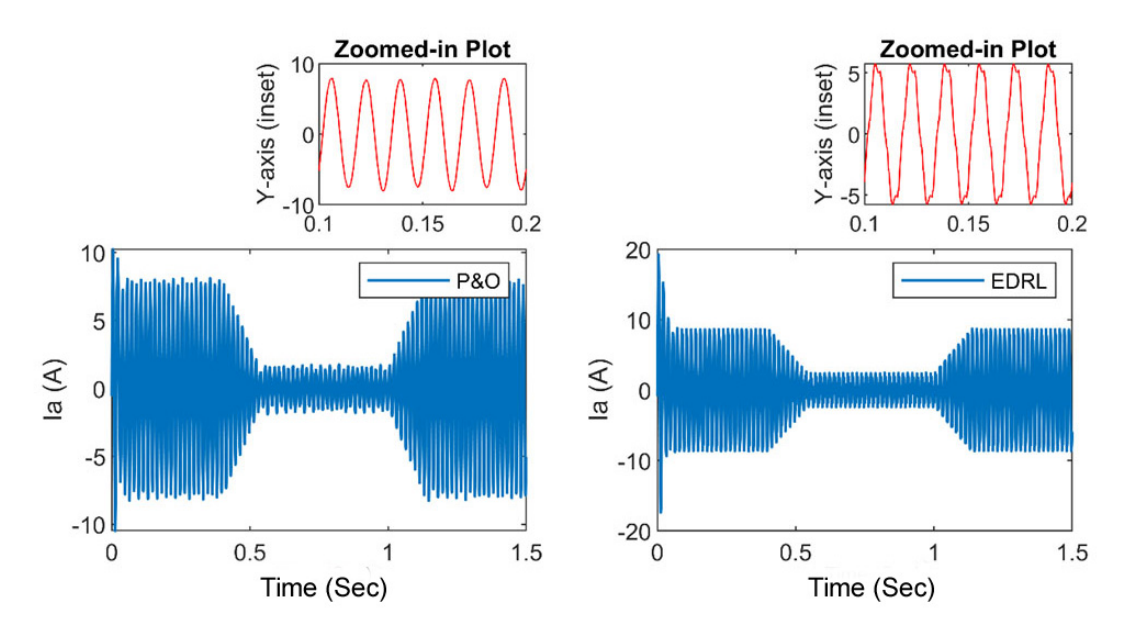


Fig 5.11 Grid current response under the P&O and EDRL based MPPT methods

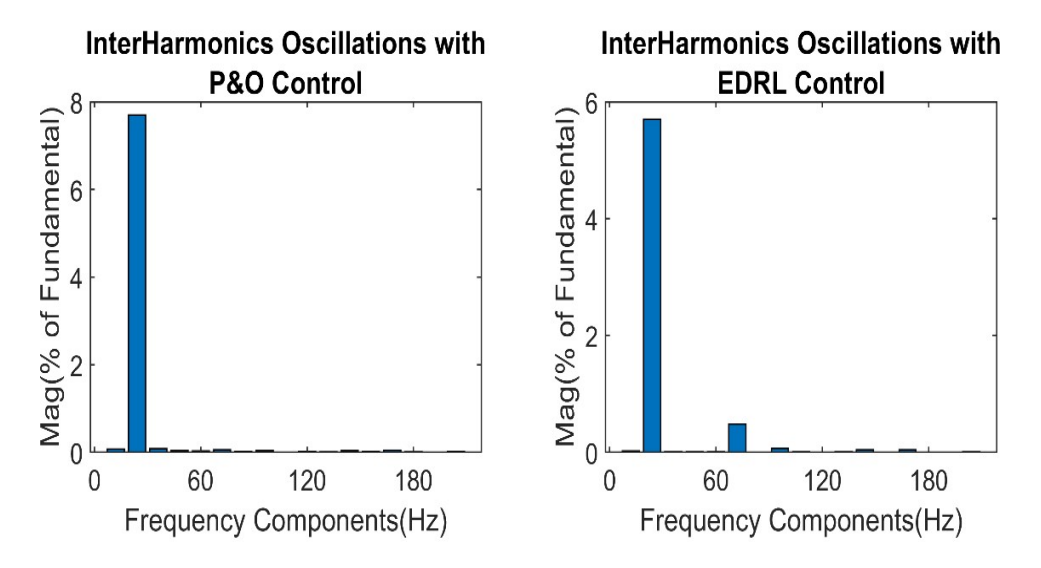


Fig 5.12 The amplitude of the fundamental frequency component observed under the P&O and EDRL-based MPPT methods

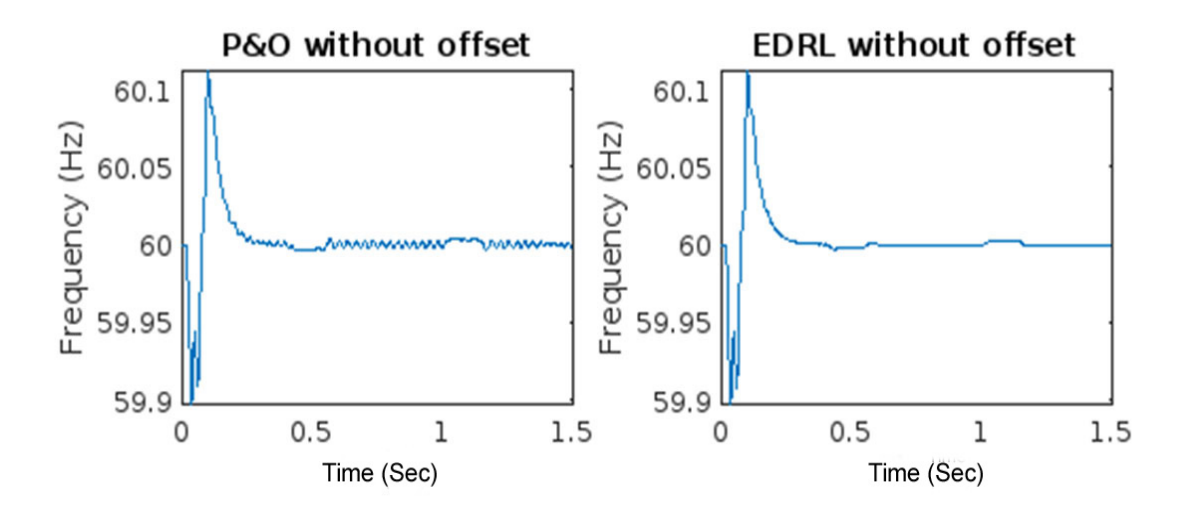


Fig 5.13 The frequency variation output under the P&O and EDRL-based MPPT methods with conventional PLL

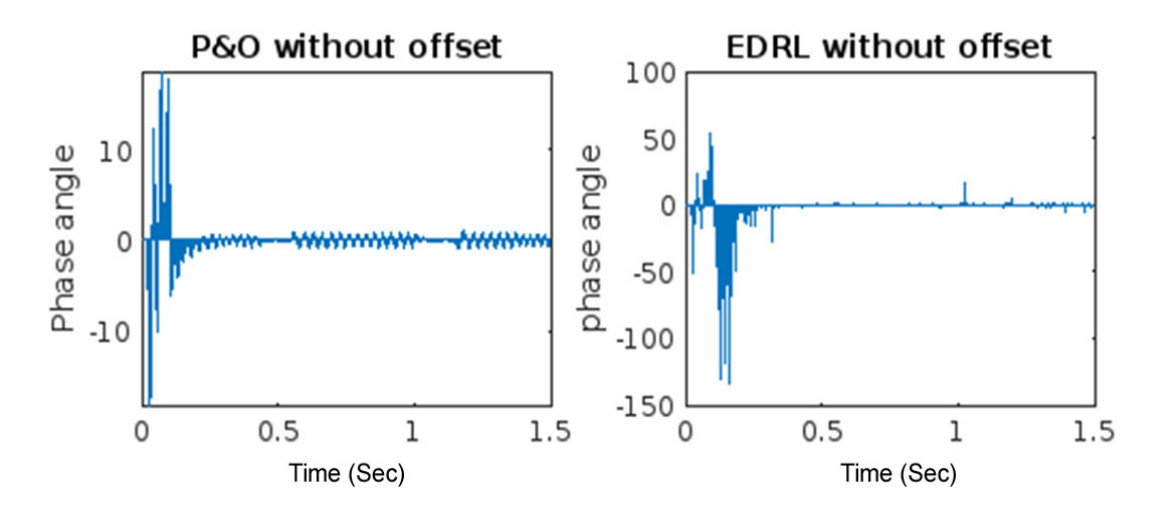


Fig 5.14 The Phase angle error under the P&O and EDRL-based MPPT methods with traditional approaches

In the third operational scenario, grid synchronization is accomplished through the integration of a COA-optimized Fuzzy-PLL and an EDRL-MPPT scheme. From the onset of operation, the system allows the grid to function at its optimal capacity. In instances where the load demand drops suddenly, any surplus energy generated by the PV system is fed back into the utility grid. To address this, the Fuzzy-PLL actively regulates the shift, where its fuzzy logic parameters are fine-tuned using results from the COA, as depicted in Fig. 5.15. This adjustment helps to suppress DC-offset and minimize grid current harmonics.

Fuzzy-PLL employs the COA to dynamically tune the fuzzy system's hyperparameters, effectively addressing phase shift issues. As illustrated in Figure 5.15, this approach significantly decreases the offset of DC and suppresses harmonic current distortion of the grid current. Figure 5.16 highlights the amplitude of the fundamental frequency component, showing an overall harmonic distortion reduction of 2.89%. Additionally, Figure 5.16 demonstrates the robust performance of the proposed Fuzzy-PLL under varying load conditions. Notably, during the interval from 0.28 to 0.33 seconds, the conventional PLL exhibits considerable frequency distortion when an offset is introduced, underscoring the superiority of the proposed method.

On the other hand, the fuzzified-PLL performs better during this time. The suggested approach performs better in a number of areas, such as steady  $V_{dc}$ , inter-harmonic rejection,

grid synchronisation, and rejection of dc offsets. A comparative assessment was conducted between the conventional P&O method combined with a standard phase lock and the proposed model integrated with a COA-based fuzzified PLL under DC-offset disturbances introduced between 0.1 and 0.3 seconds. The proposed with improved optimized PLL can provide extremely precise control signals to efficiently monitor the grid's phase angle. As seen in Figure 5.17, this produces very little phase error between a signal of reference and the output signal.

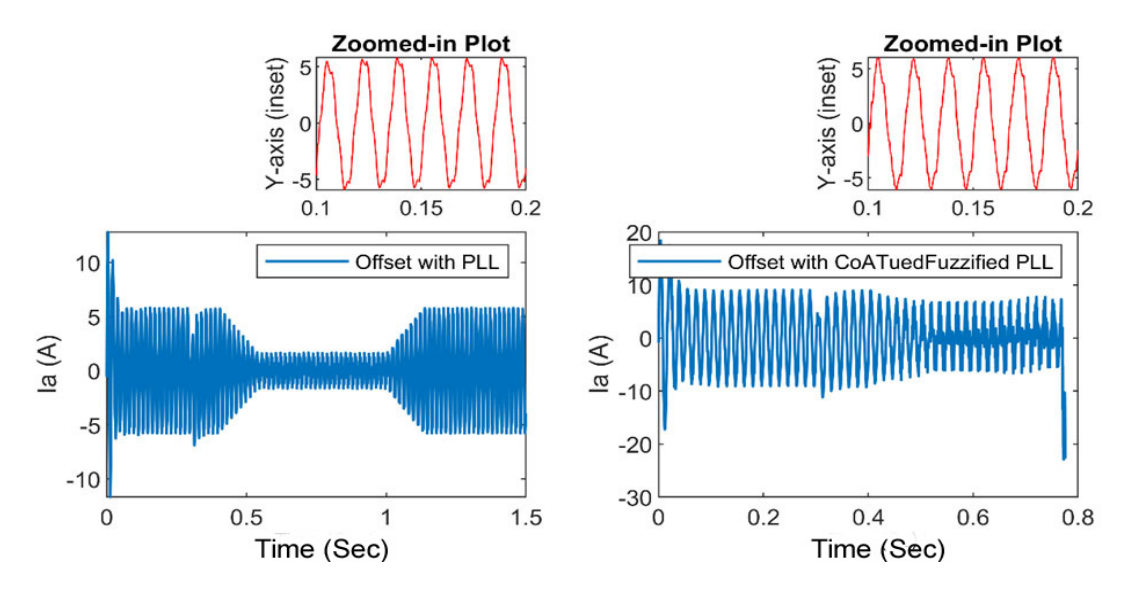


Fig 5.15 Grid current output under synchronization using the EDRL-COA-based Fuzzified PLL method.

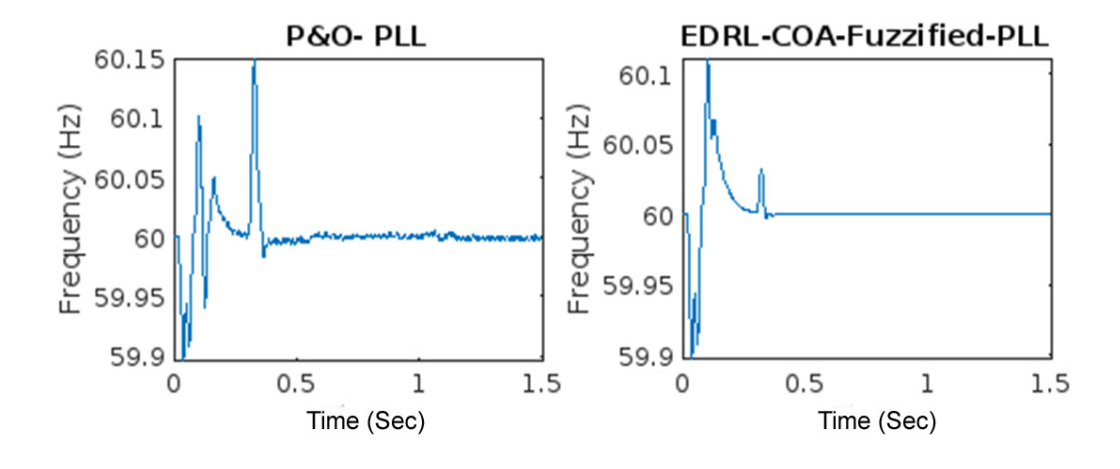


Fig 5.16 Frequency deviations observed during EDRL-based MPPT employing the COA-Fuzzified PLL method.

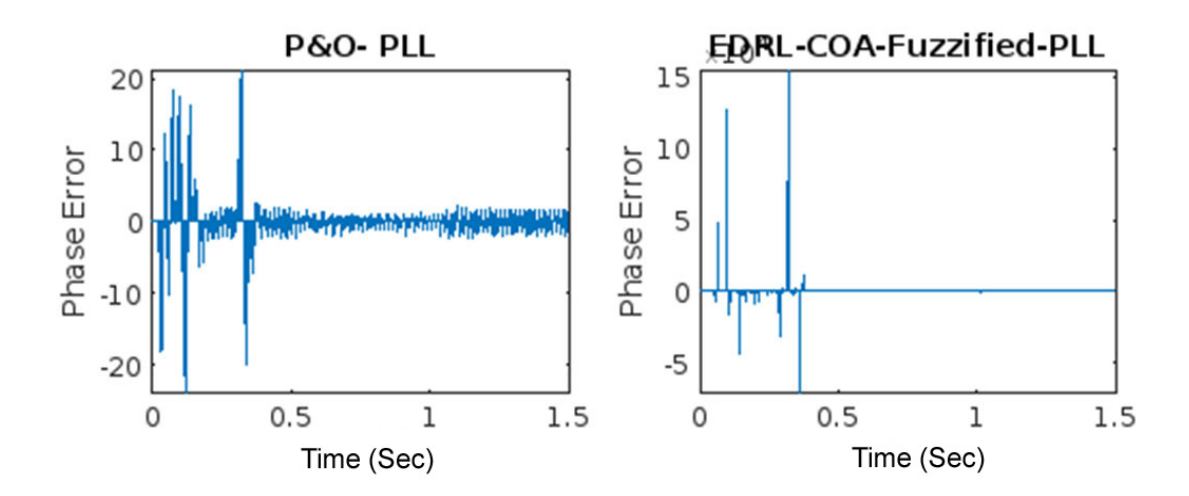


Fig 5.17 Error observed of angle of phase during the proposed approach integrated with the improved optimized PLL method

## 5.6 State-of-Art Comparison

A comparison of the improved optimized PLL method controller with many adaptive control strategies and current control strategies is shown in Table 5.5. The comparison table shown demonstrates the effectiveness of the suggested hybrid control strategy in relation to many properties, including grid current THD and DC-offset rejection. Based on results shown in Table 5.5, the proposed scheme outperforms existing control algorithms.

During transient situations, traditional MPPT algorithms using standard PLL synchronization mechanisms frequently show overshoot in the calculated phase angle, which is a momentary divergence from desirable values. The COA-fuzzified-PLL-based synchronizing system and ensemble DRL MPPT control are used in the enhanced PQ method. This reduces overshoot by using wise decision-making and adaptive control techniques. By continuously optimizing control settings in response to real-time system variations, these advance methods reduce overshoot and improve PQ and stability.

Similar to this, settling time calculates how long it takes the output of the system to stabilize following an interruption or modification in operational parameters. Longer settling durations are typically associated with traditional approaches because of slower convergence or less-than-ideal control actions. On the other hand, settling time is decreased by the COA-

fuzzified-PLL-based synchronizing system and the ensemble DRL MPPT controller using clever learning algorithms and adaptive control techniques. These cutting-edge methods enable more precise tracking of targeted operating points and quicker convergence, which lowers settling times and enhances PQ performance.

Table 5.5. The summary of performance of Different controller

Features	Conven tional PLL	FLPID- MCCF- MSOGI- FLL [193]	MCCF- SOGI [193]	MCCF [193]	Proposed COA- Fuzzified-PLL
Grid Synchronization	No	Yes	Yes	Yes	Yes
Transient Performance	Good	Good	Good	Good	Good
Oscillation	Less	Less	Less	Less	Less
DC-Offset Rejection	No	Better	No	No	Good
Interharmonics Removal	No	Yes	Yes	No	Yes
THD of Grid Current	No	Better	Less	Less	Good
Steady State Performance	Good	Good	Good	Good	Good

## 5.7 Summary

In this chapter, the design and application of an proposed Maximum PPT for eliminating harmonics of inner, a novel PLL for mitigating offset of DC, and the CC-ROGI-FLL for harmonic reduction, all aimed at the operation and control of a proposed PV System. The performance of all the above-said algorithms is carried out through simulation. The above-said control approaches successfully extract the fundamental component from nonlinear and unbalanced load current and give a fast dynamic response with reduced oscillations compared with other conventional algorithms. The performance approves the proposed control algorithms with VSC provide power compensation (active/reactive), interharmonics abatement, load leveling, DC-Offset removal, voltage & frequency stabilization, and improves overall PQ of the system under load perturbation and dynamic environments of solar.

## **CHAPTER 6**

# CONCLUSION, FUTURE SCOPE AND SOCIAL IMPACT

The main aim of thesis work is the application of power electronics for the improvement of PQ in single-phase and three-phase grid-connected PV systems feeding non-linear loads. These goals can be achieved by the designing the system components with implementation of control algorithms for the PQ improvement. The control algorithms require the synchronization techniques, control algorithms to estimate fundamental component, DC-link voltage controllers and the feed form term. Simulation and experimental work have been performed to find out the effectiveness of the system and the control algorithms. The main conclusions of the thesis work have been discussed in next section.

#### 6.1 Conclusion

Introduction of this thesis work has been presented first which discusses PQ, its reason, effect and the state of art to solve these problems. Chapter 2 presented the literature review on PV modeling, MPPT techniques, PQ problems, impacts and their solutions. The effective solution for both active power injection and the PQ improvement in single-phase and three-phase grid-connected PV system require synchronization and control techniques and are discussed here.

Chapter 3 discusses the design and development of single-phase and three-phase grid-connected PV system has been discussed in detail. Design equations and system configuration have been presented. Rating of PV string/array has been designed for single-phase and three-phase grid-connected PV system.

In Chapter 4, grid-synchronization techniques have been presented for single-phase system. In single-phase synchronization techniques PLL and non-PLL type techniques have been presented. For the variation in grid voltage, the FOGI-FLL shows best performance for both the amplitude estimation and frequency estimation. Frequency estimated by FOGI-FLL

shows zero error and faster convergence. During the polluted grid condition APF-PLL shows best performance as it filter out harmonic effectively. The performance of FOGI-FLL and APF-PLL is not satisfactory, while the performance of 1φ-CBF-FLL is observed to be the best.

In Chapter 5, the control technique for harmonic reduction have been designed and applied for operation and control of the three-phase grid-connected PV system. The performance of all the above-said algorithms is carried through simulation. The above-said control approaches successfully extract the fundamental component from nonlinear and unbalanced load current and give a fast dynamic response with reduced oscillations compared with other conventional algorithms. The performance approves the proposed control algorithms with VSC provide power compensation (active/reactive), interharmonics abatement, load leveling, DC-Offset removal, voltage & frequency stabilization, and improves overall PQ of the system under load perturbation and dynamic environments of solar.

The main aim of the thesis work is to mitigate interharmonics, DC-offset rejection, power compensation, load leveling and improvement in power quality of grid-connected solar PV system feeding non-linear loads. These goals are achieved by designing the grid-connected solar PV with VSC operating system components proposed control algorithms. The control algorithms require synchronization techniques, and to estimate the fundamental component of load current under dynamic conditions of PV system and nonlinear load. A novel ensembled Deep Reinforcement Learning (EDRL) MPPT controller, and a Coati Optimization Algorithm tuned Fuzzified-Phase Locked Loop (COA Fuzzified-PLL), Complex-Coefficient Reduced-Order Generalised Integrator-based Frequency-Locked Loop (CC-ROGI-FLL), single-phase complex band-pass filter-based frequency locked loop (1\phi-CBF-FLL), four ordered generalized integrator frequency locked loop (FOGI-FLL) and all-pass filter-based phase-locked loop (APF-PLL)based synchronizing system are proposed to improve the power quality of the system. Simulation work has been performed to find out the effectiveness of the system and the control algorithms.

## **6.2** Future Scope of Work

The development, control and analysis of the grid-connected solar PV system have been demonstrated in this work. Some conventional and new synchronization algorithm has been designed to work in adverse operating conditions. More work is still required to develop new synchronization techniques, especially under dynamic conditions of renewable energy sources. Mathematical stability analysis could also be done for the stable operation of the synchronization techniques under dynamic conditions of load and renewable energy sources.

Conventional P&O MPPT methods have been employed to achieve maximal power from the SPV in the islanded system for the fixed or changing irradiance conditions. New techniques should be developed for varying irradiance and partial shading conditions. These days PV is widely used for electricity generation.

### 6.3 Social Impact

Depending on the situation, improving the performance of grid-connected solar PV system can have a variety of beneficial social impacts. Below is a summary of the main social impacts:

- Improved solar systems can lessen energy poverty and blackouts in places with erratic networks.
- 2. The need for installation, maintenance, and engineering positions rises as solar PV systems become more widely used and efficient.
- 3. Over time, families and businesses may see a reduction in their power bills due to increased efficiency brought about by improved performance.
- 4. Better air quality results from less reliance on fossil fuels, particularly in places with high population density.
- 5. Investing in R&D to improve PV systems frequently encourages creativity and scholarly inquiry.

## **REFERENCES**

- [1] K. Sridharan and B. C. Babu, "Accurate Phase Detection System Using Modified SGDFT-Based PLL for Three-Phase Grid-Interactive Power Converter during Interharmonic Conditions," *IEEE Trans. Instrum. Meas.*, vol. 71, pp. 1–11, 2022, doi: 10.1109/TIM.2021.3136172.
- [2] N. L. Panwar, S. C. Kaushik, and S. Kothari, "Role of renewable energy sources in environmental protection: A review," *Renew. Sustain. Energy Rev.*, vol. 15, no. 3, pp. 1513–1524, 2011, doi: 10.1016/j.rser.2010.11.037.
- [3] S. Lubura, M. S'oja, S. A. Lale, and M. Ikic', "Single-phase phase locked loop with DC offset and noise rejection for PV inverters," *IET Power Electron.*, vol. 7, no. 9, pp. 2288–2299, 2014, doi: 10.1049/iet-pel.2013.0413.
- [4] S. Kundu, M. Singh, and A. K. Giri, "Synchronization and control of WECS-SPV-BSS-based distributed generation system using ICCF-PLL control approach," *Electr. Power Syst. Res.*, vol. 226, no. July 2023, p. 109919, 2024, doi: 10.1016/j.epsr.2023.109919.
- [5] A. Tuan, V. V. Pham, and X. Phuong, "Integrating renewable sources into energy system for smart city as a sagacious strategy towards clean and sustainable process," *J. Clean. Prod.*, vol. 305, p. 127161, 2021, doi: 10.1016/j.jclepro.2021.127161.
- [6] P. A. Owusu and S. Asumadu-Sarkodie, "A review of renewable energy sources, sustainability issues and climate change mitigation," *Cogent Eng.*, vol. 3, no. 1, pp. 1–14, 2016, doi: 10.1080/23311916.2016.1167990.
- [7] S. A. Rizzo and G. Scelba, "ANN based MPPT method for rapidly variable shading conditions," *Appl. Energy*, vol. 145, pp. 124–132, 2015, doi: 10.1016/j.apenergy.2015.01.077.
- [8] C. C. Yeh *et al.*, "Design of Special Protection System for an Offshore Island with High-PV Penetration," *IEEE Trans. Ind. Appl.*, vol. 53, no. 2, pp. 947–953, 2017, doi:

- 10.1109/TIA.2016.2627518.
- [9] M. Jedari Zare Zadeh and S. H. Fathi, "A New Approach for PV Arrays Modeling and Maximum Power Point Estimation in Real Operating Conditions," *IEEE Trans. Ind. Electron.*, vol. 64, no. 12, pp. 9334–9343, 2017, doi: 10.1109/TIE.2017.2711571.
- [10] A. Dolara, S. Leva, and G. Manzolini, "Comparison of different physical models for PV power output prediction," *Sol. Energy*, vol. 119, pp. 83–99, 2015, doi: 10.1016/j.solener.2015.06.017.
- [11] A. A. Desai, S. Mikkili, and S. Member, "Modelling and analysis of PV configurations (alternate TCT-BL, total cross tied, series, series parallel, bridge linked and honey comb) to extract maximum power under partial shading conditions," *CSEE J. Power Energy Syst.*, vol. 8, no. 6, pp. 1670–1683, 2020, doi: 10.17775/cseejpes.2020.00900.
- [12] S. R. Pendem and S. Mikkili, "Modeling, simulation and performance analysis of solar PV array configurations (Series, Series–Parallel and Honey-Comb) to extract maximum power under Partial Shading Conditions," *Energy Reports*, vol. 4, pp. 274–287, 2018, doi: 10.1016/j.egyr.2018.03.003.
- [13] S. N. Deshkar, S. B. Dhale, J. S. Mukherjee, T. S. Babu, and N. Rajasekar, "Solar PV array reconfiguration under partial shading conditions for maximum power extraction using genetic algorithm," *Renew. Sustain. Energy Rev.*, vol. 43, no. 2015, pp. 102–110, 2015, doi: 10.1016/j.rser.2014.10.098.
- [14] M. A. Hasan and S. K. Parida, "An overview of solar PV panel modeling based on analytical and experimental viewpoint," *Renew. Sustain. Energy Rev.*, vol. 60, pp. 75– 83, 2016, doi: 10.1016/j.rser.2016.01.087.
- [15] R. Ahmad, A. F. Murtaza, and H. A. Sher, "Power tracking techniques for efficient operation of PV array in solar applications A review," *Renew. Sustain. Energy Rev.*, vol. 101, no. November 2017, pp. 82–102, 2019, doi: 10.1016/j.rser.2018.10.015.
- [16] K. Sundareswaran, V. Vigneshkumar, P. Sankar, S. P. Simon, P. Srinivasa Rao Nayak, and S. Palani, "Development of an Improved P&O Algorithm Assisted Through a

- Colony of Foraging Ants for MPPT in PV System," *IEEE Trans. Ind. Informatics*, vol. 12, no. 1, pp. 187–200, 2016, doi: 10.1109/TII.2015.2502428.
- [17] B. N. Alajmi, K. H. Ahmed, S. J. Finney, and B. W. Williams, "Fuzzy-logic-control approach of a modified hill-climbing method for maximum power point in microgrid standalone PV system," *IEEE Trans. Power Electron.*, vol. 26, no. 4, pp. 1022–1030, 2011, doi: 10.1109/TPEL.2010.2090903.
- [18] R. I. Putri, S. Wibowo, and M. Rifa'i, "Maximum power point tracking for PV using incremental conductance method," *Energy Procedia*, vol. 68, pp. 22–30, 2015, doi: 10.1016/j.egypro.2015.03.228.
- [19] M. Seyedmahmoudian *et al.*, "State of the art artificial intelligence-based MPPT techniques for mitigating partial shading effects on PV systems A review," *Renew. Sustain. Energy Rev.*, vol. 64, pp. 435–455, 2016, doi: 10.1016/j.rser.2016.06.053.
- [20] A. K. Pandey, V. V. Tyagi, J. A. Selvaraj, N. A. Rahim, and S. K. Tyagi, "Recent advances in solar PV systems for emerging trends and advanced applications," *Renew. Sustain. Energy Rev.*, vol. 53, pp. 859–884, 2016, doi: 10.1016/j.rser.2015.09.043.
- [21] M. Yamaguchi and A. Luque, "High efficiency and high concentration in PVs," *IEEE Trans. Electron Devices*, vol. 46, no. 10, pp. 2139–2144, 1999, doi: 10.1109/16.792009.
- [22] R. Har-Lavan and D. Cahen, "40 years of inversion layer solar cells: From MOS to conducting polymer/inorganic hybrids," *IEEE J. PVs*, vol. 3, no. 4, pp. 1443–1459, 2013, doi: 10.1109/JPHOTOV.2013.2270347.
- [23] P. Reinhard, P. Blasch, F. Pianezzi, S. Nishiwaki, S. Buecheler, and A. N. Tiwari, "Review of Progress Toward 20 % Efficiency Flexible CIGS Solar Cells and Manufacturing Issues of Solar Modules," 2012, doi: 10.1109/PVSC-Vol2.2012.6656789.
- [24] Y. Chen *et al.*, "From laboratory to production: Learning models of efficiency and manufacturing cost of industrial crystalline silicon and thin-film PV technologies,"

- *IEEE J. PVs*, vol. 8, no. 6, pp. 1531–1538, 2018, doi: 10.1109/JPHOTOV.2018.2871858.
- [25] M. Gloeckler, I. Sankin, and Z. Zhao, "CdTe solar cells at the threshold to 20% efficiency," *IEEE J. PVs*, vol. 3, no. 4, pp. 1389–1393, 2013, doi: 10.1109/JPHOTOV.2013.2278661.
- [26] A. V. Pavan Kumar, A. M. Parimi, and K. Uma Rao, "Performance analysis of a two-diode model of PV cell for PV based generation in MATLAB," *Proc. 2014 IEEE Int. Conf. Adv. Commun. Control Comput. Technol. ICACCCT 2014*, no. 978, pp. 68–72, 2015, doi: 10.1109/ICACCCT.2014.7019191.
- [27] T. Wei, F. Yu, G. Huang, and C. Xu, "A Particle-Swarm-Optimization-Based Parameter Extraction Routine for Three-Diode Lumped Parameter Model of Organic Solar Cells," *IEEE Electron Device Lett.*, vol. 40, no. 9, pp. 1511–1514, 2019, doi: 10.1109/led.2019.2926315.
- [28] N. Mohamed, A. Alrahim, N. Z. Yahaya, and B. Singh, "S ingle-Diode Model and Two-Diode Model of PV Modules: A C omparison," *2013 IEEE Int. Conf. Control Syst. Comput. Eng.*, pp. 210–214, 2013, doi: 10.1109/ICCSCE.2013.6719960.
- [29] S. H. Hanzaei, S. A. Gorji, and M. Ektesabi, "A scheme-based review of MPPT techniques with respect to input variables including solar irradiance and PV arrays' temperature," *IEEE Access*, vol. 8, pp. 182229–182239, 2020, doi: 10.1109/ACCESS.2020.3028580.
- [30] A. K. Gupta and R. Saxena, "Review on widely-used MPPT Techniques for PV Applications," 2016 Int. Conf. Innov. Challenges Cyber Secur., no. Iciccs, pp. 270–273, 2016, doi: 10.1109/ICICCS.2016.7542321.
- [31] D. Singh and H. Singh, "Technical Survey and review on MPPT techniques to attain Maximum Power of PV system," pp. 265–268, 2019.
- [32] R. B. Bollipo, S. Mikkili, and P. K. Bonthagorla, "Hybrid, optimal, intelligent and classical PV MPPT techniques: A review," *CSEE J. Power Energy Syst.*, vol. 7, no. 1,

- pp. 9–33, 2021, doi: 10.17775/CSEEJPES.2019.02720.
- [33] N. Femia, G. Petrone, G. Spagnuolo, and M. Vitelli, "Optimization of perturb and observe maximum power point tracking method," *IEEE Trans. Power Electron.*, vol. 20, no. 4, pp. 963–973, 2005, doi: 10.1109/TPEL.2005.850975.
- [34] D. Sera, L. Mathe, T. Kerekes, S. V. Spataru, and R. Teodorescu, "On the perturb-and-observe and incremental conductance mppt methods for PV systems," *IEEE J. PVs*, vol. 3, no. 3, pp. 1070–1078, 2013, doi: 10.1109/JPHOTOV.2013.2261118.
- [35] I. V. Banu, R. Beniuga, and M. Istrate, "Comparative analysis of the perturb-and-observe and incremental conductance MPPT methods," 2013 8th Int. Symp. Adv. Top. Electr. Eng. ATEE 2013, no. 1, pp. 23–26, 2013, doi: 10.1109/ATEE.2013.6563483.
- [36] S. S. Satapathy and N. Kumar, "Modulated Perturb and Observe Maximum Power Point Tracking Algorithm for Solar PV Energy Conversion System," 2019 3rd Int. Conf. Recent Dev. Control. Autom. Power Eng. RDCAPE 2019, pp. 345–350, 2019, doi: 10.1109/RDCAPE47089.2019.8979025.
- [37] M. J. H. Moghaddam *et al.*, "Improved voltage unbalance and harmonics compensation control strategy for an isolated microgrid," *Energies*, vol. 11, no. 10, 2018, doi: 10.3390/en11102688.
- [38] M. Abdul and K. Aziz, "Enhancement of Power Quality in Distribution System using D-Statcom," pp. 2093–2098, 2016.
- [39] S. R. Arya, S. Member, B. Singh, and R. Niwas, "Power Quality Enhancement Using DSTATCOM in Distributed Power Generation System," pp. 1–10, 2016, doi: 10.1109/TIA.2016.2600644.
- [40] V. Kavitha and K. Subramanian, "Investigation of power quality issues and its solution for distributed power system," *Proc. IEEE Int. Conf. Circuit, Power Comput. Technol. ICCPCT 2017*, 2017, doi: 10.1109/ICCPCT.2017.8074372.
- [41] T. I. M. Slangen, "Grid Impact of Electric Vehicle Fast Charging Stations: Trends, Standards, Issues and Mitigation Measures An Overview," vol. 2, no. November

- 2020, 2021, doi: 10.1109/OJPEL.2021.3054601.
- [42] I. S. Association, *Ieee Standard 1159 1995*. 1995.
- [43] IEEE Std 1159, Monitoring Electric Power Quality Developed by the Transmission and Distribution Committee IEEE Power and Energy Society, vol. 2019. 2019.
- [44] R. G. Suryavanshi, "A review on power quality issues due to high penetration level of solar generated power on the grid," pp. 464–467, 2019.
- [45] D. Committee, I. Power, and E. Society, "IEEE Std 519<sup>TM</sup>-2014," *IEEE Std 519-2014*(Revision IEEE Std 519-1992), vol. 2014, 2014.
- [46] IEEE, "IEEE 1547 2003 Standards," 1547 TM IEEE Stand. Interconnecting Distrib. Resour. with Electr. Power Syst. Stand., no. July, 2003.
- [47] IEEE Std 1547, IEEE Standard for Interconnection and Interoperability of Distributed Energy Resources with Associated Electric Power Systems Interfaces. 2018.
- [48] S. Rahmani, A. Hamadi, S. Member, K. Al-haddad, and L. A. Dessaint, "A Combination of Shunt Hybrid Power Filter and Thyristor-Controlled Reactor for Power Quality," vol. 61, no. 5, pp. 2152–2164, 2014.
- [49] A. Kumar, "Design , Modeling and Performance of Static Synchronous Series Compensator Regulated Self- excited induction generator," pp. 519–525, 2019.
- [50] S. V. Compensator, R. K. Varma, S. Auddy, and S. Member, "Mitigation of Subsynchronous Oscillations in a Series Compensated Wind Farm with," pp. 1–7, 2006.
- [51] B. Singh and F. Ieee, "DVR Based Voltage Regulator for Isolated Asynchronous Generators Feeding Three Phase Load," pp. 1–6.
- [52] F. Dstatcom, B. Singh, P. Jayaprakash, S. Kumar, and D. P. Kothari, "Implementation of Neural-Network-Controlled Three-Leg VSC and a Transformer as Three-Phase," vol. 47, no. 4, pp. 1892–1901, 2011.

- [53] B. Jena and A. Choudhury, "Voltage and frequency stabilisation in a micro-hydro-PV based hybrid microgrid using FLC based STATCOM equipped with BESS," *Proc. IEEE Int. Conf. Circuit, Power Comput. Technol. ICCPCT 2017*, 2017, doi: 10.1109/ICCPCT.2017.8074291.
- [54] K. F. Krommydas and A. T. Alexandridis, "Modular Control Design and Stability Analysis of Isolated PV-Source/Battery-Storage Distributed Generation Systems," *IEEE J. Emerg. Sel. Top. Circuits Syst.*, vol. 5, no. 3, pp. 372–382, 2015, doi: 10.1109/JETCAS.2015.2462172.
- [55] R. R. Chilipi, B. Singh, S. S. Murthy, and L. Fellow, "Performance of a Self-Excited Induction Generator With DSTATCOM-DTC Drive-Based Voltage and Frequency Controller," vol. 29, no. 3, pp. 545–557, 2014.
- [56] M. Abdul, A. Yahiya, M. Abdul, and R. Uzair, "Performance Analysis of DVR, DSTATCOM and UPQC For Improving The Power Quality With Various Control Strategies," 2016.
- [57] S. Kaur and B. Dwivedi, "Power quality issues and their mitigation techniques in microgrid system- A review," *India Int. Conf. Power Electron. IICPE*, vol. 2016-Novem, 2016, doi: 10.1109/IICPE.2016.8079543.
- [58] C. Jain and B. Singh, "A three-phase grid tied SPV system with adaptive DC link voltage for CPI voltage variations," *IEEE Trans. Sustain. Energy*, vol. 7, no. 1, pp. 337–344, 2016, doi: 10.1109/TSTE.2015.2496297.
- [59] B. Singh, C. Jain, and A. Bansal, "An improved adjustable step adaptive neuron based control approach for grid supportive SPV system," *12th IEEE Int. Conf. Electron. Energy, Environ. Commun. Comput. Control (E3-C3), INDICON 2015*, pp. 2–7, 2016, doi: 10.1109/INDICON.2015.7443147.
- [60] S. Kumar and B. Singh, "Multi-Objective Single-Stage SPV System Integrated to 3P4W Distribution Network Using DMSI-Based Control Technique," *IEEE Trans. Ind. Appl.*, vol. 54, no. 3, pp. 2656–2664, 2018, doi: 10.1109/TIA.2017.2788886.

- [61] S. Kumar and B. Singh, "Seamless Operation and Control of Single-Phase Hybrid PV-BES-Utility Synchronized System," *IEEE Trans. Ind. Appl.*, vol. 55, no. 2, pp. 1072–1082, 2019, doi: 10.1109/TIA.2018.2876640.
- [62] R. Majumder, "Reactive Power Compensation in Single-Phase Operation of Microgrid," *IEEE Trans. Ind. Electron.*, vol. 60, no. 4, pp. 1403–1416, 2013, doi: 10.1109/TIE.2012.2193860.
- [63] J. Rocabert, A. Luna, F. Blaabjerg, and P. Rodríguez, "Control of power converters in AC microgrids," *IEEE Trans. Power Electron.*, vol. 27, no. 11, pp. 4734–4749, 2012, doi: 10.1109/TPEL.2012.2199334.
- [64] Y. Yang, K. Zhou, and F. Blaabjerg, "Current Harmonics from Single-Phase Grid-Connected Inverters-Examination and Suppression," *IEEE J. Emerg. Sel. Top. Power Electron.*, vol. 4, no. 1, pp. 221–233, 2016, doi: 10.1109/JESTPE.2015.2504845.
- [65] F. Blaabjerg, R. Teodorescu, M. Liserre, and A. V. Timbus, "Overview of control and grid synchronization for distributed power generation systems," *IEEE Trans. Ind. Electron.*, vol. 53, no. 5, pp. 1398–1409, 2006, doi: 10.1109/TIE.2006.881997.
- [66] J. Selvaraj and N. A. Rahim, "Multilevel Inverter For Grid-Connected PV System Employing Digital PI Controller," *IEEE Trans. Ind. Electron.*, vol. 56, no. 1, pp. 149– 158, 2009, doi: 10.1109/TIE.2008.928116.
- [67] A. Kumar, "Performance Enhancement of Single-Phase Grid-Connected PV System Under Partial Shading Using Cascaded Multilevel Converter," *IEEE Trans. Ind. Appl.*, vol. 54, no. 3, pp. 2665–2676, 2018, doi: 10.1109/TIA.2017.2789238.
- [68] L. Wu, Z. Zhao, and J. Liu, "A single-stage three-phase grid-connected PV system with modified MPPT method and reactive power compensation," *IEEE Trans. Energy Convers.*, vol. 22, no. 4, pp. 881–886, 2007, doi: 10.1109/TEC.2007.895461.
- [69] H. Patel and V. Agarwal, "MPPT scheme for a PV-fed single-phase single-stage grid-connected inverter operating in CCM with only one current sensor," *IEEE Trans. Energy Convers.*, vol. 24, no. 1, pp. 256–263, 2009, doi: 10.1109/TEC.2008.2005282.

- [70] E. S. Sreeraj, K. Chatterjee, and S. Bandyopadhyay, "One-cycle-controlled single-stage single-phase voltage-sensorless grid-connected PV system," *IEEE Trans. Ind. Electron.*, vol. 60, no. 3, pp. 1216–1224, 2013, doi: 10.1109/TIE.2012.2191755.
- [71] A. Datta, R. Sarker, and I. Hazarika, "An Efficient Technique Using Modified p-q Theory for Controlling Power Flow in a Single-Stage Single-Phase Grid-Connected PV System," *IEEE Trans. Ind. Informatics*, vol. 15, no. 8, pp. 4635–4645, 2018, doi: 10.1109/tii.2018.2890197.
- [72] G. P. V System, B. N. Alajmi, K. H. Ahmed, S. Member, G. P. Adam, and B. W. Williams, "Single-Phase Single-Stage Transformer less," *IEEE Trans. Power Electron.*, vol. 28, no. 6, pp. 2664–2676, 2013, doi: 10.1109/TPEL.2012.2228280.
- [73] A. Kumar, Seema, B. Singh, and R. Jain, "Double stage grid-tied solar PV system using HC-LMS control," *PIICON 2020 9th IEEE Power India Int. Conf.*, 2020, doi: 10.1109/PIICON49524.2020.9112906.
- [74] H. S. Sahu and S. K. Nayak, "Extraction of Maximum Power from a PV Array under Nonuniform Irradiation Conditions," *IEEE Trans. Electron Devices*, vol. 63, no. 12, pp. 4825–4831, 2016, doi: 10.1109/TED.2016.2616580.
- [75] M. S. Elnozahy, S. Member, and M. M. A. Salama, "Uncertainty-Based Design of a Bilayer Distribution System for Improved Integration of PHEVs and PV Arrays," *IEEE Trans. Sustain. Energy*, vol. 6, no. 3, pp. 659–674, 2015, doi: 10.1109/TSTE.2015.2405411.
- [76] G. P. V. B. System, B. Lu, and M. Shahidehpour, "Short-Term Scheduling of Battery in a," vol. 20, no. 2, pp. 1053–1061, 2005.
- [77] V. Rallabandi, O. M. Akeyo, N. Jewell, and D. M. Ionel, "Incorporating battery energy storage systems into multi-MW grid connected PV systems," *IEEE Trans. Ind. Appl.*, vol. 55, no. 1, pp. 638–647, 2019, doi: 10.1109/TIA.2018.2864696.
- [78] T. Wu, S. Member, C. Chang, L. Lin, and C. Kuo, "Power Loss Comparison of Single-and Two-Stage Grid-Connected PV Systems," *IEEE Trans. Energy Convers.*, vol. 26,

- no. 2, pp. 707–715, 2011, doi: 10.1109/TEC.2011.2123897.
- [79] S. Jain and V. Agarwal, "A single-stage grid connected inverter topology for solar PV systems with maximum power point tracking," *IEEE Trans. Power Electron.*, vol. 22, no. 5, pp. 1928–1940, 2007, doi: 10.1109/TPEL.2007.904202.
- [80] T. Sreekanth, N. Lakshminarasamma, and M. K. Mishra, "A Single-Stage Grid-Connected High Gain Buck-Boost Inverter with Maximum Power Point Tracking," IEEE Trans. Energy Convers., vol. 32, no. 1, pp. 330–339, 2017, doi: 10.1109/TEC.2016.2633365.
- [81] A. K. Singh, I. Hussain, and B. Singh, "Double-Stage Three-Phase Grid-Integrated Solar PV System With Fast Zero Attracting Normalized Least Mean Fourth Based Adaptive Control," *IEEE Trans. Ind. Electron.*, vol. 65, no. 5, pp. 3921–3931, 2018, doi: 10.1109/TIE.2017.2758750.
- [82] N. Femia, G. Petrone, G. Spagnuolo, and M. Vitelli, "A technique for improving P&O MPPT performances of double-stage grid-connected PV systems," *IEEE Trans. Ind. Electron.*, vol. 56, no. 11, pp. 4473–4482, 2009, doi: 10.1109/TIE.2009.2029589.
- [83] B. Singh, R. Sharma, and S. Kewat, "Robust Control Strategies for SyRG-PV and Wind-Based Islanded Microgrid," *IEEE Trans. Ind. Electron.*, vol. 68, no. 4, pp. 3137–3147, 2021, doi: 10.1109/TIE.2020.2978723.
- [84] S. Kewat and B. Singh, "Modified amplitude adaptive control algorithm for power quality improvement in multiple distributed generation system," *IET Power Electron.*, vol. 12, no. 9, pp. 2321–2329, 2019, doi: 10.1049/iet-pel.2018.5936.
- [85] M. Bajaj, M. Pushkarna, and A. S. Rana, "An Improved SRF based Control Algorithm for D-STATCOM under Abnormal Source Voltage," pp. 1–6, 2015.
- [86] E. Engineering and E. S. Engineering, "EPLL based Controller for Voltage Harmonic Mitigation in Grid Connected Wind Systems," no. 2, pp. 1157–1161, 2017.
- [87] S. Jiao, R. R. Krishna, and K. Rajashekara, "A Novel Phase-Locked Loop based Four-leg Converter Control for Unbalanced Load Compensation under Distorted and

- Unbalanced Grid Condition," *ECCE 2020 IEEE Energy Convers. Congr. Expo.*, pp. 4749–4754, 2020, doi: 10.1109/ECCE44975.2020.9236389.
- [88] A. J. Wang, B. Y. Ma, and C. X. Meng, "A frequency-locked loop technology of three-phase grid-connected inverter based on improved reduced order generalized integrator," *Proc. 2015 10th IEEE Conf. Ind. Electron. Appl. ICIEA 2015*, no. 1, pp. 730–735, 2015, doi: 10.1109/ICIEA.2015.7334204.
- [89] A. Kumar, S. Kewat, B. Singh, and R. Jain, "CC-ROGI-FLL based control for grid-tied PV system at abnormal grid conditions," 2020, doi: 10.1049/iet-gtd.2019.0765.
- [90] F. Wu and X. Li, "Multiple DSC Filter-Based Three-Phase EPLL for Nonideal Grid Synchronization," *IEEE J. Emerg. Sel. Top. Power Electron.*, vol. 5, no. 3, pp. 1396–1403, 2017, doi: 10.1109/JESTPE.2017.2701498.
- [91] R. Sebastián and A. Nevado, "Study and simulation of awind hydro isolated microgrid," *Energies*, vol. 13, no. 22, pp. 1–15, 2020, doi: 10.3390/en13225937.
- [92] G. Pathak, B. Singh, and B. K. Panigrahi, "Control of Wind-Diesel Microgrid Using Affine Projection-Like Algorithm," *IEEE Trans. Ind. Informatics*, vol. 12, no. 2, pp. 524–531, 2016, doi: 10.1109/TII.2016.2518643.
- [93] M. Qasim, P. Kanjiya, and V. Khadkikar, "Artificial-neural-network-based phase-locking scheme for active power filters," *IEEE Trans. Ind. Electron.*, vol. 61, no. 8, pp. 3857–3866, 2014, doi: 10.1109/TIE.2013.2284132.
- [94] M. Izadbakhsh, A. Rezvani, and M. Gandomkar, "Dynamic response improvement of hybrid system by implementing ANN-GA for fast variation of PV irradiation and FLC for wind turbine," *Arch. Electr. Eng.*, vol. 64, no. 2, pp. 291–314, 2015, doi: 10.1515/aee-2015-0024.
- [95] T. S. Babu, J. P. Ram, T. Dragičević, M. Miyatake, F. Blaabjerg, and N. Rajasekar, "Particle swarm optimization based solar PV array reconfiguration of the maximum power extraction under partial shading conditions," *IEEE Trans. Sustain. Energy*, vol. 9, no. 1, pp. 74–85, 2018, doi: 10.1109/TSTE.2017.2714905.

- [96] Z. Ding, H. Hou, G. Yu, E. Hu, L. Duan, and J. Zhao, "Performance analysis of a wind-solar hybrid power generation system," *Energy Convers. Manag.*, vol. 181, no. November 2018, pp. 223–234, 2019, doi: 10.1016/j.enconman.2018.11.080.
- [97] M. Abdolrasol, R. Mohamed, M. Hannan, A. Al-Shetwi, M. Mansor, and F. Blaabjerg, "Artificial Neural Network Based Particle Swarm Optimization for Microgrid Optimal Energy Scheduling," *IEEE Trans. Power Electron.*, vol. 36, no. 11, pp. 12151–12157, 2021, doi: 10.1109/TPEL.2021.3074964.
- [98] A. Kumar, R. Garg, and P. Mahajan, "Performance Analysis of Grid Integrated PV System using SRF and IRPT Control," 2019 1st Int. Conf. Signal Process. VLSI Commun. Eng. ICSPVCE 2019, 2019, doi: 10.1109/ICSPVCE46182.2019.9092869.
- [99] B. Singh, D. T. Shahani, and A. K. Verma, "IRPT based control of a 50 kw grid interfaced solar PV power generating system with power quality improvement," 2013 4th IEEE Int. Symp. Power Electron. Distrib. Gener. Syst. PEDG 2013 Conf. Proc., pp. 1–8, 2013, doi: 10.1109/PEDG.2013.6785601.
- [100] L. A. Pittorino, A. Horn, and J. H. R. Enslin, "Power theory evaluation for the control of an active power filter," *IEEE AFRICON Conf.*, vol. 2, pp. 676–681, 1996, doi: 10.1109/afrcon.1996.562970.
- [101] Sujono, I. Sudiharto, and O. A. Qudsi, "Application of D-STATCOM to reduce unbalanced load using synchronous reference frame theory," *EECCIS* 2020 - 2020 10th Electr. Power, Electron. Commun. Control. Informatics Semin., no. 3, pp. 65–70, 2020, doi: 10.1109/EECCIS49483.2020.9263476.
- [102] R. N. Tripathi and A. Singh, "SRF theory based grid interconnected Solar PV (SPV) system with improved power quality," Proc. 2013 Int. Conf. Emerg. Trends Commun. Control. Signal Process. Comput. Appl. IEEE-C2SPCA 2013, 2013, doi: 10.1109/C2SPCA.2013.6749390.
- [103] A. Kumar, Seema, B. Singh, and R. Jain, "ROGI with FsLMS Based Control Technique for Solar PV System under Weak Grid," *Proc. 2019 IEEE Int. Conf.*

- Environ. Electr. Eng. 2019 IEEE Ind. Commer. Power Syst. Eur. EEEIC/I CPS Eur. 2019, 2019, doi: 10.1109/EEEIC.2019.8783710.
- [104] H. Saxena, A. Singh, and J. N. Rai, "Enhanced Third-Order Generalized Integrator-Based Grid Synchronization Technique for DC-Offset Rejection and Precise Frequency Estimation," *Arab. J. Sci. Eng.*, vol. 46, no. 10, pp. 9753–9762, 2021, doi: 10.1007/s13369-021-05559-x.
- [105] B. Sahoo, S. K. Routray, and P. K. Rout, "A modified least mean square technique for harmonic elimination," *1st Odisha Int. Conf. Electr. Power Eng. Commun. Comput. Technol. ODICON* 2021, 2021, doi: 10.1109/ODICON50556.2021.9428970.
- [106] H. Saxena, A. Singh, and P. Chittora, "Modified LMS synchronization technique for distributed energy resources with DC-offset and harmonic elimination capabilities," *ISA Trans.*, no. xxxx, 2022, doi: 10.1016/j.isatra.2022.09.042.
- [107] A. Kherbachi, A. Chouder, A. Bendib, K. Kara, and S. Barkat, "Enhanced structure of second-order generalized integrator frequency-locked loop suitable for DC-offset rejection in single-phase systems," *Electr. Power Syst. Res.*, vol. 170, no. December 2018, pp. 348–357, 2019, doi: 10.1016/j.epsr.2019.01.029.
- [108] S. Golestan, J. M. Guerrero, M. J. H. Rawa, A. M. Abusorrah, and Y. Al-Turki, "Frequency-Locked Loops in Electrical Power and Energy Systems: Equivalent or Different to Phase-Locked Loops?," *IEEE Ind. Electron. Mag.*, vol. 15, no. 4, pp. 54– 64, 2021, doi: 10.1109/MIE.2021.3054580.
- [109] A. K. Giri, S. R. Arya, R. Maurya, and B. Chitti Babu, "VCO-less PLL control-based voltage-source converter for power quality improvement in distributed generation system," *IET Electr. Power Appl.*, vol. 13, no. 8, pp. 1114–1124, 2019, doi: 10.1049/iet-epa.2018.5827.
- [110] D. G. A. Krishna and A. Karthikeyan, "Design and analysis of frequency adaptive CDSC-PLL for Dynamic Voltage Restorer during adverse grid conditions," 2020 IEEE Int. Conf. Power Electron. Smart Grid Renew. Energy, PESGRE 2020, no. 1, pp. 5–9,

- 2020, doi: 10.1109/PESGRE45664.2020.9070625.
- [111] A. Jain, R. Saravanakumar, and S. Shankar, "Moving Average Filter-PLL-Based Voltage and Frequency Control of Standalone WECS," *IETE J. Res.*, vol. 68, no. 5, pp. 3628–3637, 2022, doi: 10.1080/03772063.2020.1772128.
- [112] S. Golestan, J. M. Guerrero, and J. C. Vasquez, "Three-Phase PLLs: A Review of Recent Advances," *IEEE Trans. Power Electron.*, vol. 32, no. 3, pp. 1894–1907, 2017, doi: 10.1109/TPEL.2016.2565642.
- [113] S. Golestan, J. M. Guerrero, and J. C. Vasquez, "Is Using A Complex Control Gain in Three-Phase FLLs Reasonable?," *IEEE Trans. Ind. Electron.*, vol. 67, no. 3, pp. 2480– 2484, 2020, doi: 10.1109/TIE.2019.2903748.
- [114] "IET Generation Trans Dist 2020 Saxena Adaptive spline-based PLL for synchronisation and power quality improvement.pdf.".
- [115] P. Chittora, A. Singh, and M. Singh, "Adaptive EPLL for improving power quality in three-phase three-wire grid-connected PV system," *IET Renew. Power Gener.*, vol. 13, no. 9, pp. 1595–1602, 2019, doi: 10.1049/iet-rpg.2018.5261.
- [116] B. Liu et al., "A Simple Approach to Reject DC Offset for Single-Phase Synchronous Reference Frame PLL in Grid-Tied Converters," *IEEE Access*, vol. 8, pp. 112297– 112308, 2020, doi: 10.1109/ACCESS.2020.3003009.
- [117] S. Kundu, M. Singh, and A. K. Giri, "Implementation of variable gain controller based improved phase locked loop approach to enhance power quality in autonomous microgrid," *Int. J. Numer. Model. Electron. Networks, Devices Fields*, no. November, pp. 1–19, 2022, doi: 10.1002/jnm.3082.
- [118] S. Kundu, M. Singh, and A. K. Giri, "SPV-wind-BES-based islanded electrical supply system for remote applications with power quality enhancement," *Electr. Eng.*, 2023, doi: 10.1007/s00202-023-01979-0.
- [119] M. Xie, H. Wen, C. Zhu, and Y. Yang, "DC Offset Rejection Improvement in Single-Phase SOGI-PLL Algorithms: Methods Review and Experimental Evaluation," *IEEE*

- Access, vol. 5, no. c, pp. 12810–12819, 2017, doi: 10.1109/ACCESS.2017.2719721.
- [120] Y. Han, M. Luo, X. Zhao, J. M. Guerrero, and L. Xu, "Comparative Performance Evaluation of Orthogonal-Signal-Generators-Based Single-Phase PLL Algorithms - A Survey," *IEEE Trans. Power Electron.*, vol. 31, no. 5, pp. 3932–3944, 2016, doi: 10.1109/TPEL.2015.2466631.
- [121] R. Pandey and N. Kumar, "Advanced TOGI Controller for Weak Grid Integrated Solar PV System," 2023 IEEE IAS Glob. Conf. Renew. Energy Hydrog. Technol. GlobConHT 2023, pp. 1–6, 2023, doi: 10.1109/GlobConHT56829.2023.10087502.
- [122] S. Kumar, D. Jaraniya, R. R. Chilipi, and A. Al-Durra, "Optimal Operation of WL-RC-QLMS and Luenberger Observer Based Disturbance Rejection Controlled Grid Integrated PV-DSTATCOM System," *IEEE Trans. Ind. Appl.*, vol. 58, no. 6, pp. 7870–7880, 2022, doi: 10.1109/TIA.2022.3199401.
- [123] H. Saxena, A. Singh, and J. N. Rai, "Analysis of SOGI-ROGI for synchronization and shunt active filtering under distorted grid condition," *ISA Trans.*, vol. 109, no. xxxx, pp. 380–388, 2021, doi: 10.1016/j.isatra.2020.10.025.
- [124] H. Saxena, A. Singh, and J. N. Rai, "Design and Analysis of Cascaded Generalized Integrators for Mitigation of Power Quality Problems," 2019 Int. Symp. Adv. Electr. Commun. Technol. ISAECT 2019, 2019, doi: 10.1109/ISAECT47714.2019.9069704.
- [125] C. Jain and B. Singh, "A SOGI-FLL based control algorithm for single phase grid interfaced multifunctional SPV under non ideal distribution system," 11th IEEE India Conf. Emerg. Trends Innov. Technol. INDICON 2014, pp. 0–5, 2015, doi: 10.1109/INDICON.2014.7030368.
- [126] C. Jain and B. Singh, "Luenberger observer based control algorithm for single-phase two-stage multifunctional grid connected solar energy conversion system," *9th Int. Conf. Ind. Inf. Syst. ICIIS 2014*, pp. 2–7, 2015, doi: 10.1109/ICIINFS.2014.7036471.
- [127] S. Deo, C. Jain, and B. Singh, "A PLL-Less Scheme for Single-Phase Grid Interfaced Load Compensating Solar PV Generation System," *IEEE Trans. Ind. Informatics*, vol.

- 11, no. 3, pp. 692–699, 2015, doi: 10.1109/tii.2015.2425138.
- [128] C. Jain and B. Singh, "A PEF based control for single-phase multifunctional SECS with adaptive DC link structure for PCC voltage variations," *Conf. Proc. IEEE Appl. Power Electron. Conf. Expo. APEC*, vol. 2015-May, no. May, pp. 1722–1729, 2015, doi: 10.1109/APEC.2015.7104579.
- [129] C. Jain and B. Singh, "A SOGI-Q based control algorithm for multifunctional grid connected SECS," *India Int. Conf. Power Electron. IICPE*, vol. 2015-May, pp. 0–5, 2015, doi: 10.1109/IICPE.2014.7115773.
- [130] B. Singh, S. Goel, A. Singhal, A. Garg, and C. Jain, "Power quality enhancement of grid integrated solar PV system based on adaptive noise reduction control," *IEEE Power Energy Soc. Gen. Meet.*, vol. 2015-Septe, pp. 0–4, 2015, doi: 10.1109/PESGM.2015.7286619.
- [131] B. Singh, C. Jain, S. Goel, A. Chandra, and K. Al-Haddad, "A multifunctional grid tied solar energy conversion system with ANF based control approach," 2015 IEEE Energy Convers. Congr. Expo. ECCE 2015, pp. 434–441, 2015, doi: 10.1109/ECCE.2015.7309721.
- [132] J. Philip *et al.*, "Control and Implementation of a Standalone Solar PV Hybrid System," *IEEE Trans. Ind. Appl.*, vol. 52, no. 4, pp. 3472–3479, 2016, doi: 10.1109/TIA.2016.2553639.
- [133] C. Jain and B. Singh, "An offset reduction second order generalized integrator based control algorithm for single-phase S-DSTATCOM," Proc. 2015 39th Natl. Syst. Conf. NSC 2015, pp. 1–6, 2016, doi: 10.1109/NATSYS.2015.7489076.
- [134] B. Singh, S. Kumar, S. Dwivedi, I. Hussain, and C. Jain, "A cross correlation control approach for multifunctional SPV system," 2016 IEEE 6th Int. Conf. Power Syst. ICPS 2016, pp. 1–6, 2016, doi: 10.1109/ICPES.2016.7584241.
- [135] C. Jain and B. Singh, "An adjustable DC link voltage-based control of multifunctional grid interfaced solar PV system," *IEEE J. Emerg. Sel. Top. Power Electron.*, vol. 5, no.

- 2, pp. 651–660, 2017, doi: 10.1109/JESTPE.2016.2627533.
- [136] U. I. E. P. Loop-based, C. Under, and V. Solar, "Better Control for a Solar Energy System," *IEEE Ind. Appl. Mag.*, no. April, pp. 2–14, 2017.
- [137] S. Kumar and B. Singh, "A Multipurpose PV System Integrated to a Three-Phase Distribution System Using an LWDF-Based Approach," *IEEE Trans. Power Electron.*, vol. 33, no. 1, pp. 739–748, 2018, doi: 10.1109/TPEL.2017.2665526.
- [138] B. Singh, S. Kumar, and C. Jain, "Damped-SOGI-Based Control Algorithm for Solar PV Power Generating System," *IEEE Trans. Ind. Appl.*, vol. 53, no. 3, pp. 1780–1788, 2017, doi: 10.1109/TIA.2017.2677358.
- [139] S. Kumar and B. Singh, "Self-Normalized-Estimator-Based Control for Power Management in Residential Grid Synchronized PV-BES Microgrid," *IEEE Trans. Ind. Informatics*, vol. 15, no. 8, pp. 4764–4774, 2019, doi: 10.1109/tii.2019.2907750.
- [140] A. Ranjan, S. Kewat, and B. Singh, "DSOGI-PLL with In-Loop Filter Based Solar Grid Interfaced System for Alleviating Power Quality Problems," *IEEE Trans. Ind. Appl.*, vol. 57, no. 1, pp. 730–740, 2021, doi: 10.1109/TIA.2020.3029125.
- [141] I. Member, B. Singh, and I. Fellow, "Grid Synchronization of WEC-PV-BES Based Distributed Generation System using Robust Control Strategy," vol. 9994, no. c, pp. 1–10, 2020, doi: 10.1109/TIA.2020.3021060.
- [142] B. Singh, "Intelligent Control of SPV-Battery-Hydro Based Microgrid."
- [143] V. Narayanan, S. Kewat, and B. Singh, "Real Time Implementation of CLMS Algorithm in 3P4W Solar PV-BES Based Microgrid System," vol. 9994, no. c, 2020, doi: 10.1109/TIA.2020.3031873.
- [144] A. Ranjan, S. Kewat, and B. Singh, "Reweighted L1Norm Penalized LMS Fourth Algorithm of Solar Grid Interfaced System for Alleviating Power Quality Problems," *IEEE Trans. Ind. Appl.*, vol. 56, no. 5, pp. 5352–5362, 2020, doi: 10.1109/TIA.2020.3004746.

- [145] A. Ranjan, "Reweighted Zero Attracting Maximum Correntropy Criterion Algorithm based Solar Grid Interfaced System for Alleviating Power Quality Problems," pp. 3–8, 2020.
- [146] S. Singh, S. Kewat, B. Singh, B. K. Panigrahi, and M. K. Kushwaha, "Seamless Control of Solar PV Grid Interfaced System With Islanding Operation," *IEEE Power Energy Technol. Syst. J.*, vol. 6, no. 3, pp. 162–171, 2019, doi: 10.1109/jpets.2019.2929300.
- [147] V. Narayanan, Seema, and B. Singh, "Solar PV-BES based microgrid system with seamless transition capability," 2018 2nd IEEE Int. Conf. Power Electron. Intell. Control Energy Syst. ICPEICES 2018, pp. 722–728, 2018, doi: 10.1109/ICPEICES.2018.8897358.
- [148] R. Sharma, S. Kewat, and B. Singh, "SyRG-PV-BES-Based Standalone Microgrid Using," vol. 56, no. 3, pp. 2913–2924, 2020.
- [149] P. Gawhade and A. Ojha, "Recent advances in synchronization techniques for grid-tied PV system: A review," *Energy Reports*, vol. 7, no. October, pp. 6581–6599, 2021, doi: 10.1016/j.egyr.2021.09.006.
- [150] F. Sevilmiş and H. Karaca, "An Effective Solution to Eliminate DC-Offset for Extracting the Phase and Frequency of Grid Voltage," *Math. Probl. Eng.*, vol. 2021, 2021, doi: 10.1155/2021/9742683.
- [151] A. Kulkarni and V. John, "Design of a high-performance high-pass generalized integrator based single-phase PLL," *J. Power Electron.*, vol. 17, no. 5, pp. 1231–1243, 2017, doi: 10.6113/JPE.2017.17.5.1231.
- [152] A. Dash, D. P. Bagarty, U. R. Muduli, R. K. Behera, K. Al Hosani, and P. K. Hota, "Performance Evaluation of Three-Phase Grid-Tied SPV-DSTATCOM with DC-Offset Compensation under Dynamic Load Condition," *IEEE Access*, vol. 9, pp. 161395– 161406, 2021, doi: 10.1109/ACCESS.2021.3132549.
- [153] S. C. Devi, B. Singh, and S. Devassy, "Modified generalised integrator based control

- strategy for solar PV fed UPQC enabling power quality improvement," *IET Gener. Transm. Distrib.*, vol. 14, no. 16, pp. 3127–3138, 2020, doi: 10.1049/iet-gtd.2019.1939.
- [154] S. Golestan and J. M. Guerrero, "Conventional synchronous reference frame phase-locked loop is an adaptive complex filter," *IEEE Trans. Ind. Electron.*, vol. 62, no. 3, pp. 1679–1682, 2015, doi: 10.1109/TIE.2014.2341594.
- [155] A. GHOSHAL and V. JOHN, "Performance evaluation of three phase SRF-PLL and MAF-SRF-PLL," *Turkish J. Electr. Eng. Comput. Sci.*, vol. 23, no. 6, pp. 1781–1804, 2015, doi: 10.3906/elk-1404-488.
- [156] F. SEVİLMİŞ and H. KARACA, "Performance analysis of SRF-PLL and DDSRF-PLL algorithms for grid interactive inverters," *Int. Adv. Res. Eng. J.*, vol. 3, no. 2, pp. 116–122, 2019, doi: 10.35860/iarej.412250.
- [157] Y. Singh, I. Hussain, B. Singh, S. Mishra, and S. Member, "Real Time Implementation of EPLL with Generalized Filtering in Single Phase Grid Interfaced SPV System," 2016 IEEE Uttar Pradesh Sect. Int. Conf. Electr. Comput. Electron. Eng., pp. 50–54, 2016, doi: 10.1109/UPCON.2016.7894623.
- [158] P. Rodríguez, A. Luna, M. Ciobotaru, R. Teodorescu, and F. Blaabjerg, "Advanced grid synchronization system for power converters under unbalanced and distorted operating conditions," *IECON Proc. (Industrial Electron. Conf.*, no. 2, pp. 5173–5178, 2006, doi: 10.1109/IECON.2006.347807.
- [159] M. Karimi-Ghartemani and M. R. Iravani, "A method for synchronization of power electronic converters in polluted and variable-frequency environments," *IEEE Trans. Power Syst.*, vol. 19, no. 3, pp. 1263–1270, 2004, doi: 10.1109/TPWRS.2004.831280.
- [160] F. Xiao, L. Dong, L. Li, and X. Liao, "A Frequency-Fixed SOGI-Based PLL for Single-Phase Grid-Connected Converters," *IEEE Trans. Power Electron.*, vol. 32, no. 3, pp. 1713–1719, 2017, doi: 10.1109/TPEL.2016.2606623.
- [161] S. Golestan, J. M. Guerrero, J. C. Vasquez, A. M. Abusorrah, and Y. Al-Turki, "Single-Phase FLLs Based on Linear Kalman Filter, Limit-Cycle Oscillator, and Complex

- Bandpass Filter: Analysis and Comparison with a Standard FLL in Grid Applications," *IEEE Trans. Power Electron.*, vol. 34, no. 12, pp. 11774–11790, 2019, doi: 10.1109/TPEL.2019.2906031.
- [162] C. Zhang, X. Zhao, X. Wang, X. Chai, Z. Zhang, and X. Guo, "A Grid Synchronization PLL Method Based on Mixed Second- and Third-Order Generalized Integrator for DC Offset Elimination and Frequency Adaptability," *IEEE J. Emerg. Sel. Top. Power Electron.*, vol. 6, no. 3, pp. 1517–1526, 2018, doi: 10.1109/JESTPE.2018.2810499.
- [163] P. Rodríguez et al., "Multiresonant Frequency-Locked Loop for Grid Synchronization of Power Converters Under Distorted Grid Conditions," vol. 58, no. 1, pp. 127–138, 2011.
- [164] Y. F. Wang and Y. W. Li, "Grid synchronization PLL based on cascaded delayed signal cancellation," *IEEE Trans. Power Electron.*, vol. 26, no. 7, pp. 1987–1997, 2011, doi: 10.1109/TPEL.2010.2099669.
- [165] H. A. Hamed, A. F. Abdou, E. H. E. Bayoumi, and E. E. El-Kholy, "Frequency Adaptive CDSC-PLL Using Axis Drift Control Under Adverse Grid Condition," *IEEE Trans. Ind. Electron.*, vol. 64, no. 4, pp. 2671–2682, 2017, doi: 10.1109/TIE.2016.2633524.
- [166] Z. Dai, M. Fan, H. Nie, J. Zhang, and J. Li, "A Robust Frequency Estimation Method for Aircraft Grids under Distorted Conditions," *IEEE Trans. Ind. Electron.*, vol. 67, no. 5, pp. 4254–4258, 2020, doi: 10.1109/TIE.2019.2920469.
- [167] A. A. Vedyakov, A. O. Vediakova, A. A. Bobtsov, A. A. Pyrkin, and S. V. Aranovskiy, "Frequency estimation of a sinusoidal signal with time-varying amplitude\*," *IFAC-PapersOnLine*, vol. 50, no. 1, pp. 12880–12885, 2017, doi: 10.1016/j.ifacol.2017.08.1940.
- [168] B. Widrow and M. E. Hoff, "Adaptive switching circuits," *Wescon Conference Record*. pp. 709–717, 1989.
- [169] F. J. Alcántara and P. Salmerón, "A new technique for unbalance current and voltage

- estimation with neural networks," *IEEE Trans. Power Syst.*, vol. 20, no. 2, pp. 852–858, 2005, doi: 10.1109/TPWRS.2005.846051.
- [170] H. Saxena, A. Singh, and J. N. Rai, "Design and performance analysis of improved Adaline technique for synchronization and load compensation of grid-tied PV system," *Int. Trans. Electr. Energy Syst.*, vol. 30, no. 6, pp. 1–18, 2020, doi: 10.1002/2050-7038.12388.
- [171] K. Punitha, D. Devaraj, and S. Sakthivel, "Development and analysis of adaptive fuzzy controllers for PV system under varying atmospheric and partial shading condition," *Appl. Soft Comput. J.*, vol. 13, no. 11, pp. 4320–4332, 2013, doi: 10.1016/j.asoc.2013.06.021.
- [172] L. Liu, C. Liu, J. Wang, and Y. Kong, "Simulation and hardware implementation of a hill-climbing modified fuzzy-logic for maximum power point tracking with direct control method using boost converter," *JVC/Journal Vib. Control*, vol. 21, no. 2, pp. 335–342, 2015, doi: 10.1177/1077546313486912.
- [173] M. Kermadi, Z. Salam, J. Ahmed, and E. M. Berkouk, "An Effective Hybrid Maximum Power Point Tracker of PV Arrays for Complex Partial Shading Conditions," *IEEE Trans. Ind. Electron.*, vol. 66, no. 9, pp. 6990–7000, 2019, doi: 10.1109/TIE.2018.2877202.
- [174] V. Ravindran, S. K. Rönnberg, and M. H. J. Bollen, "Interharmonics in PV systems: a review of analysis and estimation methods; considerations for selection of an apt method," vol. 13, no. v, pp. 2023–2032, 2023, doi: 10.1049/iet-rpg.2018.5697.
- [175] A. Sangwongwanich, Y. Yang, D. Sera, and F. Blaabjerg, "Interharmonics from grid-connected PV systems: Mechanism and mitigation Aalborg Universitet Interharmonics from Grid-Connected PV Systems: Mechanism and Mitigation Sangwongwanich, Ariya; Yang, Yongheng; Sera, Dezso; Blaabjerg, Frede," no. August, 2017, doi: 10.1109/IFEEC.2017.7992128.
- [176] A. Sangwongwanich, Y. Yang, D. Sera, and H. Soltani, "Analysis and Modeling of

- Interharmonics From Grid-Connected PV Systems Aalborg Universitet Analysis and Modeling of Interharmonics from Grid-Connected PV Systems Sangwongwanich, Ariya; Yang, Yongheng; Sera, Dezso; Soltani, Hamid," no. October, 2018, doi: 10.1109/TPEL.2017.2778025.
- [177] M. Y. Rizwin, H. K. R, N. Mayadevi, and V. P. Mini, "Interharmonics Mitigation in Grid-connected Solar PV Systems with P & O MPPT Algorithm," 2020.
- [178] Z. Salam, K. Ishaque, and H. Taheri, "An improved two-diode PV (PV) model for PV system," 2010 Jt. Int. Conf. Power Electron. Drives Energy Syst. PEDES 2010 2010 Power India, vol. 1, no. 4, pp. 1–5, 2010, doi: 10.1109/PEDES.2010.5712374.
- [179] K. Ishaque, Z. Salam, H. Taheri, and Syafaruddin, "Modeling and simulation of PV (PV) system during partial shading based on a two-diode model," *Simul. Model. Pract. Theory*, vol. 19, no. 7, pp. 1613–1626, 2011, doi: 10.1016/j.simpat.2011.04.005.
- [180] H. Saxena, A. Singh, and J. N. Rai, "Design and analysis of different PLLs as load compensation techniques in 1-Ø grid-tied PV system," *Int. J. Electron.*, vol. 106, no. 11, pp. 1632–1659, 2019, doi: 10.1080/00207217.2019.1600745.
- [181] D. Jena and V. V. Ramana, "Modeling of PV system for uniform and non-uniform irradiance: A critical review," *Renew. Sustain. Energy Rev.*, vol. 52, pp. 400–417, 2015, doi: 10.1016/j.rser.2015.07.079.
- [182] Y. T. Tan, D. S. Kirschen, and N. Jenkins, "A model of PV generation suitable for stability analysis," *IEEE Trans. Energy Convers.*, vol. 19, no. 4, pp. 748–755, 2004, doi: 10.1109/TEC.2004.827707.
- [183] S. Motahhir, A. El Ghzizal, S. Sebti, and A. Derouich, "Modeling of PV System with Modified Incremental Conductance Algorithm for Fast Changes of Irradiance," *Int. J. Photoenergy*, vol. 2018, 2018, doi: 10.1155/2018/3286479.
- [184] P. Shah, I. Hussain, and B. Singh, "A Novel Fourth-Order Generalized Integrator Based Control Scheme for Multifunctional SECS in the Distribution System," *IEEE Trans. Energy Convers.*, vol. 33, no. 3, pp. 949–958, 2018, doi:

- 10.1109/TEC.2018.2806191.
- [185] Q. Liu, L. Cheng, A. L. Jia, and C. Liu, "Deep Reinforcement Learning for Communication Flow Control in Wireless Mesh Networks," *IEEE Netw.*, vol. 35, no. 2, pp. 112–119, 2021, doi: 10.1109/MNET.011.2000303.
- [186] M. Dehghani, Z. Montazeri, E. Trojovská, and P. Trojovský, "Coati Optimization Algorithm: A new bio-inspired metaheuristic algorithm for solving optimization problems," *Knowledge-Based Syst.*, vol. 259, p. 110011, 2023, doi: 10.1016/j.knosys.2022.110011.
- [187] Z. Xia et al., "RLCC: Practical Learning-based Congestion Control for the Internet," Proc. Int. Jt. Conf. Neural Networks, vol. 2021-July, pp. 1–8, 2021, doi: 10.1109/IJCNN52387.2021.9533754.
- [188] Q. Lan, Y. Pan, A. Fyshe, and M. White, "Maxmin Q-Learning: Controlling the Estimation Bias of Q-Learning," 8th Int. Conf. Learn. Represent. ICLR 2020, pp. 1–20, 2020.
- [189] O. Ansehel, N. Baram, and N. Shimkin, "Averaged-DQN: Variance reduction and stabilization for Deep Reinforcement Learning," *34th Int. Conf. Mach. Learn. ICML* 2017, vol. 1, pp. 240–253, 2017.
- [190] X.-Y. Liu *et al.*, "FinRL: A Deep Reinforcement Learning Library for Automated Stock Trading in Quantitative Finance," *SSRN Electron. J.*, no. NeurIPS, pp. 1–12, 2021, doi: 10.2139/ssrn.3737859.
- [191] H. Yang, X.-Y. Liu, S. Zhong, and A. Walid, "Deep Reinforcement Learning for Automated Stock Trading: An Ensemble Strategy," SSRN Electron. J., 2020, doi: 10.2139/ssrn.3690996.
- [192] J. Zhu, F. Wu, and J. Zhao, "An overview of the action space for deep reinforcement learning," *ACM Int. Conf. Proceeding Ser.*, 2021, doi: 10.1145/3508546.3508598.
- [193] N. P. Babu, J. M. Guerrero, P. Siano, R. Peesapati, and G. Panda, "An Improved Adaptive Control Strategy in Grid-Tied PV System with Active Power Filter for Power

Quality Enhancement," *IEEE Syst. J.*, vol. 15, no. 2, pp. 2859–2870, 2021, doi: 10.1109/JSYST.2020.2985164.

# **APPENDIX**

# Rating of Single-Phase Grid-Connected PV System

S.No.	Quantity	Parameters		
1	Grid Voltage	230V, 50Hz		
2	DC-Link Capacitance	2000μF		
3	DC-Link Reference Voltage	400V		
4	Interfacing Inductor	3.20mH		
5	PV Rating	$N_{ss} = 12, \ N_{pp} = 1, \ P_{mp} = 3248W, \ V_{oc} = 528V,$		
		$V_{mp} = 416V, I_{sc} = 8A, I_{mp} = 7.7A$		

# Rating of Three-Phase Grid-Connected PV System

S. No.	Quantity	Parameters
1	Grid Voltage	120 KV
2	DC-Link Reference Voltage	480 V
3	PV arrays (series connected)	7
4	PV arrays (parallel connected)	88
5	Current of single PV array	6.09 A
6	Voltage of single PV array	85.3 V
7	Maximum power output	250 KW

## LIST OF PUBLICATIONS

#### **Details of Publications in SCI/SCIE Journals**

- 1) Singh S, Rai JN. Implementation of an adaptive control approach in a single-phase grid-tied solar PV system for power quality improvement. Int J Circ Theor Appl. 2024;1-16. doi:10.1002/cta.4032.
- 2) Singh, S., Rai, J.N. Enhancement of power quality in three-phase GC solar PVs. *Electr Eng* (2024). https://doi.org/10.1007/s00202-024-02304-z.

#### **Details of Publications in International Conferences**

- 1) S. Singh and J. N. Rai, "Design and Dynamic Response of FOGI-FLL Based Controller in Grid Tied Solar PV System," 2023 International Conference on Power, Instrumentation, Energy and Control (PIECON), Aligarh, India, 2023, pp. 1-6, doi: 10.1109/PIECON56912.2023.10085766.
- 2) Sukhbir Singh and J.N. Rai, "An Adaptive Control Approach for the Synchronization and Control of Grid-Connected Solar PV System" International Conference on Green Energy and Sustainable Technology (ICGEST), NIT, kurukshetra. India, 2023.
- 3) Sukhbir Singh and J.N. Rai "Power Quality Enhancement and Voltage Stabilization in ROGI-FLL Based Hybrid System" International Electrical and Electronics Engineering Conference (IEEEC), DTU, Delhi, India, 2021.
- **4)** Sukhbir Singh and J.N. Rai, "Power Quality Improvement in Grid-Connected PV System using Adaptive Control Algorithm" International Conference on Energy, Power and Environment (ICEPE), NIT, Meghalaya, India, 2025.

### **BIO DATA**

Sukhbir Singh
Junior Engineer
Electricity Department
(UHBVN), Haryana, India
(Govt. of Haryana)

M. No. 8683857977,

**EMAIL:** 

sss.singh149@gmail.com

**DOB:** 02<sup>nd</sup>June1990



#### **CAREEROBJECTIVE**

Looking for an entry into highly professional organization with challenging and competitive environment, where I can use my knowledge base as well as personal attributes to achieve the organizational goals.

#### EDUCATIONAL QUALIFICATIONS

QUALIFI-	SPECIALIZATION	UNIVERSITY/	SESSION	%AGE
CATION		BOARD		
Ph.D*	Performance enhancement	DTU, Delhi	2019	Course work
	of grid connected solar PV			completed with
	system.			80%
M.Tech	Power System	MDU, Rohtak	2013-2015	76%
B.Tech	Electrical Engg.	MDU, Rohtak	2007-2011	75%
10+2	Non-Medical	HBSE	2007	72%
10	All Subject	HBSE	2005	77%

### WORK EXPERIENCE

- ➤ Working as a Junior Engineer in Electricity Department (UHBVN), Haryana, India (Govt. of Haryana) since 08<sup>th</sup> Nov 2024.
- ➤ Worked as an Assistant Professor (01<sup>st</sup> May 2022 to 07<sup>th</sup> Feb 2024) in Ganga Institute of Technology & Management, Jhajjar in Electrical Engg. Department since.
- ➤ Worked as an Assistant Professor (02<sup>nd</sup> Oct 2015 to 30<sup>th</sup> April 2022) in Ganga Technical Campus, Bahadurgarh in Electrical Engg. Department.
- ➤ Worked as a Lecturer (13<sup>th</sup> Feb 2012 to 9<sup>th</sup> Sept 2013) in Bhagwan Parshuram College of Engineering, Gohana in Electrical Engg. Department.